THE HONG KONG
POLYTECHNIC UNIVERSITY
香港理工大學
Pao Yue-kong Library
包玉剛圖書館

Copyright Undertaking

This thesis is protected by copyright, with all rights reserved.

By reading and using the thesis, the reader understands and agrees to the following terms:

1. The reader will abide by the rules and legal ordinances governing copyright regarding the use of the thesis.

2. The reader will use the thesis for the purpose of research or private study only and not for distribution or further reproduction or any other purpose.

3. The reader agrees to indemnify and hold the University harmless from and against any loss, damage, cost, liability or expenses arising from copyright infringement or unauthorized usage.

Pao Yue-kong Library, The Hong Kong Polytechnic University, Hung Hom, Kowloon, Hong Kong

http://www.lib.polyu.edu.hk

TRANSIENT STABILITY CONSTRAINED

OPTIMAL POWER FLOW WITH RENEWABLE

ENERGY UNCERTAINTIES

XIA SHIWEI

Ph.D

The Hong Kong Polytechnic University

2015

The Hong Kong Polytechnic University

Department of Electrical Engineering

TRANSIENT STABILITY CONSTRAINED OPTIMAL POWER FLOW WITH RENEWABLE ENERGY UNCERTAINTIES

XIA SHIWEI

A thesis submitted in partial fulfillment of the requirements

for the Degree of Doctor of Philosophy

September 2014

CERTIFICATE OF ORIGINALITY

I hereby declare that this thesis is my own work and that, to the best of my knowledge and belief, it reproduces no material previously published or written or material which has been accepted for the award of any other degree or diploma, except where due acknowledgement has been made in the text.

_____(Signed)

_____XIA Shiwei_____(Name of student)

Abstract

Optimal Power Flow (OPF) is an essential and practical tool for power system planning and operating attributed to its ability of approaching the best economic operating point by optimally adjusting the controllable variables. However, OPF solutions without security constraints imposed would have little practical value when contingencies were encountered, especially for modern power systems with increasing load demand and decreasing stability margin. The transient stability constrained OPF (TSCOPF) capable of effectively reconciling both the economic and stability of power systems would be therefore imperative for power grid operation. Based on the foundations of pioneering research in TSCOPF, this thesis strives to further investigate this TSCOPF problem and its effective analytical and computational intelligence solution methods.

TSCOPF is a semi-infinite optimization problem with finite number of controllable variables and infinite number of constraints, thus it is difficult to solve even for small power systems. Though promising results have been obtained in solving TSCOPF, a complete solution approach to effectively solve all types of TSCOPF problems, in particular extreme unstable and over-stabilization cases, is still lacking. This thesis therefore develops an all-round analytical solution approach, in which the transient stability constraint for each contingency is incorporated into the OPF model as a single stability constraint derived from the minimum kinetic energy for normal unstable case or the minimum accelerating power distance for extreme unstable case using SIngle Machine Equivalent (SIME) theory with trajectory sensitivity strategy based on time domain simulation. The proposed constraint is robust and scalable for large power systems as well as applicable to multi-swing unstable, normal unstable and extreme unstable cases. In addition, this stability constraint is further refined

I

to overcome the issue of over-stabilization by guiding the solution gradually across the stability boundary in the optimization process. As a whole, a complete solution method capable to solve all types of TSCOPF problems is established.

With the fast development of electronic technology and the rapid expansion of power network, many complex dynamic components such as FACTS devices are now widely applied in power grids. Coupled with the extensive use of discrete control devices, such as transformer taps and capacitor banks for power system preventive control, and the physical operation limitations, such as prohibited operation zone (POZ) and valve point effects in thermal generators, the TSCOPF problem has become much more challenging and needs to be solved as a non-differentiable and discontinuous optimization problem. As a remedy, a general non-convex Mixed Integer Nonlinear Program (MINLP) TSCOPF model with consideration of discrete control variables, generation POZ and valve-point effects as well as applicable to all complex dynamic components is proposed and solved using an Enhanced Particle Swarm Optimization (EPSO) with dynamic adjusted inertia weight and shrinking Gaussian distribution disturbance. The effectiveness and efficiency of this MINLP-TSCOPF model and EPSO solution approach have been comprehensive evaluated using a well-established bench-marking mathematical function and two representative power systems with FACTS devices.

Since MINLP is a hard mathematical problem and TSCOPF with semi-infinite feature is tough to solve, the proposed MINLP-TSCOPF model would pose a huge challenge for any optimization methods. Though the proposed EPSO method is capable to search for effective solutions, further exploration for a better method with improved quality and consistency of MINLP-TSCOPF solutions is still needed. Inspired by the encouraging optimization capability of the Group Search Optimization (GSO) algorithm in many engineering problems, an enhanced version referred as improved GSO (IGSO) is developed with new features including backward searching strategy, Cauchy mutation and inheritance

operator. Comparison study with seven representative artificial intelligence algorithms including EPSO on the WSCC 9-bus system, New England 39-bus system, and IEEE 145-bus system has confirmed the outperformance and superiority of the proposed IGSO method in solving this MINLP-TSCOPF problem.

Over the years, TSCOPF model has been mostly handled as a deterministic optimization problem with pre-assumed conditions while uncertainties in real power grids, such as stochastic load injections, uncertain generations and protection device activation time, are seldom considered. Meanwhile, due to the worldwide growing concerns on the depletion of fossil resources and their environmental effects, recent installation surge of wind power generations has led to even higher level of uncertainties and higher risk to the safe operation of power systems. In the coming era of smart grid, a new generation of stochastic TSCOPF models considering economic, stability and uncertainty simultaneously will be essential and indispensable for power system preventive control. In this thesis, a novel probabilistic TSCOPF (P-TSCOPF) model is therefore proposed. In this model, not only the detailed wind generator model with rotor flux magnitude and angle control strategy but also uncertainties including probabilistic load injections, stochastic fault clearing time and multiple correlated uncertain wind generations will all be considered. While the correlated uncertainties are efficiently handled using the $2m+1$ Point Estimated (PE) method with Cholesky decomposition, the proposed IGSO algorithm is further developed to form a new IGSO-PE solution approach to effectively solve this P-TSCOPF problem. The validity of the proposed P-TSCOPF model and the capability of the proposed IGSO-PE solution method have been thoroughly tested on a modified New England 39-bus system with correlated uncertain wind generations and validated using the Monte Carlo (MC) simulations.

Acknowledgement

First, I would like to express my deep and sincere appreciation to my chief supervisor, Dr. Kevin K. W. Chan, for his continuous support and painstaking effort throughout my PhD study and research. His critical thinking and meticulous research attitude have always inspired me that 'Learning without thought is labour lost' and 'keep asking and be cautious of your research'. It has been an honour to study under his guidance, and the academic experience with him will have a profound influence on the professional and personal development through my life.

I also own thanks to the members in the research team for the comfortable and invigorative academic atmosphere they have created during my research period. I wish to give special thanks to Dr. B. Zhou and Mr. X. Luo. They not only have always encouraged me to move forward when I was frustrated, but also have given me so many valuable suggestions and practical helps on my research. My sincere appreciations also go to many other coworkers, with whom I have a wonderful and unforgettable research journey.

Moreover, I would like to thank all the staff in the Department of Electrical Engineering for their direct or indirect assistances. I would also like to appreciate the reviewers and editors of my papers as well as my thesis examiners for their valuable comments to enable the improvements of my thesis. I am grateful to The Hong Kong Polytechnic University for the research scholarship to support my Ph.D. study and academic research.

Finally yet importantly, I am indebted to my dear parents whose sustainable and unconditional love has been with me for so many years. Special thanks to my wife Mrs. X. M. Wang for her thoughtfulness, empathy and love intensely motivating me to concentrate on my research.

Table of Contents

Lists of Figures, Tables and Abbreviations

List of Figures

List of Tables

List of Abbreviations

AIs	Artificial Intelligence algorithms
ANN	Artificial Neural Network
ARMS	Average Root Mean Square
AVR	Automatic Voltage Regulator
B&B	Branch and Bound
BCU	Boundary of stability region based Controlling Unstable equilibrium point
BD	Benders Decomposition
CDF	Cumulative Distribution Function
CM	Critical Machine
COI	Centre Of Inertia
CPSO	PSO with Constriction factor
CUEP	Controlling Unstable Equilibrium Point
DAEs	Differential Algebraic Equations
DE	Differential Evolution
DFIG	Doubly Fed Induction Generator
DOPF	Dynamic Optimal Power Flow
ED	Economic Dispatch
EEAC	Extended Equal Area Criterion
EP	Evolutionary Programming
EPSO	Enhanced Particle Swarm Optimization
FACTS	Flexible AC Transmission System

FC	Fuel Cost
FMAC	Rotor Flux Magnitude and Angle Control
FP	Function evaluation and Position update
GA	Genetic Algorithm
GSC	Grid Side Converter
GSO	Group Search Optimization
GSOISW	Group Search Optimization with an Improved Small World topology
HPSO	Hybrid Particle Swarm Optimization
IGSO	Improved Group Search Optimization
IGSO-PE	Point Estimated method with Improved Group Search Optimization
IPM	Interior Point Method
IPSO	Improved Particle Swarm Optimization
MC	Monte Carlo
MGSO	Modified Group Search Optimization
MINLP	Mixed Integer Non-Linear Program
MINLP-TSCOPF	Mixed Integer Non-Linear Program TSCOPF
MPSO	Modified Particle Swarm Optimization
NM	Non-critical Machine
OA/ER	Outer Approximation with Equality-Relaxation
OGSOMDE	Opposition-based GSO method with Modified Differential Evolution
OMIB	One Machine Infinite Bus
OPF	Optimal Power Flow

PDF	Probability Density Function
PE	Point Estimated method
PEBS	Potential Energy Boundary Surface
PF	Power Flow
POZs	Prohibited Operation Zones
PSO	Particle Swarm Optimization
PTSA	Probabilistic Transient Stability Analysis
P-TSCOPF	Probabilistic TSCOPF
SD	Standard Deviation
SIME	SIngle Machine Equivalent
SOPF	Static Optimal Power Flow
SPSO	Standard Particle Swarm Optimization
SVC	Static VAr Compensators
TCSC	Thyristor-Controlled Series Capacitors
TEF	Transient Energy Function
TS	Transient Simulation
TSB	Transient Stability Boundary
TSC	Transient Stability Constraint
TSCOPF	Transient Stability Constrained Optimal Power Flow
TSM	Transient Stability Margin
UEP	Unstable Equilibrium Point
WFs	Wind Farms

Chapter I

Introduction

1.1 Research Background

As one of the most important man-made complex project, power systems consisting of a huge number of generation plants, substation facilities, transmission and distribution devices as well as various electricity consumers have been developed with a long history of more than 130 years aiming to conveniently provide human beings with indispensable power energy. However, how to make the best energy utilization or obtain the most economic operation status of a power system is always a timeless issue in power industry. Optimal Power Flow (OPF) is a useful tool specially developed since 1960s for this purpose. The core principle of OPF is to find the most economic operating point of a power system with a given objective such as minimum fuel cost, minimum power losses, maximum transfer capacity, etc. by optimally adjusting the controllable variables.

Historically, the classical Economic Dispatch (ED), targeted to economically allocating the total load demand among all the dispatchable generation units with the equal marginal cost, was a precursor of OPF. The classical ED only considers a single constraint in term of the total active power balance to obtain a crude optimization solution. Due to its fast computing speed, ED has been widely used in the power dispatch centre to reduce the total generation cost. However, as ED focuses mainly on power system economic operation without considering either the network topology or any static security constraints, the resulted solutions would most often violate the system operation security limits, such as exceeding

the allowable range of node voltage or overloading the transmission line. As a complement to the classical ED, the OPF problem was consequently put forward to support various complicated operational constraints, particularly the electric network physical constraints [1, 2].

So far, OPF has been persistently expanded and constituted by a vast class of models with a wide range of industrial applications in the field of power system optimization. Though different OPF models do have different objectives and constraints, their core works the same to optimally adjust the controllable variables for a given economic target, such as saving fuel cost, reducing power losses [3], enhancing available transfer capacity [4], etc. or combination of those [5, 6] without violating any static constraints in the base case [7] or under any contingencies [8, 9]. Meanwhile, a wide variety of optimization techniques has been developed to solve these OPF models, for instance nonlinear programming [10-12], linear programming [9], quadratic programming [13-16], interior point method [17] and even the heuristic methods [18-22]. With the increased variable dimensions of OPF model for large-scale modern power networks, many decomposition methods have been proposed to divide the high-dimensional optimization problem into multiple sub-problems such that the original complicated OPF model can be effectively addressed. The Min-Cut algorithm in [8] and Benders decomposition in [23, 24] have been successfully applied to solve large-scale non-convex optimization problems with satisfactory solutions within an acceptable time period. As these OPF models consider only the security constraints of a power system in a given time without considering any time-related constraints between successive time instances, they are categorised as Static OPF (SOPF) [25].

However, when SOPF solutions obtained in a given time series were implemented in a real power grid, the following two major issues would arise and as a result hindered its applications: 1) Due to the physical device limits, it is not practical or desirable to allow dramatic sequential parameter changes in

power systems operating over a time period. For instance, transformer taps will be adjusted too frequently and the total number of tap changes per day will be over the daily limit if SOPF solution for each time interval was followed, or generator outputs are overrun the ramp up/down rate limit between successive time intervals. 2) The sum of all the individual optimal solutions for a given time in the time series is not necessary the optimal solution of the given time period, i.e. the overall cost covered the entire time period is not necessary minimum. Consequently, the so-called Dynamic OPF (DOPF) was proposed as an extended SOPF with consideration of transitional constraints over a time interval, such as the unit ramp rate, charge / discharge dynamics of storage devices, long term water reservoir capacity and electricity supply contracts [26-28]. Obviously, DOPF over a long time period is highly complicated due to the huge dimensional constraints and its computation speed is a major concern to its implementation in a real power grid. Based on the special block structure of DOPF, a decomposed predictor-corrector interior point algorithm was proposed in [29] to first decouple the large-scale DOPF problem into many sub-problems and then solve using an inequality iteration strategy to obtain a satisfactory solution in terms of robustness, computing time and convergence speed.

With the increasing concerns on energy saving and growing enthusiasms in the deregulated power market, the unremitting pursuit for high-quality optimal solutions has compelled modern power grids to operate closer to their stability limit than ever before. Large scale blackouts [30-32] caused by power system instability in recent years have showed the increasing importance of power system stability in the safe operation of a power grid, and that modern power systems operated with economic consideration alone but low ability to withstand credible contingencies will not be sufficient. Stability constrained OPF model taken into account of both dynamic security and economic operation has therefore been proposed and actively researched in recent years. In [33-37], a voltage stability constrained OPF model based on the active power-voltage curve

3

was presented. In [38, 39], a small signal stability constrained OPF was developed with linearization around the operation point in concern. On the other hand, angle stability constrained OPF problems were investigated in [40-45] to ensure the transient angle stability against large disturbances.

In [46], the IEEE/CIGRE Joint Task Force has provide a physically based definition for power system stability as *the ability of an electric power system, for a given initial operating condition, to regain a state of operating equilibrium after being subjected to a physical disturbance, with most system variables bounded so that practically the entire system remains intact.* Among various categories of stability problems, transient instability is one of the most dominant stability issues and has been obtained much attention from the industry [47-50]. In this thesis, transient stability has been identified as one of the main concerns in addition to the traditional static constraints in optimizing the operation of modern power grids, and the so-called Transient Stability Constrained Optimal Power Flow (TSCOPF) is selected as the core research issue to simultaneously reconcile power system economics and transient angle stability in the new emerging smart grid paradigm with high penetration of renewable energy.

1.2 Incentives of Thesis

In today's much stressed power grid and deregulated power market, the transient stability and economic of power system should be reconciled simultaneously. Meanwhile, with the increasing concerns on the energy-saving policy and in the environmental-friendly strategic framework in power industries, more and more wind power generations have been incorporated into power grids. This not only provides the power system with a valuable opportunity to be green and sustainable but also brings new challenges and concerns to power system safe operation. One of the immediate concerns is how to maintain the safe and economic operation of the power system with high uncertainty for example due

to the intermittency of wind or solar power generation. This thesis would therefore focus on the problem of TSCOPF aimed to develop new effective solution methods to overcome the following difficulties faced nowadays.

1) TSCOPF problem involves a huge number of Differential Algebraic Equations (DAEs) and transient stability inequality constraints covering the entire simulation period. It is a difficult semi-infinite optimization problem with finite number of controllable variables but infinite number of constraints [44]. How to deal with the constraints imposed by the dynamic components and generate a suitable transient stability index for use in the TSCOPF model is the key for solving this challenging problem. There are mainly two types of derivative-based methods: a) generation rescheduling strategy - it coarsely shifts generation from the most advanced generator to the least advanced generator based on trajectory sensitivities [45, 51, 52] and would usually obtain conservative suboptimal solutions; b) numerical discretization method - it discretizes the DAEs as a large set of small-step algebraic inequalities and equalities by means of implicit trapezoidal integration, and then solves the TSCOPF problem using Interior Point Method (IPM) [53-56]. The limitation of this discretization approach is that the number of constraints would rise sharply with the growing of system size, number of contingencies, simulation period, etc. and would lead to a high dimensional complexity or even unsolvable 'dimension disaster'. Therefore, a non-conservative TSCOPF solution method with low dimensional constraint using the minimum kinetic energy for normal unstable case or the minimum accelerating power distance for extreme unstable case is proposed in the thesis based on the trajectory sensitivity and SIngle Machine Equivalent (SIME) strategy. So far, most of previously published works on TSCOPF mainly concerned the normal unstable cases while the extreme unstable cases are not mentioned, and the issue of over-stabilization in the optimization process is also not handled. Therefore, the first incentive for this thesis is to develop an all-round solution

method capable to cope with all TSCOPF problems including extreme unstable cases and handle the issue of over-stabilization.

2) Considering that a) with the rapid development of power electronics, more and more sophisticated power electronics devices such as flexible AC transmission system (FACTS) are widely adopted in modern power grids; b) real thermal generators do exhibit the so-called valve-point effects due to the valve opening characteristics of multi-valve steam turbines [26, 57, 58]; and c) discrete control devices such as transformer taps and capacitor banks are commonly found in the power system optimization formulation, a general TSCOPF model readily accommodating to those would be indispensable. Consequently, a non-convex Mixed Integer Nonlinear Program TSCOPF (MINLP-TSCOPF) model with consideration of generation valve-point effects and discrete control variables as well as applicable to all complex dynamic components is proposed in the thesis. So far, there is no satisfactory published method for solving this type of TSCOPF with non-convex MINLP characteristics. Since the updating of control variables in any gradient-based methods requires the derivatives of constraint-error, applying gradient-based methods to solve such MINLP-TSCOPF problem with complex power system models and discrete control variables will not only be cumbersome but also require major development effort for any changes in the system models. More importantly, due to the non-convexity of TSCOPF, gradient-based algorithms would likely be trapped in suboptimal solutions [59]. As the second incentive in this thesis, a heuristic method referred as Enhanced Particle Swarm Optimization (EPSO) algorithm is proposed to solve this difficult MINLP-TSCOPF problem.

3) Heuristic algorithms are derivative-free and capable of finding the global optimal or a sufficiently good solution with no strict requirements for neither the convexity nor the differentiability of the model. Many such heuristic algorithms have been presented as promising tools for power system

optimization [3-7, 19-22]. Most notably, for solving the TSCOPF model, several swarm intelligence algorithms including Genetic Algorithm (GA), Particle Swarm Optimization (PSO) and Differential Evolution (DE) have been adopted in [43, 44, 60] to generate a set of encouraging optimal solutions. However, those algorithms have only been implemented and tested on simple and continuous TSCOPF models with limited attention on MINLP-TSCOPF problems characterized to have high discontinuity, non-convex features and multiple minima. Based on the No Free Lunch theorem, "for any algorithm, any elevated performance over one class of problems is exactly paid for in performance over another class" [61], an optimal solution method should therefore be specially designed for solving this MINLP-TSCOPF problem effectively. Consequently, the third incentive of this thesis is to develop a better solution method referred as an improved Group Search Optimization (IGSO) method for solving this MINLP-TSCOPF problem.

4) So far, most literatures such as [42, 43, 45, 62-66] have handled TSCOPF as a deterministic optimization problem and successfully solved it using either gradient-based methods or heuristic methods with encouraging results. While these approaches have made valuable contributions and advancements in TSCOPF, uncertainties in power systems are not considered and statistical information on the likelihood of constraint violations as well as stability risk level are seldom provided. However, the practical operation of a power system do involve uncertainties stemming from, for instances, stochastic load injections, uncertain generations and probabilistic fault clearing time imposed by practical relay operations. Furthermore, growing global concerns on the depletion of fossil resources and their environmental effects have driven the rapid deployment of renewable energy, among which wind power is the most dominated type [67, 68]. The recent installation surge of large-scale wind farms with intermittent nature has leaded to even higher level of uncertainties and threatened the safe operation of power systems with high wind

penetration. Therefore, as the last but not the least incentive of this thesis is to first propose a new probabilistic TSCOPF model with consideration of the operation and generation uncertainties in power system transient stability, and then design an effective solution approach named IGSO-PE to ensure the economic and secure operation of power system with uncertainties.

1.3 Primary Contributions

Transient stability and economic should be reconciled with each other in TSCOPF for modern stressed power systems incorporated with intermittent renewable energy. The following are the main achievements in this research work: 1) developed a complete approach to analytically solve all types of TSCOPF problems; 2) proposed a general MINLP-TSCOPF model with support for various dynamic components; 3) developed two solution methods to effectively solve the MINLP-TSCOPF; and 4) established a new probabilistic TSCOPF (P-TSCOPF) model to accommodate the generation, load and operation uncertainties in transient stability and proposed a corresponding effective solution method.

To be specific, this thesis has made the following original contributions:

- Foremost, the SIME power distance is introduced as the transient stability constraint for extreme unstable case in traditional TSCOPF model, and then the model is iteratively solved by a trajectory sensitivity based analytical method. Meanwhile, the over-stabilization issue in TSCOPF is properly addressed by guiding the solution gradually across the stability boundary. As a result, an all-round solution approach which accommodates all types of TSCOPF problems including multi-swing unstable, normal unstable and extreme unstable cases for multi-contingency with over-stabilization is established.

- Secondly, a general non-convex MINLP-TSCOPF model with many minima and support for any dynamic components and discrete control variables is proposed. A newly developed EPSO method is presented to effectively solve this MINLP-TSCOPF problem.

- Thirdly, an improved GSO (IGSO) method is specially established with backward searching strategy, Cauchy mutation and inheritance operator for solving the MINLP-TSCOPF problem. Comprehensive benchmarking study of IGSO with published heuristic methods has validated the prowess of IGSO in solving this MINLP-TSCOPF problem.

- Finally, for the first time a P-TSCOPF model simultaneously considering power system transient stability and various practical operating uncertainties is proposed for power system preventive control. A new IGSO-PE approach based on the Point Estimated (PE) strategy and IGSO is developed to solve this P-TSCOPF model with satisfactory solutions.

1.4   Organization of Thesis

This thesis consists of seven chapters and is organized as follows:

Chapter I first introduces the background and motivation of this research, and then briefly outlines the primary contributions and the organization of this thesis.

In Chapter II, fundamentals and essentials of transient stability constrained optimal power flow with uncertainties are reviewed and discussed. Firstly, the transient stability analysis method and the mathematical formulation of traditional TSCOPF model are introduced, and then a comprehensive literature survey on various TSCOPF solution methods is conducted. The current state of art techniques to deal with uncertainties in transient stability are then presented and followed by some basic definitions in probability theory for random variables. Gram-Charlier expansion is finally introduced as the essentials to handle uncertainties in the P-TSCOPF problem presented in Chapter VI.

In Chapter III, the TSCOPF problem is divided into traditional OPF and stability analysis processes and solved iteratively by IPM. Based on the SIME theory, a single stability constraint derived from the minimum accelerating power distance is proposed for extreme unstable multi-machine TSCOPF problems. Issue of over-stabilization, if there is any, is overcome by gradually guiding the solution across the stability boundary. As a result, a complete solution method capable of solving multi-contingency TSCOPF problems in normal unstable or extreme unstable conditions with over-stabilized issue is established. The performance of this proposed method has been fully evaluated using the New England 39-bus system and the IEEE 50-generator system.

In Chapter IV, valve-point effects and discrete control variables are considered to form a more general non-convex MINLP-TSCOPF model, in which the energy based transient angle and voltage constraints are included as an integrated stability control process. A new EPSO method with dynamic adjusted inertia weight and shrinking Gaussian distribution disturbance is proposed to solve this MINLP-TSCOPF problem and tested firstly with a benchmarking MINLP mathematical function. Two representative power systems with FACTS devices are prepared to fully evaluate the validity of the proposed MINLP-TSCOPF model and the full capability of the proposed EPSO method.

In Chapter V, based on the good performance of group search optimization, an IGSO algorithm is developed with enhancements of backward searching strategy, Cauchy mutation and inheritance operator to effectively solve the challenging MINLP-TSCOPF problem. The outperformance of IGSO method have been tested and validated by four comprehensive case studies on the WSCC 9-bus system, New England 39-bus system, and IEEE 145-bus system benchmarking with several typical heuristic methods in the state of art.

Chapter VI puts forward a probabilistic TSCOPF model to accommodate the generation and operation uncertainties in the transient stability for power system preventive control. The detailed model of wind generator with Rotor Flux

Magnitude and Angle Control (FMAC) strategy is introduced in the P-TSCOPF to describe the dynamic behaviours of wind generators. Also, typical uncertainties, such as probabilistic load injections, stochastic fault clearing time and multiple correlated uncertain wind generations, are incorporated in the P-TSCOPF model. Furthermore, based on PE method with Cholesky decomposition and IGSO algorithm, an IGSO-PE approach is designed to effectively solve the challenging P-TSCOPF problem. The effectiveness of the proposed P-TSCOPF model and the IGSO-PE approach is thoroughly tested on the modified New England 39-bus system with correlated uncertain wind generations and benchmarked with Monte Carlo (MC) simulations.

Finally, some concluding remarks of the thesis are summarized in Chapter VII, and the prospective extensions of the thesis are discussed as the future work in that chapter.

1.5 List of Publications

Journal papers published

1. S. W. Xia, K. W. Chan, and Z. Guo, "A novel margin sensitivity based method for transient stability constrained optimal power flow," *Electric Power Systems Research*, vol. 108, pp. 93-102, March 2014.

2. S. W. Xia, K. W. Chan, X. Bai, and Z. Guo, "Enhanced particle swarm optimization applied for transient angle and voltage constrained discrete optimal power flow with FACTS," *IET Generation, Transmission & Distribution*, vol. 9, no. 1, pp. 61-74, January 2015.

3. S. W. Xia, B. Zhou, K. W. Chan, and Z. Guo, "An Improved GSO Method for Discontinuous Non-convex Transient Stability Constrained Optimal Power Flow with Complex System Model," *International Journal of Electrical Power & Energy Systems*, vol. 64, pp. 483-492, January 2015.

4. X. Luo, S. W. Xia, and K. W. Chan, "A decentralized charging control strategy for plug-in electric vehicles to mitigate wind farm intermittency and enhance frequency regulation," *Journal of Power Sources*, vol. 248, pp. 604-614, Feb. 2014.

Journal papers under review or in preparation

5. S. W. Xia, X. Luo, and K. W. Chan, "Probabilistic transient stability constrained optimal power flow for power systems with multiple correlated uncertain wind generations," submitted to *IEEE Transactions on Sustainable Energy,* Manuscript ID: TSTE-00101-2015.

6. S. W. Xia, X. Luo, and K. W. Chan, "Optimal sizing of energy storage system for power grid planning with intermittent wind generations," submitted to IET Generation, Transmission & Distribution, Manuscript ID: GTD-SI-2015-0171.

7. S. W. Xia, X. Luo, and K. W. Chan, "Optimal sizing and siting of energy storage system for reliability constrained power network operation with high penetration of renewable generations," in preparation for submission to IEEE Transactions on Power Systems.

8. S. W. Xia, X. Luo, and K. W. Chan, "A fully distributed charging control strategy for multiple energy storages to smooth wind power fluctuation and strengthen frequency regulation," in preparation for submission to IEEE Transactions on Smart Grid.

Papers presented at international Conferences

9. S. W. Xia, X. Luo, and K. W. Chan, "A framework for self-healing smart grid with incorporation of Multi-Agents," *The 6th International Conference on Applied Energy*, May 30-June 2, 2014, Taipei, Taiwan.

10. X. Luo, S. W. Xia, and K. W. Chan, "A simple decentralized charging control scheme of plug-in electric vehicles for alleviating wind farm

intermittency," *The 6th International Conference on Applied Energy*, May 30-June 2, 2014, Taipei, Taiwan.

Chapter II

Essentials for Transient Stability Constrained Optimal Power Flow with Uncertainties

2.1 Essentials for TSCOPF problem

2.1.1 Overview of Transient Stability Analysis

Transient stability is the ability of a power system to regain a stable equilibrium operation point when exposed to a severe disturbance such as a three-phase ground fault, where the dynamic behaviours and interactions of multiple complex dynamic components should be considered [69]. Power system transient stability is directly or indirectly inferred from the solutions of high dimensional DAEs, and it is closely related to the initial condition of DAEs, i.e. power system initial operation point. So far, transient stability analysis methods can be categorized into the following three branches: 1) time domain simulation method; 2) direct energy function method; and 3) hybrid method.

In time domain simulation method, DAEs describing the system dynamic behaviours in transient stability are usually solved using classical mathematical integration algorithms, such as Euler method [70] or implicit trapezoid method [71], to obtain the state variables. Consequently, the power system transient stability can be determined from these state variables, such as through comparing the generator angles with a heuristically assumed threshold. Time domain simulation method is straightforward for transient stability analysis, and with good flexibility to support various complex dynamic models in large-scale power systems. Therefore, time domain simulation method has been widely adopted in the industry and plays the important role as a benchmark for other stability

analysis methods [72]. However, the major deficiency of time domain simulation method is the lack of direct quantitative information on the transient stability margin [73]. In addition, the heavy computation burden or expensive CPU time cost is also a concern for its on-line applications though vast improvements have been made in recent years to enhance its efficiency using, for example, parallel computation [74-79] and Taylor series techniques with large integration step-sizes [80-84].

Direct energy function method is an alternative tool for transient stability analysis capable of determining the power system stability margin directly from the perspective of system energy [85]. Based on Lyapunov's stability theory, this method compares the accumulated system energy during the contingency period with the predefined critical energy, and hence the system transient stability can be directly derived without calculating generator angle trajectories over the entire simulation period. Based on how this critical energy is defined, the direct energy function method can be categorized as: 1) Controlling Unstable Equilibrium Point (CUEP) method [86]; 2) Potential Energy Boundary Surface (PEBS) method [87]; 3) Boundary of stability region based Controlling Unstable equilibrium point (BCU) method [88-90]; and 4) Extended Equal Area Criterion (EEAC) method [91]. Compared with time domain simulation, direct energy function method is more efficient and effective to quantify transient stability margin and calculate various critical parameters, such as the critical clearing time, etc. However, the limitations of direct energy function method are: 1) the accuracy cannot be guaranteed due to various assumptions made on the calculation of critical stable energy; 2) the transient stability margin of power systems with complex dynamic components cannot be readily obtained [92] while high-order synchronous generator models, complex excitation systems and power electronic devices are quite common in modern power systems nowadays.

The hybrid method is the third method for transient stability assessment [73, 93-95]. In this method, a time domain simulation is first performed beyond the

fault clearing time, and then transient stability margin is determined using the concept of SIME by examining the candidate critical and non-critical machines [93]. The SIME theory is based on the fact that if a power system with multiple machines is transient unstable, the machines will first be separated into two groups and then may further be split into many groups. Therefore, the two equivalent groups can be mapped into SIME, and the system stability could then be observed [73]. The hybrid method inherits not only the high flexibility of time domain simulation method in power system modelling but also the high computation efficiency and quantified stability margin of direct method. Hence, SIME has been recognized and widely adopted as the most promising method for transient stability assessment [42, 66, 96].

2.1.2   Overview of Transient Stability Constrained OPF

The mathematical formulation of TSCOPF problems is formulated as follows.

$$\text{Minimize} \quad f(x,u) \tag{2.1}$$

$$\text{Subject to} \quad g(x,u) = 0 \tag{2.2}$$

$$h(x,u) \leq 0 \tag{2.3}$$

$$\dot{x} = y(x_0,u) \tag{2.4}$$

$$TSI \leq \varepsilon \tag{2.5}$$

where u is a set of control variables and x is a set of dependent variables corresponding to u, $f(x,u)$ is the objective function, which could be the total generation cost, total power grid loss or total compensation cost, and so on. $g(x, u)$ and $h(x,u)$ stand for the system operating equality and inequality constraints in normal state; $y(x_0,u)$ is the differential equations for generators and dynamic components, such as synchronous generators, rotating excitation systems, speed governors, induction machines, etc. The exact descriptions of the dynamic constraints would depend on which dynamic models were adopted to mimic the power system dynamic characteristics. The transient stability index TSI is

typically expressed in term of the generator angle margin to a heuristically fixed angle threshold.

2.2   State of the Art Methodologies for TSCOPF

With stress from power system deregulation and increasing load demand, power systems are operating much closer to its security limit than ever before [97, 98], and the so-called TSCOPF problem has therefore been widely investigated to effectively reconcile the economics and security for power system operation. So far, there are mainly three approaches for solving the TSCOPF problem, namely generation rescheduling method, numerical discretization method and Artificial Intelligence algorithms (AIs).

Generation rescheduling is a typical TSCOPF strategy used in [45, 51, 52] to shift power from the most advanced generator in terms of generator rotor angles to the least advanced generator [94, 99, 100] so as to drive the system to move to a stable operating point. Since power generation is only re-dispatched among the most advanced and least advanced generators, the solution is sub-optimal.

In numerical discretization method, the semi-infinite TSCOPF problem is first transformed to a generalized large-scale nonlinear programming problem, and then solved by classical optimization methods such as IPM in [45, 53-55, 101, 102], etc. In [103], an enhanced numerical discretization method was proposed to reduce the burden of optimization by relaxing and transforming the equality constraints to inequality constraints. In [65, 104-106], the difficulty of semi-infinite optimization was overcome by substituting the infinite constraints with a constraint transcription based on functional transformation techniques, which transformed the infinite transient constraints into lower dimension inequality constraints, and then incorporated into the conventional OPF and solved by IPM. The SIME strategy was also introduced in many publications to reduce the number of generator stability constraints. In [38], a method based on substituting

the original multi-machine by a SIME machine was presented to reduce the generator constraints for each time step; however, the OPF model still involves many transient stability constraints during the entire heuristic simulation period. In [66], though a SIME method with partial simulation period discretized was proposed to reduce the number of constraints, the computation of Jacobian and Hessian matrices is still included in the discretization of differential equations during the unstable period and hence resulted in an expensive time consuming optimization process. In [64], an improved SIME method was proposed to reduce the stability constraints to one SIME angle constraint applied only at the initial time with the angle threshold $\delta_{sh} = \delta_{UT}^{t_0} - \lambda \delta_{UT}^{t_0}$ updated by renewing λ or using linear extrapolation or interpolation between the changes of unstable margin and variations of generator angles of two successive iterations. While the initial λ shall be heuristically and properly selected, the One Machine Infinite Bus (OMIB) mode may change in successive iterations and complex handling would be required to cope with the change of OMIB m-swing structure [64]. In [107], a two-step strategy using trajectory sensitivities based on time domain simulation was proposed in which trajectory sensitivities calculation and OPF are run in turn to form an iterative process to solve the TSCOPF problem. However, the same problems of large number of angle constraints over the whole simulation period and heuristically fixed angle threshold still exist. In [108], the trajectory sensitivity theory and the SIME method were further applied to solve the TSCOPF problem iteratively. It accurately and directly formulates the transient stability constraint using the unstable margin, instead of a heuristic angle constraint as in [64], to reduce the dimension of transient stability constraints for the normal unstable case; this strategy thus made the TSCOPF optimization dimension comparable to a conventional OPF. In [40], a nonlinear transient stability boundary (TSB) trained by the Artificial Neural Network (ANN) for a large number of operating points using time domain simulation was incorporated into OPF to address the TSCOPF problem.

All these gradient-based optimization methods in above indeed enriched the content of solving TSCOPF. However, they still share a few common shortcomings such as high sensitivity to initial conditions due to their dependence on derivatives. In addition, these derivative based optimization methods would encounter high dimensional constrains and possibly diverge in their optimization processes in large-scale power systems with many complicated dynamic components. In the worst case, some TSCOPF problems may even be un-differentiable and discontinuous, and thus shall not be solved with classical gradient-based methods. On the other hand, AIs which mimic the behaviour of nature biological species have been developed as an alternative TSCOPF solution approach to overcome the above drawbacks. AIs such as DE [43], evolutionary programming (EP) [109], GA [110] and PSO [44, 111-115] are population-based stochastic optimizations, which do not rely on derivatives, and therefore are the promising methods for readily handling the non-derivative and non-convex optimization problems.

So far, the most noticeable reported applications of AIs for solving the TSCOPF problem are GA, PSO, and DE. Encouraged by the good performance for some hard optimization problems with faster and stable convergence, [44] has adopted the PSO with constriction factor (CPSO) to solve a TSCOPF problem with multiple contingencies, while [43] has obtained a satisfactory TSCOPF solution effectively based on a well-tuned DE algorithm. In [60], an orthogonal array based GA was successfully applied to solve a TSCOPF problem in the New England system and obtained quite good solutions.

2.3   State of the Art Methodologies for TSCOPF with Uncertainties

Currently, the efforts of considering various typical uncertainties in power system operations are mainly spent in the field of probabilistic power flow

problem instead of TSCOPF problem because of the high complexity involved in solving TSCOPF. So far, there are three main approaches to deal with uncertainties in the probabilistic power flow analysis, namely the Monte Carlo (MC) method, the analytical method, and the point estimated (PE) method. 1) The MC method firstly solves the traditional power flow in a deterministic manner for a large number of system samples, and then summarizes all the solutions [116-118] to obtain the statistics distribution of the concerning output variables. 2) The analytical method transforms the power flow equations into a quasi-linear form or second-order Taylor expansions of uncertain inputs, and then obtains the probability density function of random outputs by convolution computing [119]. 3) The PE method is the third promising tool for handling probabilistic power flow problems [120, 121] based on the deterministic solutions of only a few concentrations inferred from the first several central moments of random inputs.

Though uncertainties in power flow problem can now be addressed readily, efficient handling of uncertainties in transient stability analysis is still difficult due to the complicated nature of the problem. The state-of-the-art Probabilistic Transient Stability Analysis (PTSA), including the basic theories for extended research and development, were comprehensively reported in [122, 123] and further investigated in [124]. While a PTSA approach based on the regression of the critical clearing time in terms of system load distribution was proposed in [125-127], recent research has focused on analyzing the uncertainties of fault occurrence, fault location, fault type, and fault clearing time for PTSA using the Monte Carlo (MC) method and conditional probability theory. A probabilistic stability index considering random characteristics of pre-fault loading condition, fault type and location was calculated using the Bayes' theorem in [128], such that the system "weak points" were identified by the probabilistic stability index. In [129], a conceptual framework based on the steady-state and dynamic security regions was proposed to first assess the probabilistic distribution of critical

clearing time and then analyze the system probabilistic security. A stochastic modelling of high-speed reclosing was investigated in [130] for quantitative assessment of the effect of the occurrence of a transmission line fault on the likelihood of system instability. A risk-based security index in terms of both probability of instability and impact of instability was calculated by MC method in [131] to determine the operating limits for a stability-restricted power system. In [132], the probabilistic transient stability of a large scale B.C. Hydro system was assessed using a modified shell of B.C. Hydro's on-line transient stability program and MC formulation, and it was found that BC Hydro's operation was very conservative under the traditional deterministic criteria with a probabilistic instability lower than 0.2%. A probabilistic methodology based upon an approximated quadratic stability region, taking into account the randomness of fault clearing time, reclosing time and fault location, was proposed in [133] to determine the probabilistic transient stability margin. A set of stochastic differential equations was utilized to analyze the stochastic transient stability and solved by stochastic Euler and Milstein schemes in [134]. Most notably and recently, with the rapid development of wind power generations, a probabilistic-based approach was presented in [48] to evaluate the probabilistic transient stability for a wind farm with two-mass shaft wind turbines using the electromagnetic transient program. In order to enhance the PTSA efficiency, a corrected transient energy function-based probabilistic approach was adopted in [135] to speed up the calculation process of PTSA while grid-computing technique was also introduced in [136] for PTSA.

Though MC method is straightforward, accurate and well-tested, it is quite time consuming for PTSA as a large number of random time domain simulations are needed to determine the probabilistic transient stability index. Its further application to address the uncertainties in TSCOPF problem, which embeds the PTSA in an optimization problem, would be even more computational expensive and time consuming.

As an alternative, the analytical method, which handles uncertainties by linearizing the relationship between output and input and obtains the probability of random output variables using convolution computing of inputs, seems more computationally effective. An analytical approach based on EEAC was successfully implemented on a simple single-machine system in [125-127] without any further consideration on neither its application in large-scale system with multiple machines and complicated dynamic components nor the correlations among uncertainties.

Generally, for solving PTSA on multiple-machine systems with correlated uncertainties, the analytical method first requires some mathematical assumptions to simplify the relationship between the concerned output and uncertain inputs [120]; and then based on this simplified linear relationship, the probability expansion theory could be used to estimate the probability distribution of output random variables. Though the linearization of transient stability margin to the random inputs could be obtained from the trajectory sensitivity calculations of DAEs, it would be arduous to derive the probabilistic transient stability index in the term of multiple correlated uncertain inputs for large power systems with complicated dynamic components, and hence has prohibited its practical application.

The PE method is capable of calculating the raw moments of output random variables using only the deterministic solutions of very few concentrations. Compared to the large sample set required in MC and the complicated linearization of transient stability margin involved in the analytical method, uncertainties in complicated power systems could be readily and effectively addressed by the PE method. Among the common PE variants such as 2m and 4m+1 schemes, 2m+1 PE scheme has been found to provide the best performance with satisfactory accuracy of results at the cost of relatively low computational burden [120].

2.4   Basic Probabilistic Theory for Uncerinties

2.4.1 Basic Definitions

The uncertainties for discrete random variables are usually described by discrete probability at each point while for continuous random variables it is described by probability density function (PDF). The following are some basic definitions of expectation, variance and covariance, etc. which are fundamental and essential to the research in Chapter VI.

1) Mathematic expectation

Suppose the discrete random variable X has a series value $x_1, x_2, \ldots, x_n$ with a probability of $p_1, p_2, \ldots, p_n$, namely $P(X = x_i) = p_i$, its mathematic expectation denoted as $E(X)$ or $\overline{X}$ is [137, 138]

$$E(X) = \overline{X} = \sum_{i=1}^{n} x_i p_i \tag{2.6}$$

If X is a continuous random variable with a PDF as $f(x)$, its mathematic expectation is [137, 138]

$$E(X) = \int_{-\infty}^{+\infty} x f(x) dx \tag{2.7}$$

2) Variance

The variance of a discrete variable X, denoted as σ^2, is [137, 138]

$$\sigma^2 = E[(X - \overline{X})^2] = \sum_{i=1}^{n} (x_i - \overline{X})^2 p_i \tag{2.8}$$

where σ is the standard derivation which measures the degree of points scattering around its mathematic expectation.

The variance of continuous variable X is [137, 138]

$$\sigma^2 = E[(X - \overline{X})^2] = \int_{-\infty}^{+\infty} (x_i - \overline{X})^2 f(x) dx \tag{2.9}$$

3) Covariance

Suppose Y is another discrete variable with the expectation $\overline{Y}$, then the covariance between X and Y, denoted as C_{XY}, is [137, 138]

$$C_{XY} = E[(X - \overline{X})(Y - \overline{Y})] \qquad (2.10)$$

4) Correlation coefficient

The correlation coefficient ρ_{XY} between X and Y is defined as the covariance C_{XY} divided by standard derivation σ_X and σ_Y, namely [137, 138]

$$\rho_{XY} = \frac{C_{XY}}{\sigma_X \sigma_Y} \qquad (2.11)$$

5) Moment

Suppose X is a discrete random variable with series value $P(X = x_i) = p_i$, its r-order moment, denoted as m_r, is [138, 139]

$$m_r = E(X^r) = \sum_{i=1}^{n} x_i^r p_i \qquad (2.12)$$

If X is a continuous random variable with the PDF as $f(x)$, its r-order moment is [138, 139]

$$m_r = E(X^r) = \int_{-\infty}^{+\infty} x^r f(x) dx \qquad (2.13)$$

For a random vector $X = [X_1, X_2, ... X_n]^T$, the r-order mixed moment of X is [138, 139]

$$m_r^{(e_1, e_2 ... e_n)} = E(\prod_{i=1}^{n} X_i^{e_i}) \qquad (2.14)$$

where $r = \sum_{i=1}^{n} e_i$.

6) Central Moment

The r-order central moment of discrete random variable X, denote as M_r is

$$M_r = E[(X - \overline{X})^r] = \sum_{i=1}^{n} (x_i - \overline{X})^r p_i \qquad (2.15)$$

If X is a continuous variable with a PDF as $f(x)$, its r-order central moment is calculated as [138, 139]

$$M_r = E[(X - \overline{X})^r] = \int_{-\infty}^{+\infty} (x - \overline{X})^r f(x) dx \qquad (2.16)$$

For a random vector $[X_1, X_2, \ldots X_n]$, the r-order mixed central moment can be expressed as [138, 139]

$$M_r^{(e_1, e_2 \ldots e_n)} = E[\prod_{i=1}^{n} (X_i - \overline{X})^{e_i}] \tag{2.17}$$

where $r = \sum_{i=1}^{n} e_i$.

There is also a compact relationship between central moment and moment as expressed in the following form.

$$M_1 = 0$$

$$M_2 = m_2 - (m_1)^2$$

$$M_3 = m_3 - 3m_1 m_2 + 2(m_1)^3$$

$$M_4 = m_4 - 4m_1 m_3 + 6 \, m()^2 m_2 - 3(m_1)^4 \tag{2.18}$$

$$M_5 = m_5 - 5m_1 m_4 + 10(m_1)^2 m_3 - 10(m_1)^3 m_2 + 4(m_1)^5$$

$$M_6 = m_6 - 6m_5 m_1 + 15(m_1)^2 m_4 - 20(m_1)^3 m_3 + 15(m_1)^4 m_2 - 5(m_1)^6$$

$$M_7 = \sum_{j=0}^{7} C_7^j m_{7-j}(-m_1)^j$$

where M_j and m_j are the jth order central moment and j^{th} order moment of X, and C_7^j is the mathematical combinatorial number.

7) Cumulant

As the moments of a random variable are the characteristics to represent its probability distribution, the cumulants are also important attributes to describe its probability distribution, which can be calculated from moments or central moments. The following gives the first seven order cumulants in the term of central moments [138, 139].

$$K_1 = m_1$$

$$K_2 = M_2$$

$$K_3 = M_3$$

$$K_4 = M_4 - 3M_2 M_2$$

$$K_5 = M_5 - 10M_3 M_2$$

$$K_6 = M_6 - 15M_4 M_2 - 10M_3 M_3 + 30(M_2)^3$$

$$K_7 = M_7 - 21M_5 M_2 - 35M_4 M_3 + 210M_3 M_2 M_2$$

(2.19)

where K_r is the r-order cumulant.

8) Normal distribution

If a continuous random variable X has a probability density function in the following form

$$f(x) = \frac{1}{\sigma\sqrt{2\pi}} e^{-(x-\overline{X})^2/2\sigma^2}$$

(2.20)

X is a normal distribution with an expectation of $\overline{X}$ and variance σ^2, and recorded as $N(\overline{X}, \sigma^2)$ [138, 139]. The expectation $\overline{X}$ determines the displacement of density curve and variance σ^2 determines the shape of density curve. The cumulative distribution function (CDF) is

$$P(X \leq x) = \frac{1}{\sigma\sqrt{2\pi}} \int_{-\infty}^{x} e^{-(u-\overline{X})^2/2\sigma^2} du$$

(2.21)

If $\overline{X} = 0$ and $\sigma = 1$, the normal distribution is specially called standard normal distribution, denoted as $N(0,1)$. In addition, any normal distribution can be standardized by

$$\tilde{X} = \frac{X - \overline{X}}{\sigma}$$

(2.22)

where $\tilde{X}$ obeys $N(0,1)$ with a PDF as

$$f(\tilde{x}) = \frac{1}{\sqrt{2\pi}} e^{-\tilde{x}^2/2}$$

(2.23)

and its CDF is

$$P(\tilde{X} \leq \tilde{x}) = \frac{1}{\sqrt{2\pi}} \int_{-\infty}^{\tilde{x}} e^{-u^2/2} du$$

(2.24)

2.4.2 Gram-Charlier Expansion for Probability Estimation

The PDF of a random variable can be calculated from its moments or cumulants by the Cornish-Fisher expansion, Edgeworth expansion or Gram-Charlier expansion [137, 140]. In this thesis, the Gram-Charlier expansion is adopted for PDF estimation in Chapter VI, and the following is the related theory.

If X is standardized by $\tilde{X} = \dfrac{X - \overline{X}}{\sigma}$ and its r-order normalized cumulant is denoted as g_r, g_r can be calculated as

$$g_r = \frac{K_r}{\sigma^r} \tag{2.25}$$

where K_r is the r-order cumulant of X and σ is the standard derivation of X.

According to the Gram-Charlier expansion, the CDF of X can be estimated by normalized cumulants as [140, 141]

$$P(X \le x) = \int_{-\infty}^{\tilde{x}} N(u)d\tilde{u} + N(\tilde{x})[\frac{g_3}{3!}H_2(\tilde{x}) + \frac{g_4}{4!}H_3(\tilde{x}) + \frac{g_5}{5!}H_4(\tilde{x})$$
$$+ \frac{g_6 + 10g_3^2}{6!}H_5(\tilde{x}) + \frac{g_7 + 35g_3g_4}{7!}H_6(\tilde{x}) + ...] \tag{2.26}$$

where $\tilde{x} = \dfrac{x - \overline{X}}{\sigma}$, $\overline{X}$ and σ are the expectation and standard deviation of X; $N(u) = \dfrac{1}{\sqrt{2\pi}}e^{-u^2/2}$ is the PDF of standard normal distribution; and $H_r(\tilde{x})$ is r-order Hermite polynomial function with the specific expression as

$$H_0(\tilde{x}) = 1$$
$$H_1(\tilde{x}) = \tilde{x}$$
$$H_2(\tilde{x}) = \tilde{x}^2 - 1$$
$$H_3(\tilde{x}) = \tilde{x}^3 - 3\tilde{x}$$
$$H_4(\tilde{x}) = \tilde{x}^4 - 6\tilde{x}^2 + 3 \tag{2.27}$$
$$H_5(\tilde{x}) = \tilde{x}^5 - 10\tilde{x}^3 + 15\tilde{x}$$
$$H_6(\tilde{x}) = \tilde{x}^6 - 15\tilde{x}^4 + 45\tilde{x}^2 - 15$$

When (2.25) and (2.27) are substituted into (2.26), the CDF of X can be expressed as the function of the first several order cumulants as [140]

$$P(X \le x) = \int_{-\infty}^{\tilde{x}} N(u)du - N(\tilde{x})[\frac{K_3}{3!\sigma^3}(\tilde{x}^2 - 1) + \frac{K_4}{4!\sigma^4}(\tilde{x}^3 - 3\tilde{x}) \\ + \frac{K_5}{5!\sigma^5}(\tilde{x}^4 - 6\tilde{x}^2 + 3) + ...]$$

(2.28)

and the PDF of X can be estimated by

$$f(x) = N(\tilde{x})[1 + \frac{K_3}{3!\sigma^3}(\tilde{x}^3 - 3\tilde{x}) + \frac{K_4}{4!\sigma^4}(\tilde{x}^4 - 6\tilde{x}^2 + 3) + \\ \frac{K_5}{5!\sigma^5}(\tilde{x}^5 - 10\tilde{x}^3 + 15\tilde{x}) + ...]$$

(2.29)

2.5 Summary

In this chapter, the fundamentals of transient stability constrained optimal power flow have been reviewed. The traditional TSCOPF model is first represented using a compact mathematical formulation, then the current state of art algorithms for solving this TSCOPF problem are reviewed and categorized into the following three solution approaches: 1) iterative generation rescheduling, 2) analytical method by discretizing the DAEs, and 3) various AIs. In addition, methodologies to handle the TSCOPF problem with uncertainties are comprehensively reviewed. Last but not least, some basic definitions in the probability theory are introduced for describing random variables, and the Gram-Charlier Expansion for probability distribution estimation is briefly introduced to serve as the foundations to handle uncertainties in the P-TSCOPF model proposed in Chapter VI.

Chapter III

A Novel Energy Sensitivity Based Method for Transient Stability Constrained Optimal Power Flow

3.1   Introduction

Transient stability constrained optimal power flow (TSCOPF) is a difficult optimization problem for power system planning and operation. The key concern is how to deal with the transient stability constraint efficiently using a proper method to reduce the optimization burden. Since the number of TSCOPF constraints would rise sharply with the increasing power system scale, number of contingencies, transient stability simulation time, etc., a huge dimension complexity and expensive computation time would be resulted for solving TSCOPF problem by the discretized method. In addition, the usual transient stability constraint described by a heuristic generator angle threshold or energy based stability margin is applicable only to the normal unstable TSCOPF while the extreme unstable TSCOPF problem was often neglected. Furthermore, the issue of over-stabilization in the TSCOPF optimization procedure has not yet been fully addressed in the current state of art algorithms.

In this chapter, the TSCOPF problem is decomposed into two iterative processes as in [64, 107, 108], namely the OPF process and the stability analysis process. As compared to [64], the proposed method adopted the trajectory sensitivities technique [108] to 1) eliminate the problem of changed OMIB mode and the need for properly set of initial angle decrement's percentage λ in [64], and 2) handle the extreme unstable cases and over-stabilization. In the OPF

process, for each contingency, one linear energy constraint for unstable case or one power balance constraint for extreme unstable case derived from the transient stability analysis will be added to the conventional OPF model. In the stability analysis process, the stability margin constraint is constructed using the well-established trajectory sensitivities technique with enhancements to handle extreme unstable cases and over-stabilization. As a whole, this chapter presents a complete analytical solution method for solving all types of TSCOPF problems.

3.2 Traditional TSCOPF Model

The objective of TSCOPF could be in many different forms. For example, it could be the minimum power loss of network, the minimum fuel cost of generators, or the participants' bids in a deregulated electricity market. Here, the quadratic fuel cost functions of the generators are adopted as the OPF objective as

$$F_G = \sum_{i=1}^{n_G} a_i P_{Gi}^2 + b_i P_{Gi} + c_i \tag{3.1}$$

where a_i, b_i, c_i are the cost coefficients for active power P_{Gi}, and n_G is the number of generators.

The static constraints include the following power flow equalities.

$$\begin{cases} 0 = P_{Gi} - P_{Di} - V_i \sum_{j=1}^{n_b} V_j (G_{ij} \cos \theta_{ij} + B_{ij} \sin \theta_{ij}) \\ 0 = Q_{Gi} - Q_{Di} - V_i \sum_{j=1}^{n_b} V_j (G_{ij} \sin \theta_{ij} - B_{ij} \cos \theta_{ij}) \end{cases} \tag{3.2}$$

where $i = 1, 2, ..., n_b$; n_b is the total number of nodes; P_{Di} and Q_{Di} are the active and reactive load demand; Q_{Gi} is the generator reactive power; V_i is the voltage magnitude of node i; θ_{ij} is the angle difference between node i and j.

The pre-fault security inequalities include the following.

$$P_{Gi\min} \le P_{Gi} \le P_{Gi\max} \ (i = 1, 2, ..., n_G) \tag{3.3}$$

$$Q_{Gi\min} \le Q_{Gi} \le Q_{Gi\max} \ (i = 1, 2, ..., n_G) \tag{3.4}$$

$$V_{i\min} \leq V_i \leq V_{i\max} \, (i = 1, 2, ..., n_b) \tag{3.5}$$

$$S_{l\min} \leq S_l \leq S_{l\max} \, (i = 1, 2, ..., n_l) \tag{3.6}$$

where n_l is the number of branches; $V_{i\min}$ and $V_{i\max}$ are the lower and upper limits of node voltage magnitude, respectively; $S_{l\min}$ and $S_{l\max}$ are transmission line loading limits.

The dynamic constraints include the DAEs describing the following system dynamic behaviours and the transient stability.

$$\begin{cases} \dot{x} = f(x(t), y(t), \alpha), x(t_0) = x_0 \\ 0 = g(x(t), y(t), \alpha), y(t_0) = y_0 \end{cases} \tag{3.7}$$

where x is a vector of dynamic state variables such as generator angle and speed etc., y is a vector of algebraic variables, and α stands for the control parameters to be optimized. The DAEs (3.7) can be solved for instance by implicit trapezoidal integration in time domain simulation.

In most references, the transient stability is constrained by a heuristic angle threshold. However, for different threshold settings, the optimization results could be very different. Here, as a better alternative, the proposed method adopts a SIME-based transient stability margin constraint instead.

3.3　SIME Method

The Transient Energy Function (TEF) method, such as the BCU method, is an important tool for power system transient stability analysis. The BCU method is based on the correct controlling Unstable Equilibrium Point (UEP) obtained by two numerical integrations (one for the PEBS crossing on faulted system and the other for the reduced gradient system) and one Newton iteration for the nonlinear algebraic equations. While these extra efforts can consistently ensure the exact controlling UEP of the BCU method and offer higher accurate analysis of transient stability, the analysis will be slowed down [88, 142]. On the other hand, the SIME is a hybrid temporal-direct method with fast execution speed for multi-

machine system transient stability analysis. It uses the results from the time domain simulation of the full multi-machine system to (1) observe the system stability in a SIME frame by examining the candidate critical machines and the unstable conditions, and then (2) determine the stability margin [143]. SIME has been widely adopted as an effective method for transient stability assessment in [93, 94, 96] and TSCOPF problem in [42, 52, 64, 66, 108]. Based on the SIME theory, if the system is separated into two groups of Critical Machines (CMs) and Non-critical Machines (NMs) by the decomposition pattern method [42, 94], the original system can be mapped to the SIME model as

$$
\begin{cases}
M_E \dfrac{d\omega_E}{dt} = P_a = P_{mE} - P_{eE} \\
\dfrac{d\delta_E}{dt} = \omega_E
\end{cases}
\tag{3.8}
$$

where $M_E = M_C M_N / (M_C + M_N)$ is the equivalent inertial coefficient in OMIB with subscripts 'C' and 'N' stood for CMs and NMs and the inertia coefficients defined as $M_C = \sum_{k \in C} M_k$ and $M_N = \sum_{j \in N} M_j$; $\delta_E = \delta_C - \delta_N = M_C^{-1} \sum_{k \in C} M_k \delta_k - M_N^{-1} \sum_{j \in N} M_j \delta_j$ and $\omega_E = \omega_C - \omega_N = M_C^{-1} \sum_{k \in C} M_k \omega_k - M_N^{-1} \sum_{j \in N} M_j \omega_j$ are the OMIB angle and speed. The equivalent mechanical power and electric power are $P_{mE} = M_E (M_C^{-1} \sum_{k \in C} P_{mk} - M_N^{-1} \sum_{j \in N} P_{mj})$ and $P_{eE} = M_E (M_C^{-1} \sum_{k \in C} P_{ek} - M_N^{-1} \sum_{j \in N} P_{ej})$, respectively.

Based on the SIME theory, the system stability could be assessed via the accelerating area A_{acc} and the decelerating area A_{dec} as

$$
\eta = A_{dec} - A_{acc}
\tag{3.9}
$$

For normal unstable case, η can be derived from the residual dynamic energy at the exit point when the potential energy is totally offset by the dynamic energy. At this exit point, the characteristic of electric and mechanical power satisfies

$$
\begin{cases}
P_a(t_u) = P_{mE}(t_u) - P_{eE}(t_u) = 0 \\
\dot{P}_a(t_u) = \dfrac{dP_a}{dt} > 0
\end{cases}
\tag{3.10}
$$

and the stability margin is

$$\eta_u = -\frac{1}{2}M_E(\omega_E(t_u))^2 \tag{3.11}$$

For stable case, before the system approaches the exit point, the system stops its excursion at δ_r and returns for the reverse swing. For this stable condition, the characteristics of system are

$$\begin{cases} \omega(t_r) = 0 \\ P_a(t_r) < 0 \end{cases} \tag{3.12}$$

and the stability margin is

$$\eta_s = -\int_{\delta_r}^{\delta_u} P_a d\delta \approx |P_{ar}|(\delta_u - \delta_r)/2 \tag{3.13}$$

where δ_u is the angle at time t_u when the generator active power crosses mechanical power by the second kick method [96], δ_r are the return angle at time t_r, and P_{ar} is the active power at δ_r.

It shall be noted that condition (3.10) alone is not sufficient to cover all the unstable cases. For extreme unstable case, the mechanical power P_{mE} would remain larger than the electric power P_{eE} even after the fault was cleared. The generator speed will therefore continue to increase, and as a result, the generator angle will rapidly increase and the system loses stability quickly. Since there is no intersection point between P_{mE} and P_{eE}, condition (3.10) cannot be satisfied, and the accelerating power distance [94], which is the minimum distance between P_{mE} and P_{eE}, is adopted and redefined as the stability margin for the extreme unstable cases as (3-14).

$$\eta_u = -P_{a\min} = -\min \{P_{mE}(t) - P_{eE}(t), t > t_c, P_a(t) > 0\} \tag{3.14}$$

where t_c is the fault clearing time. It is also worth to mention that the stability margins defined in (3.11) and (3.14) are not directly comparable as the former is the kinetic energy of a normal unstable system whereas the later is the accelerating power distance of an extreme unstable system. In Section 3.4, the sensitivities of these margins will be derived and used to pull the system from extreme unstable to normal unstable and then finally economic stable.

3.4   Proposed Approach for TSCOPF

3.4.1   Proposed Stability Constraint for TSCOPF

So far the transient stability constraints proposed in [64, 108] are not applicable to extreme unstable TSCOPF. As mentioned above, for extreme unstable cases, there is no intersection between the mechanical and electrical powers and a redefined power criterion (3.14) is therefore used to measure the stability margin and its sensitivities can be used to effectively improve the system instability. Also, in order to reduce the computation burden, transient stability simulation could be stopped once the system is detected as unstable when the generator angle in Centre Of Inertia (COI) frame is greater than, say, 2π.

For an extreme unstable case with the redefined stability margin (3.14), the stability constraint can be formulated as (3.15) to drive the system from extreme unstable to normal unstable.

$$P_{a\min}^k + \frac{dP_{a\min}^k}{dP_{mi}^k}\Delta P_{mi} < 0 \tag{3.15}$$

where $dP_{a\min}^k / dP_{mi}^k$ is a function of the sensitivities of the generator angle when the power unbalance is minimum $P_{a\min}$. From (3.14), instability under extreme unstable conditions is measured by the accelerating power distance, and the constraint (3.15) would improve the stability by reducing the minimum distance between the mechanical and electrical power. When there is an intersection, the system effectively reaches the range of normal unstable (as shown in Fig. 3.2 in Section 3.5).

Once the system has pulled back to a normal unstable operation point, the stability margin η as defined in (3.11) with condition (3.10) can be computed using the SIME method and its sensitivity can be expressed as follows [108]:

$$\frac{d\eta_u}{dP_{mi}} = -\frac{dE_{equ}}{dP_{mi}} = -M_E\omega_E(t_u)\frac{d\omega_E(t_u)}{dP_{mi}} \tag{3.16}$$

where t_u is the unstable time defined by condition (3.10). The stability constraint

for the $k+1^{\text{th}}$ iteration can then be described as (3.17) based on the kth iteration results for normal unstable case.

$$\eta_u^{k+1} = \eta_u^k + \sum_{i=1}^{n} \frac{d\eta_u^k}{dP_{mi}} \Delta P_{mi} = \eta_u^k - M_E^k \sum_{i=1}^{n} [\omega_E^k(t_u) \frac{d\omega_E^k(t_u)}{dP_{mi}^k}] \Delta P_{mi} > 0 \qquad (3.17)$$

where k is the iteration number and $d\omega_E^k / dP_{mi}^k$ is the sensitivities of speed to generator power in SIME for the kth iteration.

In case the stabilized system is over-stabilized, say with a stability margin over a pre-defined stability margin tolerance η_t, the following strategy is applied to gradually drive the system from unstable to stable without the system being over-stabilized via a series of continuous unstable operating points. The process is as follows: if the system is unstable in the kth iteration but over-stabilized in the $k+1^{\text{th}}$ iteration, the stability constraint (3.17) is refined as constraint (3.18).

$$\eta_u^{k+1} = \lambda_j \eta_u^k + \sum_{i=1}^{n} \frac{d\eta_u^k}{dP_{mi}} \Delta P_{mi} > 0 \qquad (3.18)$$

where $\lambda_j = 0.5\lambda_{j-1}$ with $\lambda_0 = 1$ and j is the number of times that the system was over-stabilized based on the same solution of kth iteration. By gradually reducing the stability margin η_u^k by a factor of λ_j, the unstable operating point will gradually move across the stability boundary without the system being over-stabilized. Compared with [64], the handling of over-stabilization is only applied in the final stage by reducing the compensated stability margin $\lambda_j \eta_u^k$ so as to reduce the generation perturbation in the last one or two iterations, instead of re-starting the whole TSCOPF process from the beginning as in [64]. Nevertheless, whether a system is over-stabilized or not is a relative concept depending on the stability margin tolerance η_t which could be set differently to meet the requirements of different systems. Here, the same tolerance (0.1 pu-rad) as in [64] is used to determine whether a system is over-stabilized or not, i.e. a system with stability margin higher than 0.1 pu-rad is considered as over-stabilized.

3.4.2 Trajectory Sensitivities Calculation

According to $\omega_E = M_C^{-1} \sum_{k \in C} M_k \omega_k - M_N^{-1} \sum_{j \in N} M_j \omega_j$ in SIME, the sensitivities $d\omega_E / dP_{mi}$ in (3.17) are obviously a function of $d\omega / dP_{mi}$ while dP_a / dP_{mi} in (3.15) can be calculated from $d\delta / dP_{mi}$ based on $P_a = P_{mE} - P_{eE}$ which is a function of generator angles. Therefore, their sensitivities depends on $dx / dP_{mi} = [d\delta / dP_{mi}, d\omega / dP_{mi}]$ which can be calculated by trajectory sensitivities strategy as follows.

For power system dynamics described by DAEs (3.7), the trajectory sensitivities with respect to control parameters α are obtained by deriving (3.7) by α at both sides [100, 144, 145].

$$\dot{x}_\alpha = f_x(x, y, \alpha)x_\alpha + f_y(x, y, \alpha)y_\alpha + f_\alpha(x, y, \alpha), x_\alpha(t_0) = \frac{dx_0}{d\alpha} \tag{3.19}$$

$$0 = g_x(x, y, \alpha)x_\alpha + g_y(x, y, \alpha)y_\alpha + g_\alpha(x, y, \alpha) \tag{3.20}$$

where $f_x(x, y, \alpha) = \partial f(x, y, \alpha) / \partial x$, $f_y(x, y, \alpha) = \partial f(x, y, \alpha) / \partial y$ and $f_\alpha(x, y, \alpha) = \partial f(x, y, \alpha) / \partial \alpha$ for differential equation (3.19); $g_x(x, y, \alpha) = \partial g(x, y, \alpha) / \partial x$, $g_y(x, y, \alpha) = \partial g(x, y, \alpha) / \partial y$ and $g_\alpha(x, y, \alpha) = \partial g(x, y, \alpha) / \partial \alpha$ for algebraic equation (3.20).

Equations (3.19) and (3.20) describe the trajectory sensitivities of the DAEs (3.7). If further denoting $x^k = x(t_k)$, $y^k = y(t_k)$, $x_\alpha^k = x_\alpha(t_k)$ and $y_\alpha^k = y_\alpha(t_k)$, and assuming x^k and y^k are readily available from the results of implicit trapezoidal integration of DAEs (3.7) in time domain simulation, the trajectory sensitivities x_α^k and y_α^k can be derived from (3.19) and (3.20) by the implicit trapezoidal rule as

$$\begin{bmatrix} I - \dfrac{\Delta t}{2} f_x(x^k, y^k, \alpha) & -\dfrac{\Delta t}{2} f_y(x^k, y^k, \alpha) \\ g_x(x^k, y^k, \alpha) & g_y(x^k, y^k, \alpha) \end{bmatrix} \begin{bmatrix} x_\alpha^k \\ y_\alpha^k \end{bmatrix} = \begin{bmatrix} A^{k-1} + \dfrac{\Delta t}{2} f_\alpha(x^k, y^k, \alpha) \\ -g_\alpha(x^k, y^k, \alpha) \end{bmatrix} \tag{3.21}$$

where Δt is the integration step, I is the identity matrix and A^{k-1} contains values from previous step in a form of

$$A^{k-1} = x_\alpha^{k-1} + \frac{\Delta t}{2}[f_x(x^{k-1}, y^{k-1}, \alpha)x_\alpha^{k-1} + f_y(x^{k-1}, y^{k-1}, \alpha)y_\alpha^{k-1} + f_\alpha(x^{k-1}, y^{k-1}, \alpha)]$$

(3.22)

Since the coefficient matrix on the left hand side of (3.21) can be obtained as a by-product at each integration step in the calculation of x^k and y^k using the implicit trapezoidal integration algorithm in time domain simulation, the calculation burden of trajectory sensitivities x_α^k and y_α^k at each integration step would be about the same as one extra Newton iteration at each time step of the numerical integration, and would therefore not add a heavy calculation burden to the time domain simulation for x^k and y^k [100, 145, 146]. When a discontinuity occurs, say transiting from during-fault to post-fault conditions, the trajectory sensitivities would undergo a jump and a re-initialization would be needed as reported in [45, 146, 147] and is adopted here to handle any discontinuity or network switching.

3.4.3 Procedures for the Proposed Approach

The following summarizes the steps of the proposed energy sensitivity based TSCOPF method.

Step 1: Run a standard OPF to find the initial optimal point without any transient stability constraints and record as OP^i where i is the iteration number. If all contingencies are stable, go to *Step 6*.

Step 2: For each contingency k, run the transient stability simulation with initial operating point OP^i. Stop the simulation if the simulation period is reached or there is any rotor angle exceeded the predefined threshold, say 2π, in the COI frame.

Step 3: For each stable case, stability margin (3.13) is checked against the stability margin tolerance for over-stabilized case. Stability constraint will be relaxed using (3.18) for any over-stabilized case.

Step 4: For each early terminated case, construct and update the stability constraint by (3.15) or (3.17) for contingency k using the trajectory sensitivity technique. In particular, for unstable case with condition (3.10) satisfied, identify t_u^k for the formulation of energy stability constraint by (3.17), otherwise update the constraint with minimum accelerating power distance using (3.15) for the extreme unstable case.

Step 5: Unless all contingencies are stable with at least one contingency being non-over-stabilized or the maximum number of iteration is reached, re-run the OPF with constraint (3.1)-(3.6) and update stability constraint (3.15), (3.17) or (3.18) depending on the stability status to find a new OP^{i+1}, and then go back to *Step 2*.

Step 6: Terminate the TSCOPF optimization and output the solution OP^i, number of iteration i, etc.

The above iterative process would first start with the OPF solution without any transient stability constraints as the base case. If convergence cannot be reached after a predefined number of iterations, say 10, a random perturbation using a normal distribution within a 20% range would be applied to modify the initial conditions of the next iteration so as to overcome the convexity problem and allow the process to converge via a different path [42]. So far in the case studies, the use of the base case solution as the start point is sufficient for the iteration process to converge within 5 iterations. Furthermore, restriction on the maximum generation perturbation size in step 5 as adopted in [100] is not generally needed as suggested from the case studies. For rare cases which do have problems on this would be caught as cases with convergence problem and handled as outlined above. If all else fails, restriction on the maximum generation perturbation size could be applied as a last resort at the expense of convergence speed and solution time.

3.4.4 Remarks

The entire TSCOPF objective and constraints are concisely formulated as (3.1)-(3.7), (3.15), (3.17) or (3.18), and solved iteratively using the following two processes: (1) regular OPF with an additional SIME stability constraint for each contingency, and (2) transient stability simulation with stability margin sensitivities calculation. Those two processes will run in turn and continue until the system is stabilized. The following are the main features of this TSCOPF solution approach.

1) Based on the redefined power balance stability margin, the extreme unstable TSCOPF, which is not considered in [64] or [108], can be effectively solved by an iterative process, namely OPF and concise formulation of stability constraint, while existing well-tested OPF and transient stability simulation program can be used with little customization.

2) Only one additional energy or power constraint will be added for each contingency in normal unstable or extreme unstable case, respectively, instead of $n_G \times T/t_{step}$ angle constraints as in discretization method. This constraint eliminates the need for complex Hessen matrix calculation and bestows the proposed approach with a good scalability for large power systems.

3) The issue of over-stabilization is properly handled by guiding the solution gradually across the stability boundary.

4) The proposed framework is the first complete solution capable to deal with multi-swing unstable, normal unstable and extreme unstable case with multi-contingency as well as issue of over-stabilization in TSCOPF problems.

3.5   Numerical Examples

The effectiveness of the proposed TSCOPF approach has been extensively

validated using the New England 10-generator 39-bus system and the IEEE 50-generator 145-bus system. Each contingency will be simulated for 5s with 10ms time step. While MATPOWER 4.1 [148] was adopted as the OPF engine, both the transient stability program and the stability margin sensitivity calculation were developed in-house running under MATLAB R2010b on a PC with a 3.0 GHz Intel CPU and 4GB RAM.

3.5.1 New England 10-Generator 39-Bus System

Firstly, the widely used New England 10-machine 39-bus system is adopted as the benchmarking system for validating the proposed TSCOPF formulation and solution. While the full network and dynamic data of this system is collected from [149], generation cost coefficients and ratings are obtained from [42, 45]. Three scenarios, including two single-contingencies and one multi-contingency, are tested on this system. Here, a multi-contingency in a TSCOPF problem is defined as a set of separate single contingencies considered for transient stability analysis to have a common stable solution for each of the individual contingency.

1) Contingency A

Contingency A (CTG A) is the case D in [42] which is a single contingency: a three-phase-to-ground fault occurs at the end of line 21-22 near bus 21 and is cleared after 0.16s by tripping line 21-22.

As shown in Table 3.1, the initial OPF solution without any transient stability constraint is first obtained by the IPM method as the starting point in which the system is unstable but with the lowest Fuel Cost (FC) of 60918.79 $/h and G10 as the least advanced generator as shown in Fig. 3.1(a). The system is then gradually alleviated as shown in Fig. 3.1 (b) and (c) which indicate that the system has become multiple-swing unstable for the solutions of TSC-1 and TSC-2 in Table 3.1. After three iterations, the system is stabilized as shown in TSC-3 in Table 3.1 and Fig. 3.1(d) with FC of 60937.93 $/h, which is close to but not as

good as the cost 60937.85 $/h obtained in [42]. The corresponding stability margin is 0.032 pu-rad which can be further improved with constraint (3.18) if it is considered as over-stabilized; otherwise, the optimization can be stopped. In the 4th iteration, 50% of the stability margin plus the sensitivities of TSC-2 is used to produce a continuous unstable operating point TSC-4, and then a better solution is obtained in TSC-5 with lower FC of 60937.33 $/h and smaller stability margin of 0.0181 pu-rad as shown in Table 3.1 and Fig. 3.1(f). Thus, this scenario has illustrated the process of proposed approach to improve the solutions of a multi-swing unstable with over-stabilized TSCOPF problem.

Table 3.1 TSCOPF solutions for contingency A of New England system

Gen	Base OPF	Proposed method for CTG A					[42]
		TSC-1	TSC-2	TSC-3	TSC-4	TSC-5	
G1(MW)	242.39	245.57	247.25	247.78	247.6	247.63	245.94
G2(MW)	566.94	573.22	573.27	572.52	572.33	572.74	572.56
G3(MW)	642.73	647.65	649.02	649.08	648.86	649.03	648.11
G4(MW)	629.5	629.34	628.4	627.05	627.13	627.22	627.56
G5(MW)	507.9	507.14	506.35	505.03	505.13	505.27	505.91
G6(MW)	650.38	631.73	625.55	624.5	625.39	624.74	628.12
G7(MW)	557.99	541.17	535.38	534.5	535.3	534.73	539.01
G8(MW)	534.76	539.15	541.1	541.66	541.43	541.5	539.94
G9(MW)	829.38	833	833.97	834.25	834.09	834.47	833.38
G10(MW)	977.57	990.98	998.45	1002.24	1001.4	1001.31	998.56
Margin (pu-rad)	-0.9832	-1.6091	-0.3781	0.032	-0.1785	0.0181	--
Iterations	--	3			5		37
Cost ($/h)	60918.79	60927.79	60935.49	60937.93	60936.64	60937.33	60937.85
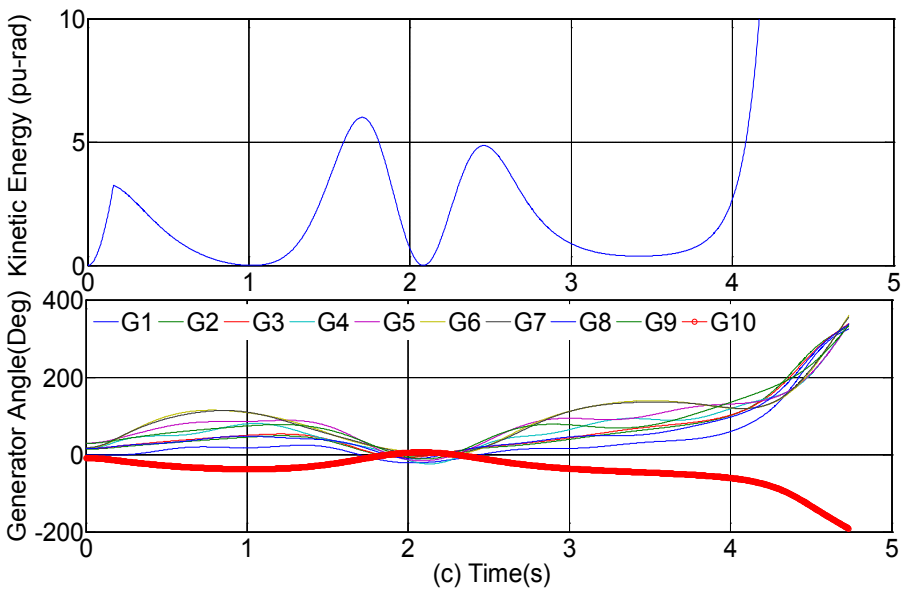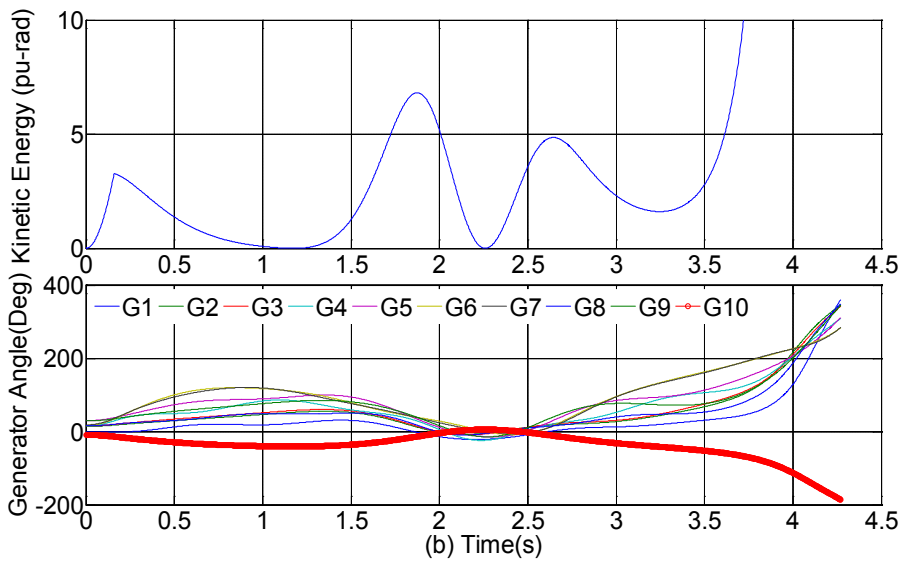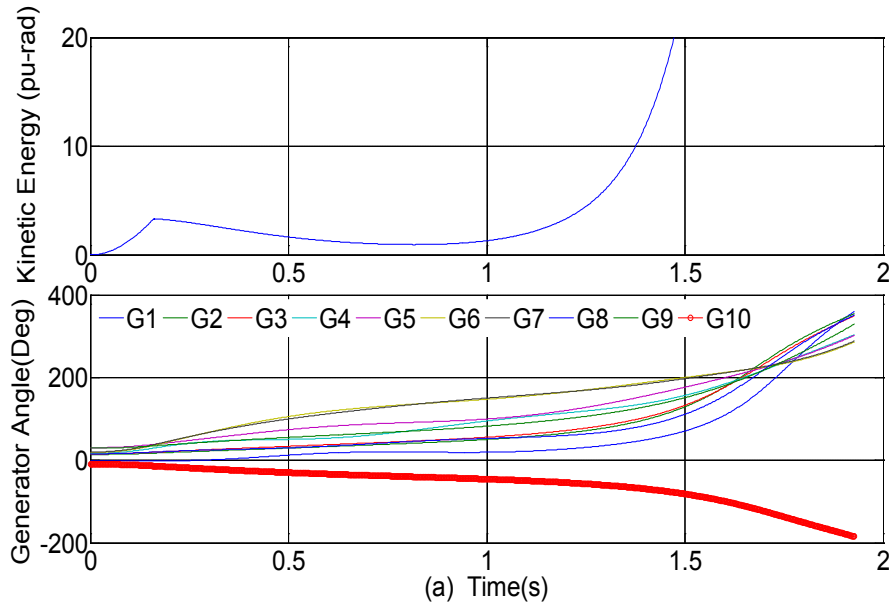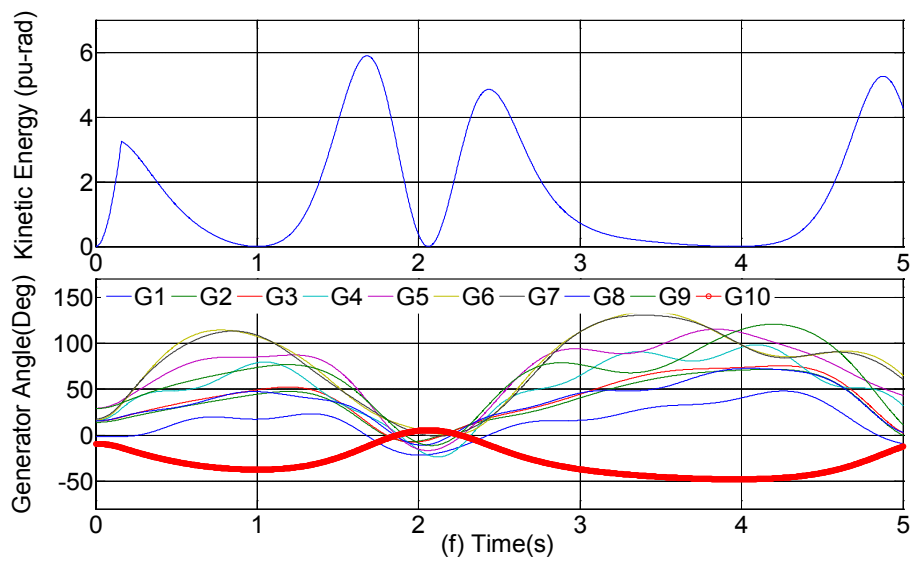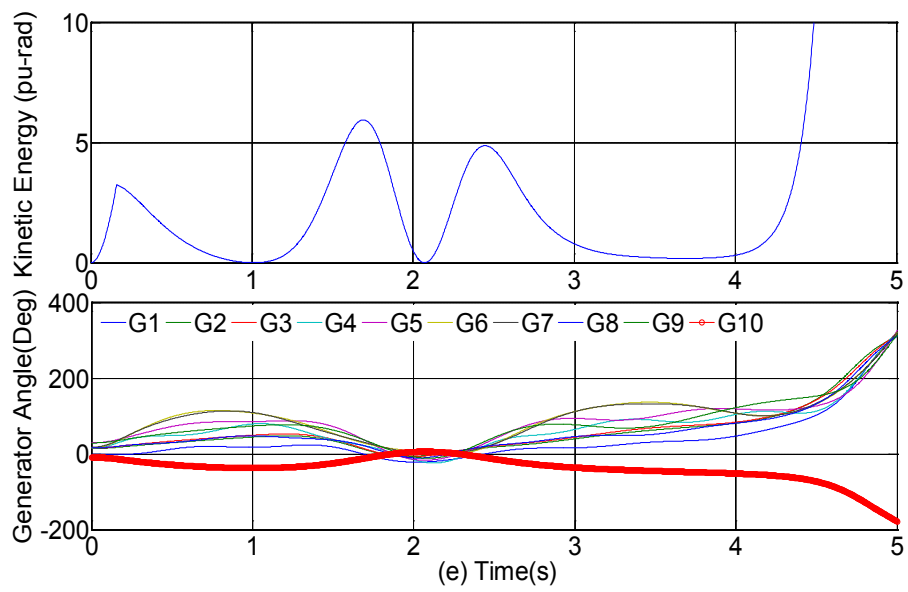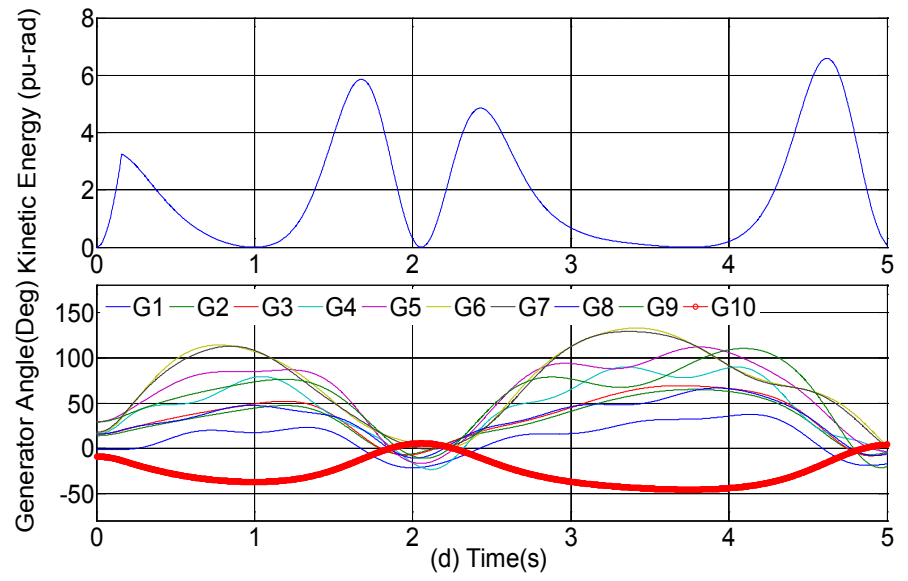
Fig. 3.1 TSCOPF process for contingency A of New England system

2) Contingency B

Contingency B (CTG B) is an extreme unstable single contingency with a three-phase-to-ground fault occurred at the end of line 28-29 near bus 29 and cleared after 0.35s by tripping line 28–29.

Table 3.2 TSCOPF solutions for contingency B of New England system

Gen	Base OPF	Proposed method for CTG B				
		TSC-1	TSC-2	TSC-3	TSC-4	TSC-5
G1(MW)	242.39	249.66	255.66	265.72	260.76	264.47
G2(MW)	566.94	581.67	593.9	623.76	611.73	622.48
G3(MW)	642.73	656.64	668.09	686.13	676.92	683.73
G4(MW)	629.5	646.87	661.27	681.2	670.26	678.39
G5(MW)	507.9	519.72	529.42	542.77	535.39	540.84
G6(MW)	650.38	667.38	681.46	700.8	690.14	698.09
G7(MW)	557.99	574.06	587.41	606.15	595.97	603.61
G8(MW)	534.76	551.08	564.74	586	575.03	582.68
G9(MW)	829.38	692.06	580.25	403.17	491.82	425.72
G10(MW)	977.57	996.85	1012.42	1039.38	1026.28	1034.8
Margin (pu-rad)	(-6.617)[*]	(-1.501)[*]	-8.1647	0.8837	-3.6834	0.036
Iterations	--	5				
Cost ($/h)	60918.79	61089.49	61482.00	62575.78	61955.89	62405.08

Note:( )[*] is the margin defined by (3.14) for extreme unstable with unit as per unit (pu).

First, OPF results without any transient stability constraint are used as the starting point with FC of 60918.79 $/h. The system is extreme unstable with G9 as CMs and all other machines as NMs. There is no intersection between the SIME mechanical and electric power, and the minus of the minimum accelerating power distance, i.e. -6.617 pu, is used as the stability margin according to (3.14) as shown in Fig. 3.2(a). Constraint (3.15) is then used to obtain an alleviated unstable solution TSC-1 as shown in Table 3.2 and Fig. 3.2(b), where the system is still extreme unstable but with a smaller minimum accelerating power distance, i.e. smaller power unbalance. The system then evolves to normal unstable with

FC increased to 61482.00 $/h and results shown as TSC-2 in Table 3.2 and Fig. 3.2(c). After three iterations, this system is stabilized with FC of 62575.78 $/h and stability margin of 0.8837 pu-rad which is considered as over-stabilized if the tolerance is set to 0.1 pu-rad as adopted in [64]. Using the sensitivities of TSC-2 and relaxed constraint (3.18) with $\lambda_1 = 0.5$, a further alleviated unstable solution is obtained as TSC-4 in Table 3.2 and Fig. 3.2(e). Finally, the system is stabilized as TSC-5 with the best FC of 62405.08 $/h and non-over-stabilized stability margin 0.036 pu-rad as shown in Table 3.2 and Fig. 3.2(f).

(a) Time(s)

(b)Time(s)

(c) Time(s)

(d) Time(s)

(e)Time(s)

46
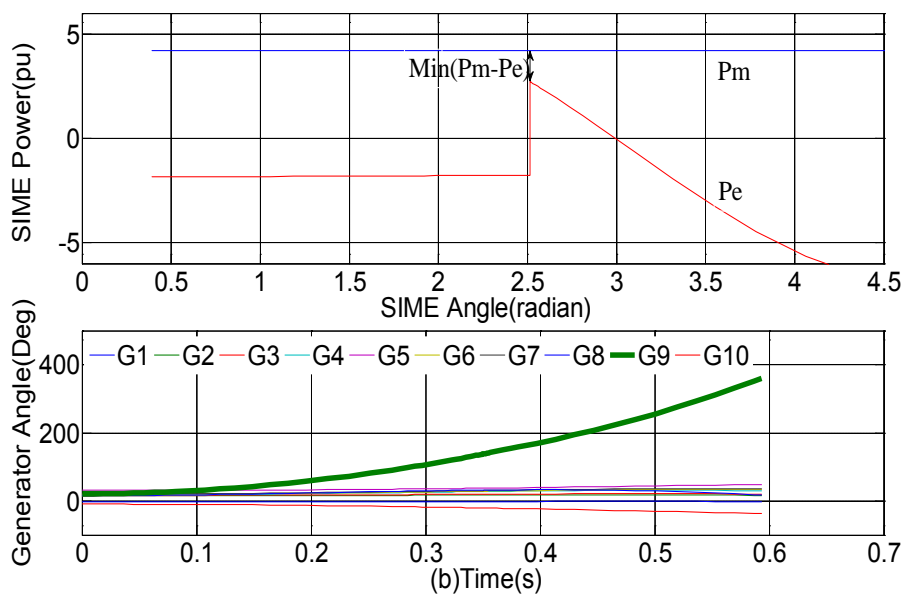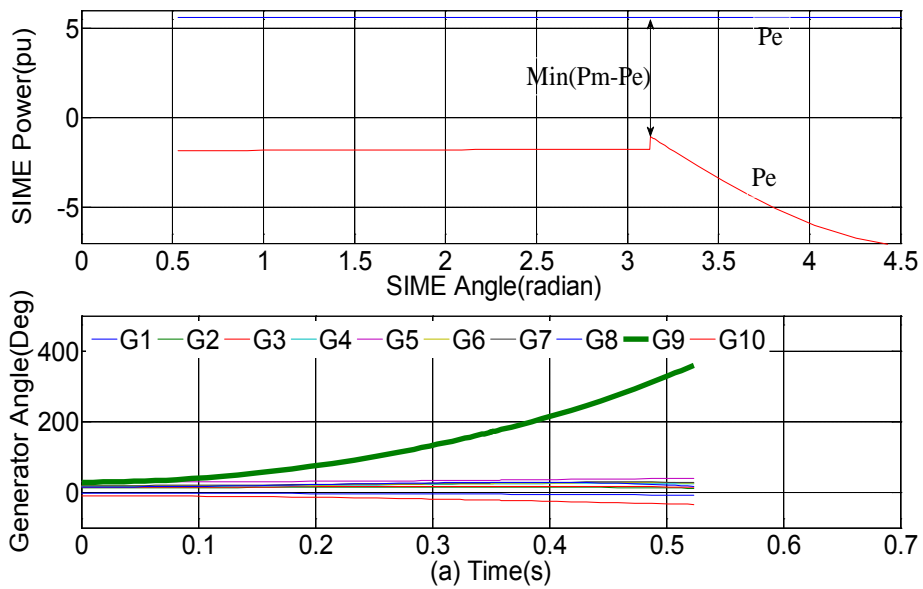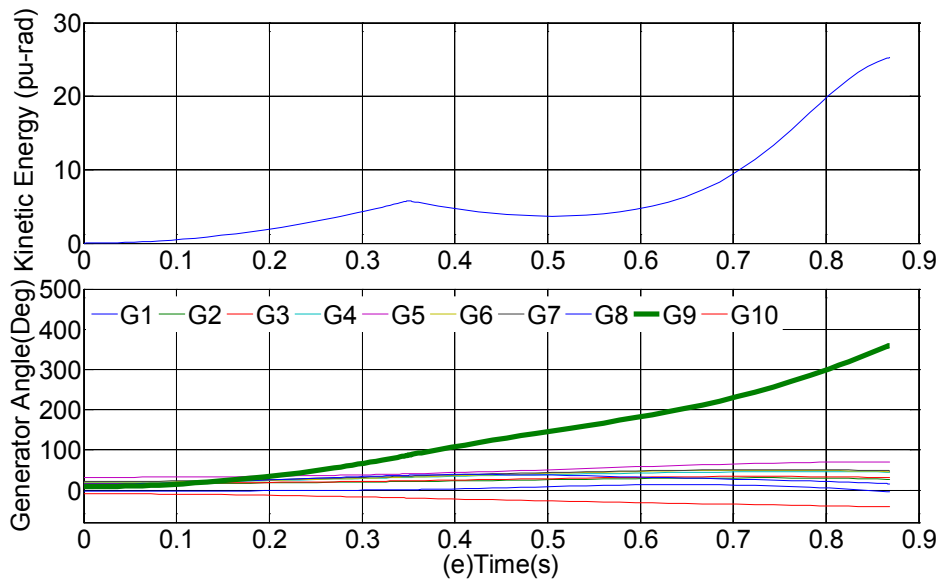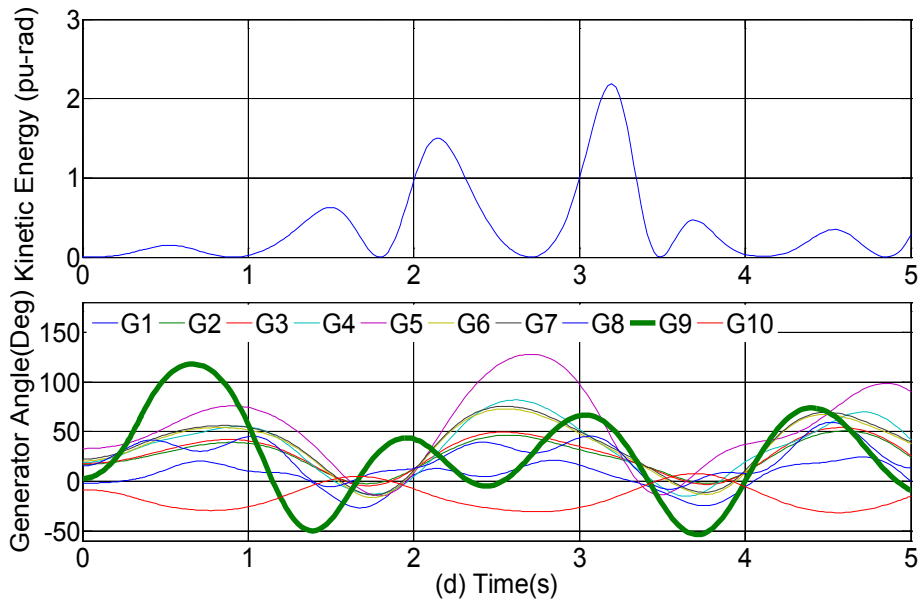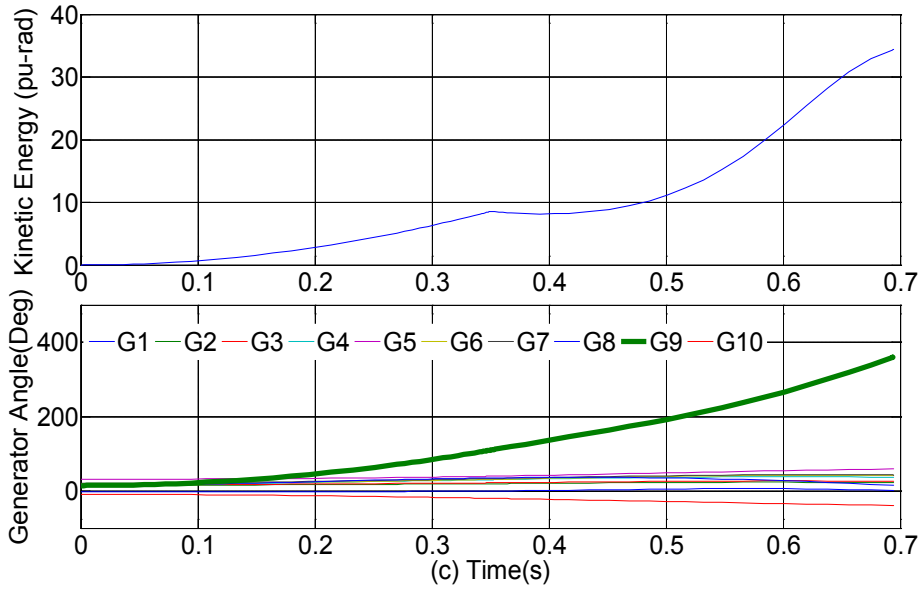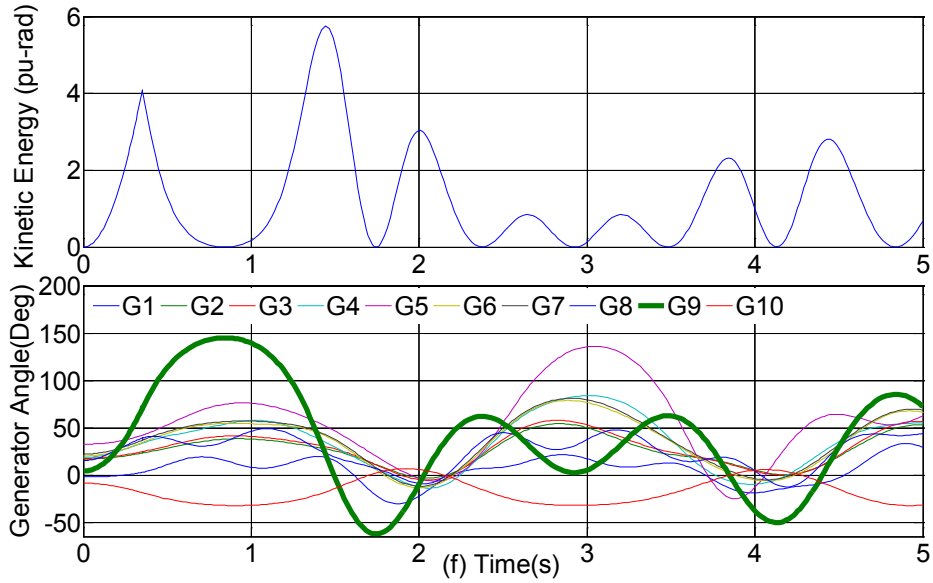
Fig. 3.2 TSCOPF process for contingency B of New England system

3) Multi-contingency A+B

The third scenario is a multi-contingency consisting of contingency A and B (CTG A+B) presented in above for evaluating the capability of the proposed method in handling multiple contingencies simultaneously. The main feature of this multi-contingency is that contingency A and B do possess different SIME modes, namely contingency A is normal unstable with G10 as NMs and others as CMs versus contingency B is extreme unstable with G9 as CMs and others as NMs.

One stability constraint per contingency is constructed, using (3.17) or (3.15) respectively for contingency A and B, and added to the OPF model at each iteration for searching a common stable operating point for the two contingencies. After 3 iterations, the system is over-stabilized for contingency B with FC 62751.74 $/h and stability margin of 0.2494 pu-rad as shown in TSC-3 in Table 3.3 while contingency A is still unstable. Therefore the stability constraint for contingency B is relaxed according to (3.18) with $\lambda_1 = 0.5$ and sensitivities of TSC-2 while the one for contingency A is updated by (3.17) using TSC-3 results. The system is finally stabilized after 4 iterations with FC of 62756.8 $/h, which is as expected to be slightly more expensive than the ones for contingency A or B

alone, and with stability margin of 0.0667 pu-rad and 0.2419 pu-rad for contingency A and B, respectively. The corresponding generator angles for this multi-contingency are plotted in Fig. 3.3.

Table 3.3 TSCOPF solutions for Contingency A+B of New England system

Gen	Base OPF	Proposed method for CTG A+B			
		TSC-1	TSC-2	TSC-3	TSC-4
G1(MW)	242.39	255.38	265.68	282.04	282.94
G2(MW)	566.94	592.88	611.46	645	644.63
G3(MW)	642.73	665.59	682.82	706.63	706.37
G4(MW)	629.5	647.36	661.17	675.64	674.39
G5(MW)	507.9	518.92	528.16	533.47	531.9
G6(MW)	650.38	637.02	632.6	631.63	631.04
G7(MW)	557.99	546.73	542.92	543.37	542.96
G8(MW)	534.76	559.35	579.09	608.77	610.58
G9(MW)	829.38	691.09	578.79	398.5	398.44
G10(MW)	977.57	1020.49	1050.13	1107.31	1109.05
Margin A (pu-rad)	-0.9832	-2.1355	-0.7341	-0.1857	0.0667
Margin B (pu-rad)	(-6.617)*	(-1.489)*	-8.13	0.2494	0.2419
Iterations	--	4			
Cost ($/h)	60918.79	61114.37	61546.52	62751.74	62756.8

Note:( )* is the margin defined by (3.14) for extreme unstable with unit as per unit (pu).

(a) Time(s)
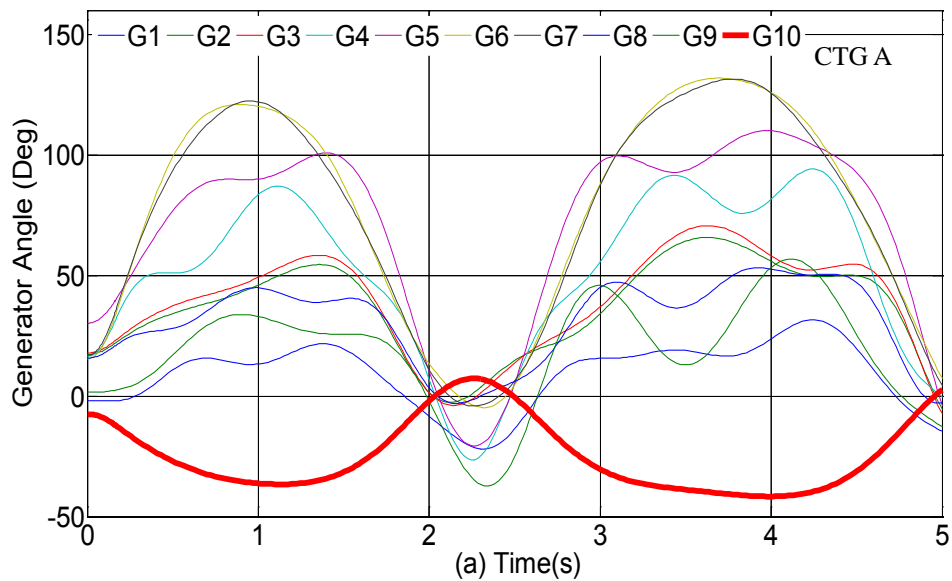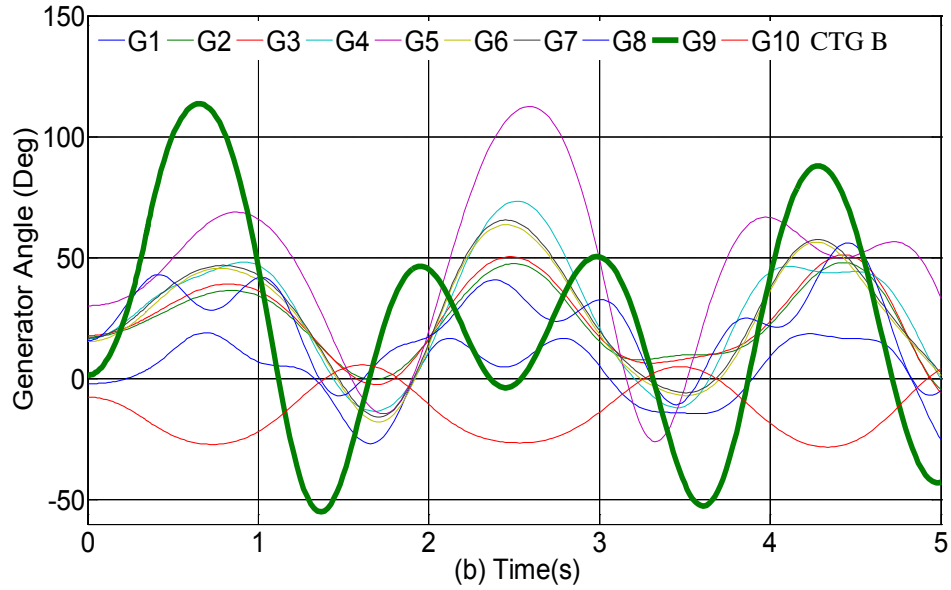
Fig. 3.3 Rotor angles for multi-contingency A+B of New England system

3.5.2 IEEE 50-Generator 145-Bus System

The proposed TSCOPF has been further evaluated with the larger IEEE 50-generator 145-bus system [150] using the following three contingencies with bus voltages limited to $0.9 < V_i < 1.15$.

Contingency A: three-phase earth fault at the end of line 60-59 near bus 60 at t=0ms, and cleared by tripping line 60-59 at tcl=200ms;

Contingency B: three-phase earth fault at the end of line 89-103 near bus 89 at t=0ms and cleared by tripping line 89-103 at tcl=420ms;

Contingency C: three-phase earth fault at the end of line 108-73 near bus 108 at t=0ms and cleared by tripping line 108-73 at tcl=260ms.

Table 3.4 shows the solutions obtained with the proposed TSCOPF method for single contingency A, B or C, and multi-contingency A+B+C (CTG A+B+C), and compared with the base case solution without any transient stability constraints. For contingency A, B or C, the increase in FC for stabilizing the system is little, ranged from 0.0031% to 0.0192%. For multi-contingency A+B+C, the FC is further increased to 51,449,579.07 $/h, i.e. increased by 0.0323% compared to the base case, in order to simultaneously stabilize all the

contingency A, B and C as shown in Fig. 3.4. It is noted that this is a strong and stable system with maximum rotor swing close to 200° as shown in Fig. 3.4(a) for contingency A. However, this contingency would be considered as unstable if a heuristic angle threshold criteria was used instead with a limit of 100° or 2/3 π as suggested in [104, 106]. Also, the convergence rate of the proposed method for this 50-generator system has not been deteriorated with the increase in number of contingencies, and some of the generators have reached their generation limit. However, since the OPF optimization would drive the system along different directions under different contingencies, and as a result, different generators would reach their generation limits for different single contingency A, B, C and multi-contingency A+B+C.

Table 3.4 TSCOPF solutions for IEEE 50-generator system

Gen No.	Base OPF (MW)	CTG A (MW)	CTG B (MW)	CTG C (MW)	CTG A+B+C (MW)
G1	71.40	61.06	71.40	71.40	62.96
G2	1480.80	1501.33	1485.91	1485.11	1509.91
G3	201.68	226.03	219.71	202.47	244.10
G4	0.00	0.00	0.00	0.00	0.00
G5	98.00	98.00	98.00	98.00	98.00
G6	360.14	357.99	217.00	361.20	215.72
G7	30.80	28.23	30.80	30.80	29.86
G8	89.60	89.60	89.60	89.60	89.60
G9	980.00	980.00	980.00	980.00	980.00
G10	210.15	216.68	211.13	210.17	219.48
G11	183.40	138.58	183.40	183.40	137.96
G12	84.00	84.00	84.00	84.00	84.00
G13	196.00	196.00	196.00	196.00	196.00
G14	466.74	448.43	480.31	470.06	474.93
G15	280.00	280.00	280.00	280.00	280.00
G16	172.21	169.50	185.38	172.70	185.16
G17	434.00	434.00	434.00	434.00	434.00
G18	2505.14	2436.77	2503.15	2506.16	2462.48
G19	112.48	111.70	129.94	112.68	130.24

G20	1267.68	1252.03	1284.93	1276.25	1294.02
G21	1365.05	1358.70	1385.13	1379.86	1414.87
G22	1282.95	1272.19	1302.33	1296.92	1326.85
G23	1120.00	1120.00	1120.00	937.95	678.46
G24	72.80	72.80	72.80	72.80	72.80
G25	980.00	980.00	980.00	980.00	980.00
G26	1391.58	1380.91	1406.85	1399.57	1418.89
G27	420.00	420.00	420.00	420.00	420.00
G28	3490.20	3490.20	3490.20	3490.20	3490.20
G29	3798.20	3798.20	3798.20	3798.20	3798.20
G30	2380.31	2402.73	2378.89	2380.17	2395.54
G31	5908.00	5908.00	5908.00	5908.00	5908.00
G32	12675.60	12675.60	12675.60	12675.60	12675.60
G33	3829.44	3881.35	3828.83	3932.00	4096.72
G34	1094.10	1098.35	1094.59	1093.82	1096.24
G35	2362.75	2408.38	2366.82	2365.76	2406.61
G36	14403.59	14324.03	14413.77	14451.29	14517.60
G37	8311.80	8311.80	8311.80	8311.80	8311.80
G38	19394.78	19487.08	19402.64	19379.28	19407.52
G39	4088.95	4082.24	4084.85	4083.34	4063.33
G40	17267.31	17316.91	17275.20	17271.90	17318.88
G41	7576.64	7601.76	7575.72	7576.60	7599.68
G42	43663.39	43613.95	43658.04	43663.28	43630.02
G43	14467.30	14467.30	14467.30	14467.30	14467.30
G44	48545.27	48524.16	48543.00	48544.89	48529.33
G45	27885.33	27885.33	27885.33	27885.33	27885.33
G46	31070.94	31166.48	31079.34	31069.99	31132.90
G47	21558.11	21550.53	21548.70	21545.53	21505.04
G48	7355.60	7355.60	7355.60	7355.60	7355.60
G49	15955.80	15955.80	15955.80	15955.80	15955.80
G50	15401.05	15343.29	15393.68	15398.32	15351.00
Iterations	-----	4	2	2	3
Margin (pu-rad)	-----	0.028	0.063	0.0597	A: 0.0087 B: 0.3947 C: 0.6096
Cost($/h)	51432959.2	51438622.84 (0.0110%)	51434583.83 (0.0031%)	51442836.48 (0.0192%)	51449579.07 (0.0323%)
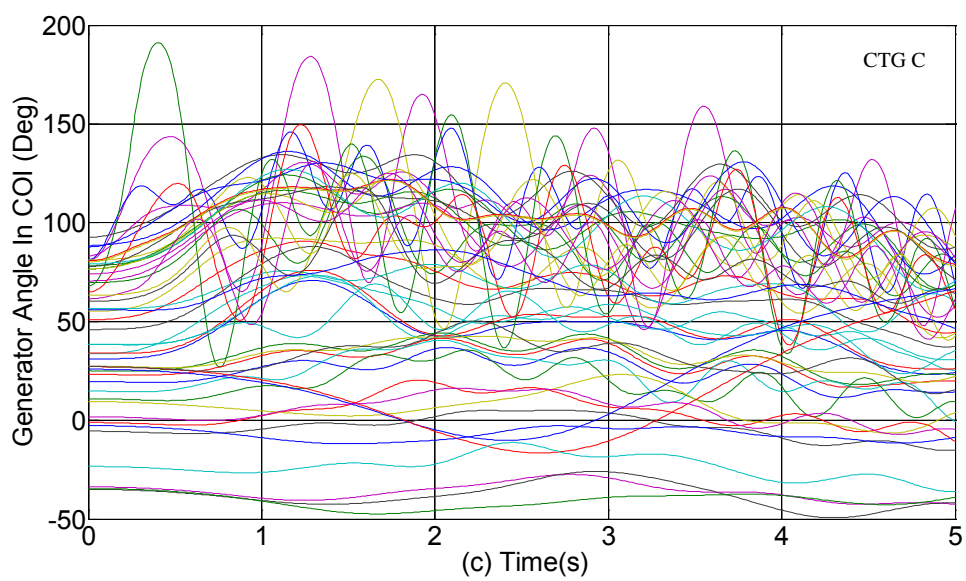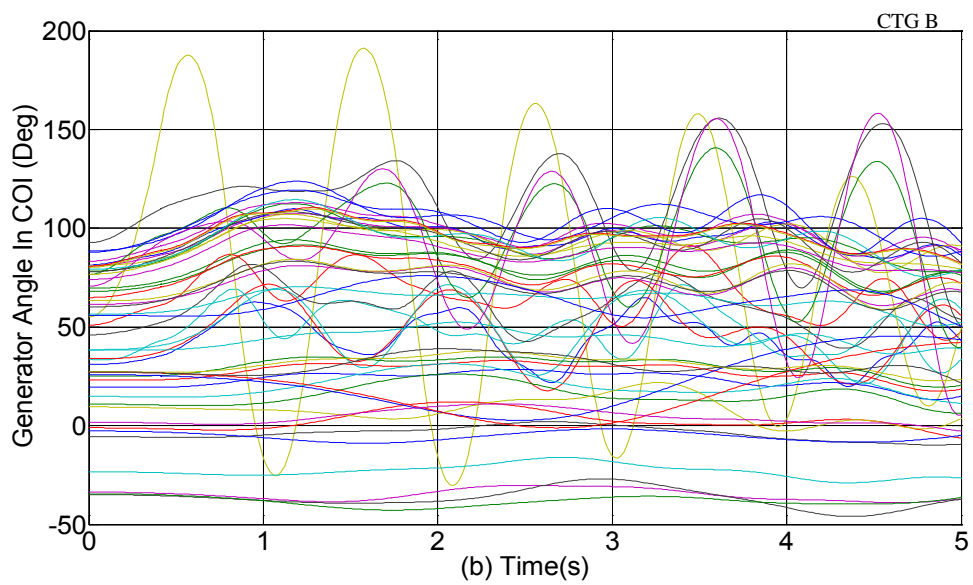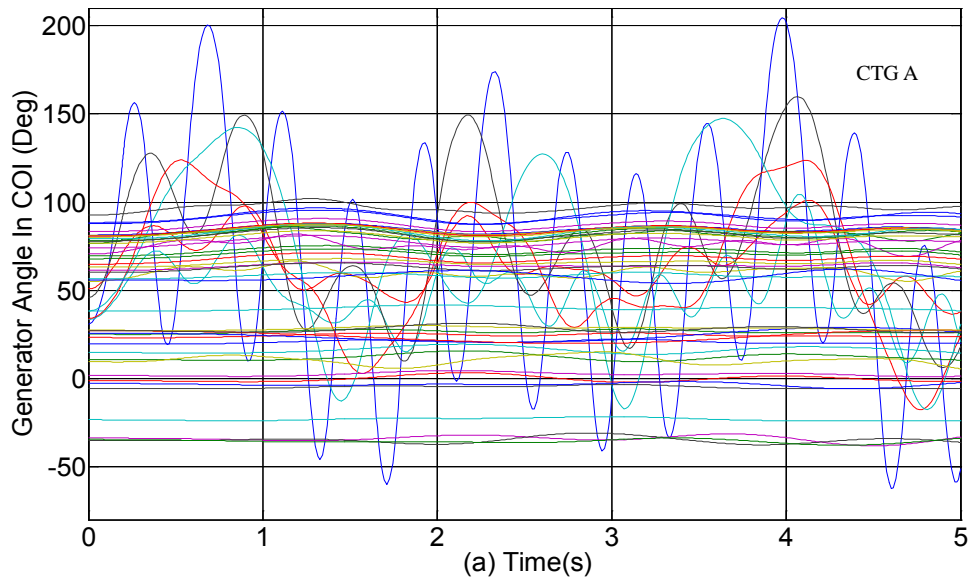
Fig. 3.4 Rotor plots for multi-contingency A+B+C of IEEE 50-generator system

3.5.3 Computation Time Analysis

Table 3.5 shows the computation times of the proposed method for solving the TSCOPF problem on the two different sized systems with single/multi-contingency. In column 2, A, B and C are the entries corresponding to contingency A, B and C with the Jacobian matrix formed in the final Newton iteration in the time domain simulation reused to improve the sensitivity calculation speed. Column 3 and 4 show the total number of iterations and the total CPU time with break downs on the time taken for solving the OPF and forming the Transient Stability Constraint (TSC).

Table 3.5 Computation times for solving various TSCOPF problems

Systems	Iterations		OPF+TSC=Total Time (s)
New England 10-Gen	A	3	0.95+7.16=8.11
	B	5	1.31+7.13=8.44
	A-B	4	1.02+13.32=14.34
IEEE 50-Gen	A	4	3.51+52.91=56.42
	B	2	2.18+17.50=19.68
	C	2	2.08+19.69=21.77
	A-B-C	3	3.24+93.56=96.80
	A-B-C (parallel)	3	3.35+39.76=43.11

For the New England 10-generator system, 3 iterations were required to complete the optimization process for contingency A as compared to 37 iterations in [42] with similar solution. The total time taken is 8.11s. For contingency B, 5 iterations and 8.44s were required for the optimization; whereas for multi-contingency A+B, 4 iterations were needed and the total CPU time taken increased to 14.34s due to the number of transient stability simulations increased in each iteration.

For the 50-generator system, the execution times for single contingency A, B, or C were 56.42s for 4 iterations, 19.68s for 2 iterations and 21.77s for 2 iterations, respectively. The time taken for the 46-gen Mexican power system, which is comparable in size to the IEEE 50-gen system, is 33.34s as reported in [64]. Thus, the timing for the two methods is roughly comparable or in the similar order of magnitude. The time taken for stabilizing the multi-contingency A+B+C increased to 96.80s for 3 iterations due to the increased number of contingencies. When parallel processing technique is used to evenly distribute the computation burden among 3 PCs, the CPU time is significantly reduced to 43.11s with speedup and efficiency increased to 2.25 and 74.8%, respectively.

In general, the proposed method could solved the TSCOPF problem with satisfied solutions in an acceptable time scale with the help of the following: (1) only one transient stability constraint for each contingency would be introduced irrespective of system size or simulation period; (2) the reuse of the Jacobian matrix in time domain simulation for trajectory sensitivity calculation.

3.5   Summary

A novel energy sensitivity based transient stability constrained OPF for multi-machine power system is proposed in this chapter. Since only a single stability constraint is introduced for each extreme unstable contingency based on the SIME power distance of the whole system instead of angles of multiple machines, the dimension of the stability constraints in TSCOPF is greatly reduced. The proposed method splits the TSCOPF into two sub-processes solving iteratively in turn to obtain the stable and economic operating point with convergence characteristic comparable to traditional OPF. The issue of over-stabilization of TSCOPF optimization is also properly handled by guiding the solution gradually across the stability boundary. Consequently, an all-round approach is proposed for the first time to effectively solve all types of TSCOPF problems. The

proposed approach has been extensively tested and validated on the New England 10-generator 39-bus system and the IEEE 50-generator 145-bus system. Simulations showed that the proposed approach is capable of handling multi-swing and extreme instability with multiple contingencies and possible over-stabilized TSCOPF problem and can effectively obtain the stable and economic solutions.

Chapter IV

Enhanced Particle Swarm Optimization Applied for Transient Angle and Voltage Constrained MINLP-TSCOPF Problem with FACTS

4.1   Introduction

In Chapter III, a basic TSCOPF model was introduced and solved analytically by the trajectory sensitivity-based method. With the rapid development of power electronics technologies, many new dynamic complicated components such as FACTS devices are now widely used in power systems, which make the system much more complex and bring new challenges to TSCOPF solving. Meanwhile, real generators do have valve-point effects in power generations, and discrete control variables such as transformer taps and capacitor banks are common in power system optimization. In order to properly consider all these factors, the TSCOPF will have to transform to a non-differential and discrete optimization problem. As a timely development, in this chapter, a general non-convex Mixed Integer Non-Linear Program TSCOPF (MINLP-TSCOPF) model is proposed to support any complicated dynamic components and discrete control variables.

The proposed MINLP-TSCOPF model is highly discontinuous and non-convex with multiple minima and thus very difficult to be addressed. The Branch and Bound (B&B) algorithm is a classical algorithm proposed in 1960 which can deal with discrete variables and its combination with a gradient-based method could in principle solve this non-convex MINLP-TSCOPF. However, as the B&B algorithm is based on a systematic enumeration of all the potential solutions in which large subsets of candidates are compared and discarded so as to find the

final solution, the resulted hybrid algorithm will be too complicated for solving any practical TSCOPF problems with large number of discrete control variables. More important, due to the non-convexity of TSCOPF, B&B hybrid with gradient-based algorithm would likely be trapped in suboptimal solutions [59]. So far, there is no successful deterministic method published for solving any non-convex MINLP-TSCOPF problems.

Intelligent methods such as DE [43], ANN [40], EP [109], GA [110] and PSO [44, 111-115] are population-based stochastic optimizations which do not rely on derivatives and therefore could handle non-derivative and non-convex problems. From the simplicity and practical point of view, PSO imitating the social behaviours of bird flocking is a good stochastic optimization algorithm with only a few parameters needed to be tuned [151]. Coupled with the encouraging performance for some hard optimization problems with fast and stable convergence, PSO has been widely and successfully applied in power system optimization such as the PSO method with Constriction factor (CPSO) proposed in [44] for solving traditional TSCOPF.

In this chapter, an MINLP-TSCOPF model is first presented to consider the generation valve-point effects, discrete control variables and complicated behaviours of FACTS devices. A signal energy expression is also proposed to form the transient voltage constraint such that the transient angle and transient voltage performance can be coordinated as an integrated stability control process in the MINLP-TSCOPF model and solved by a new enhanced PSO (EPSO) method. Last but not least, the proposed MINLP-TSCOPF model and proposed EPSO solution method are investigated and validated using two representative power systems with complex generator models and FACTS devices.

4.2   Proposed MINLP-TSCOPF Model

As widely adopted in [42-44, 64, 66], the generation fuel cost is adopted as

the objective function in this thesis for benchmarking with published methods. Due to the sharp increase of fuel losses in the valve opening process of turbine, generators would have valve point effects on the heat rate curve with ripples [26, 57, 58], which makes the objective function become high order nonlinear, non-convex with many minima. A refined model with consideration of the valve point effects is therefore expressed as a sum of quadratic polynomials and sinusoidal terms of active power as follows.

$$F_G = \sum_{i=1}^{n_G} \{a_i P_{Gi}^2 + b_i P_{Gi} + c_i + |e_i \sin(f_i(P_{Gi\min} - P_{Gi}))|\} \qquad (4.1)$$

where n_G is the numbers of generators; P_{Gi} is the generator active power; a_i, b_i, c_i, e_i, and f_i are fuel cost coefficients. Control variables include active power P_{Gi} of generators, discrete capacity of compensation capacitors and discrete tap ratio of on-load tap changers. It shall be noted that, though the valve load point effect is considered in the TSCOPF objective to form a non-differential optimization problem from the viewpoint of economy, the valve opening dynamic process for prime mover control is not included and thus a constant mechanical power is adopted during transient stability analysis as in [42-44, 64-66] for TSCOPF.

Static constraints are the following power flow equalities and static security inequalities.

1) Equality constraints of power flow

$$0 = P_{Gi} - P_{Di} - V_i \sum_{j=1}^{n_b} V_j (G_{ij} \cos\theta_{ij} + B_{ij} \sin\theta_{ij}) \qquad (4.2)$$

$$0 = Q_{Gi} - Q_{Di} - V_i \sum_{j=1}^{n_b} V_j (G_{ij} \sin\theta_{ij} - B_{ij} \cos\theta_{ij}) \qquad (4.3)$$

where $i = 1, 2......, n_b$ and n_b is the number of buses; P_{Gi} and Q_{Gi} are the generator active and reactive power; P_{Di} and Q_{Di} are the active and reactive load demand; V_i and θ_i are voltage magnitude and angle of bus i.

2) Inequality constraints for static security [42, 66]

$$P_{Gi\min} \leq P_{Gi} \leq P_{Gi\max} (i = 1, 2, ..., n) \qquad (4.4)$$

$$Q_{Gi\min} \leq Q_{Gi} \leq Q_{Gi\max} \ (i=1,2,...,n) \tag{4.5}$$

$$V_{i\min} \leq V_i \leq V_{i\max} \ (i=1,2,...,n_b) \tag{4.6}$$

$$S_{l\min} \leq S_l \leq S_{l\max} \ (i=1,2,...,n_l) \tag{4.7}$$

$$T_{i\min} \leq T_i \leq T_{i\max} \ (i=1,2,...,n_t) \tag{4.8}$$

where S_l and T_i are the line flow and transformer tap ratio, respectively; n_l and n_t are the number of transmission lines and transformers, respectively.

The proposed TSCOPF model also includes transient constraints for detailed generators, Static VAr Compensators (SVC), and Thyristor-Controlled Series Capacitors (TCSC) as follows.

3) Equality constraints of generator motion

The dynamic for a n-generator power system in the COI frame is generally described by [152]

$$\begin{cases} M_i \dfrac{\mathrm{d}\omega_i}{\mathrm{d}t} = P_{mi} - P_{ei} - \dfrac{M_i}{M_T} \sum_{i=1}^{n} (P_{mi} - P_{ei}) \equiv f_i(\cdot) \\ \dfrac{\mathrm{d}\delta_i}{\mathrm{d}t} = \omega_i \, (i=1,2,...,n) \end{cases} \tag{4.9}$$

where M_i is inertia constant of machine, and $M_T = \sum_{i=1}^{n} M_i$; P_{mi} and P_{ei} are the mechanical power input and electrical power output of machine i. The expressions for P_{ei} would vary with different generator models, and the detailed equations involved in computing P_{ei} can be found in [150]. Here, a two-axis transient generator model with Automatic Voltage Regulator (AVR) is adopted as a representative complex generation system [149, 150] for the evaluation of the proposed TSCOPF model and solution method.

4) Equality constraints of SVC

The static model of SVC can be simply represented as a susceptance B_{svc} with reactive power output dependent on the bus voltage as follows [4]

$$Q = B_{svc} V_i^2 \tag{4.10}$$

where V_i is the voltage magnitude of the bus to which the SVC is connected. Its dynamics can be modelled as a lead-lag controller and an inertial block with anti-

windup limiter as shown in Fig. 4.1(a). The corresponding differential equations are as follows:

$$
\begin{cases}
T_2 \dfrac{dx}{dt} = (1 - \dfrac{T_1}{T_2})(V_{ref} - V_i) - x \\[4mm]
T_B \dfrac{dB_{svc}}{dt} = [x + (V_{ref} - V_i)\dfrac{T_1}{T_2}]K_B - B_{svc}
\end{cases}
\tag{4.11}
$$

where V_{ref} is the reference voltage of SVC.
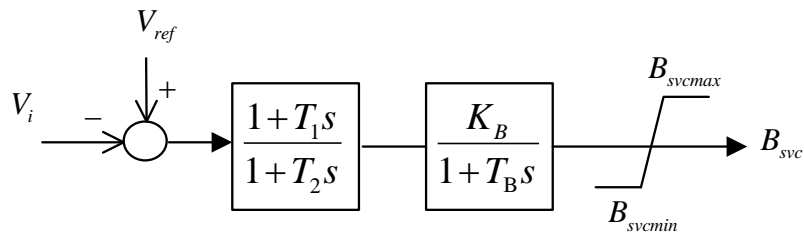
(a)   Block diagram of SVC controller
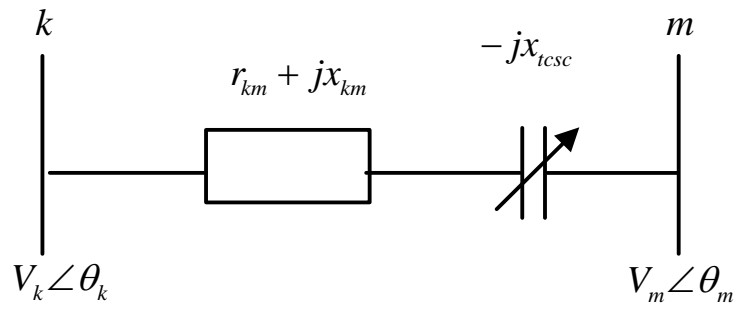
(b)   Module of TCSC
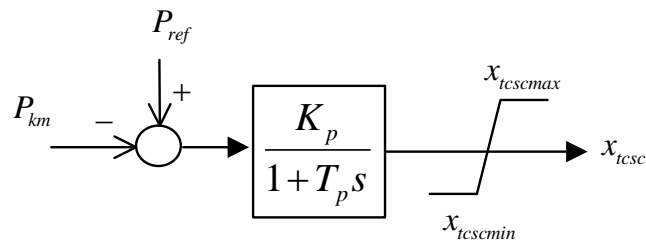
(c)   Block diagram of TCSC controller

Fig. 4.1 Models of SVC and TCSC

5) Equality constraints of TCSC

    TCSC can be considered as a controllable reactance inserted in a transmission line as shown in Fig. 4.1(b) with its power flow equations written as [153]:

$$P_{km} = V_m^2 g_{km} - V_k V_m g_{km} \cos(\theta_k - \theta_m) - V_k V_m b_{km} \sin(\theta_k - \theta_m)$$

$$Q_{km} = -V_m^2 b_{km} - V_k V_m g_{km} \sin(\theta_k - \theta_m) + V_k V_m b_{km} \cos(\theta_k - \theta_m)$$

$$P_{mk} = V_n^2 g_{km} - V_k V_m g_{km} \cos(\theta_k - \theta_m) + V_k V_m b_{km} \sin(\theta_k - \theta_m)$$

$$Q_{mk} = -V_n^2 b_{km} + V_k V_m g_{km} \sin(\theta_k - \theta_m) - V_k V_m b_{km} \cos(\theta_k - \theta_m)$$

$$(4.12)$$

where P_{km} and Q_{km} are the active power and reactive power transferred from bus k to m; $g_{km} = r_{km}/[r_{km}^2 + (x_{km} - x_{tcsc})^2]$, $b_{km} = (x_{tcsc} - x_{km})/[r_{km}^2 + (x_{km} - x_{tcsc})^2]$, and x_{tcsc} is the TCSC series reactance. While (4.12) is used to calculate the power flows of the lines with TCSC installed for constraint (4.7), x_{tcsc} will be lumped to the line reactance as shown in Fig. 4.1(b) in considering the power flow constraints in (4.2) and (4.3).

The TCSC controller is modelled as an inertial block with anti-windup limiter as shown in Fig. 4.1(c). The input signal is the active power error of the controlled transmission line, and the output signal is the series reactance of TCSC. Its differential equation is as follows.

$$T_p \frac{dx_{tcsc}}{dt} = (P_{ref} - P_{km})K_p - x_{tcsc} \qquad (4.13)$$

where P_{ref} is the active power reference of the controlled transmission line.

6) Inequality constraints of transient voltage

Recently, power system network frequently encountered problems of poor transient voltage causing, for example, disconnections of wind generators with poor Low Voltage Ride Through capability, stalling of induction motor, or mal-tripping of relay. Most utilities have adopted the North American Electric Reliability Committee [154] criteria for assessing the transient voltage performance. As a result, the transient voltage performance is becoming a concern and therefore shall also be considered in the TSCOPF model together with the transient angle stability. With reference to the energy expression of a signal [155], the transient voltage performance can be expressed as follows.

$$\frac{1}{(t_f - t_{cl})} \int_{t_{cl}}^{t_f} (\frac{V_t - V_s}{V_s})^T \cdot W \cdot (\frac{V_t - V_s}{V_s}) \le N \cdot \gamma^2 \qquad (4.14)$$

where t_{cl} and t_f are the fault clearing time and the total simulation time, respectively; V_t and V_s are the transient voltages during the simulation period and the reference voltage of the corresponding buses; $\boldsymbol{W}$ is the weight matrix; N is the number of buses, and γ is the threshold for the average derivation of voltage. V_s usually is the pre-fault steady-state voltage of each bus. During the transient, voltage could typically vary in the range of [0.8, 1.2] and γ could therefore be set to 20%. Thus, (4.14) represents the acceptable energy derivation during the simulation period.

7) Inequality constraints of transient angle stability

Transient angle stability constraints are commonly defined heuristically as a maximum allowable generator angle in COI frame such as π in [45], 100° in [55] and 120° in [44, 65, 104]. It is obvious that such heuristic constraints would be system dependent and lead to sub-optimal results, and there will be n_G inequality constraints resulted for n_G generators as this angle constraint is tied to the individual generator. On the other hand, the SIME method is an effective method for transient stability analysis [93, 94, 96], therefore, the SIME method introduced in Chapter III is adopted here to calculate the transient stability margin (*TSM*) for precise formulation of the transient angle stability constraints in the proposed MINLP-TSCOPF model.

Based on SIME theory [93, 94, 96], the calculation of *TSM* depends on the post-fault trajectory simulation. For a normal unstable case, it is defined as the negative value of the SIME kinetic energy at the exit point; for a stable case, the *TSM* is defined as the SIME potential energy increment from the return point of post-fault trajectory to the exit point of the reinserted permanent fault trajectory, which give a measure of how much more kinetic energy the post-fault system can withstand before becoming unstable. The approach to evaluate *TSM* is summarized as follows:

Step 1: Determine the system state at fault clearing and then continue the

simulation of the post-fault power system and keep track of ω_E along the simulation trajectory, where ω_E is the equivalent SIME speed [93, 94]. If ω_E passes through a positive minimum value indicated as ω_c, go to *Step 2*; if ω_E changes its value from positive to negative, go to *Step 3*; if ω_E continuously increases without a minimum, go to *Step 4*.

Step 2: Normal unstable case: *TSM* is evaluated as the negative minima of SIME kinetic energy, i.e. $TSM = -M_E \omega_c^2 / 2$.

Step 3: Stable case: Perform a "reinserted fault-on" simulation commencing at the return point to locate the exit point, then $TSM = |P_{ar}|(\delta_u - \delta_r)/2$.

Step 4: Extreme unstable case: calculate the redefined stability margin by $TSM = -P_{a\min} = -\min\{P_{mE}(t) - P_{eE}(t), t > t_c, P_a(t) > 0\}$, where t_c is the fault clearing time [94].

In short, (i) *TSM* is positive if and only if the system is stable; (ii) *TSM* is negative if and only if the system is dynamic unstable; (iii) when *TSM* is zero, the system is critical; (iv) the stability margin defined for extreme unstable case is not directly comparable to the stable or normal unstable case as the former is defined as the accelerating power distance while the latter is defined in term of energy.

As a result, the proposed transient stability constraint can be expressed as

$$TSM \geq 0 \quad \text{or} \quad -TSM \leq 0 \tag{4.15}$$

which not only is a precise constraint for transient stability but also reduces the number of constraints to one for the complete system instead of n_G for all the generators.

While equality constraints (4.2), (4.3) and (4.10) are implicitly handled in the Newton-Raphson power flow calculation and equality constraints (4.9), (4.11) and (4.13) are implicitly addressed in the time domain simulation, the remaining inequality constraints (4.4)-(4.8), (4.14) and (4.15) are grouped as:

$$H_i(x,u) \leq 0 \quad i = 1, 2, 3, ..., n_{ueq} \tag{4.16}$$

and handled using the external penalty method [44, 114, 115, 156] with a new objective function expressed as:

$$Min \ \tilde{F}(x,u) = f(x,u) + \beta_i [\max(0, H_i(x,u))]^2 \qquad (4.17)$$

where β_i is the penalty factor which should be properly selected to sufficiently penalize the violations and also guarantee a good flexible solution [156]. As a rule of thumb derived from experiments, the penalty factor β_i in this thesis is set to one order of magnitude higher than the objective function value $f(x,u)$.

4.3 Improved Particle Swarm Optimization

4.3.1 Standard Particle Swarm Optimization

The Standard PSO (SPSO) algorithm is an optimization method based on the foraging behaviour of birds. Each possible optimal solution is a 'bird' in a search space, and is called 'particle' in the algorithm. The particle in the group moves to a better area according to its fitness. The core of the algorithm is the 'speed-displacement' search model described mathematically as follows. Assuming there are m particles in the D-dimensional search space, and the position of ith particle is $X_i = (x_{i1}, x_{i2}, ..., x_{iD})$; the best position of each particle is $PBest_i = (p_{i1}, p_{i2}, ..., p_{iD})$ with corresponding fitness $fPBest_i$; the best position of the swarm is $Best_g = (p_{g1}, p_{g2}, ..., p_{gD})$ and the corresponding fitness is global best $fGBest$. Denoted the flight speed of particles as $V_i = (v_{i1}, v_{i2}, ..., v_{iD})$, their velocities and positions are updated by (4.18) [112].

$$\begin{cases} V_i^{k+1} = \omega V_i^k + c_1 \cdot Rand_1() \cdot (Pbest_i^k - X_i^k) + c_2 \cdot Rand_2() \cdot (Best_g^k - X_i^k) \\ X_i^{k+1} = X_i^k + V_i^{k+1} \quad i = 1, 2, ..., m \end{cases} \qquad (4.18)$$

where k is the number of iterations; ω is the inertia weight factor; c_1 and c_2 are cognitive and social constants, and they are typically set to 2.0; $Rand_1$ and $Rand_2$ are the uniform random number in range of (0, 1). The inertia weight decreases linearly as (4.19) [112]

$$\omega = \omega_{max} - \frac{\omega_{max} - \omega_{min}}{k_{total}} * k \qquad (4.19)$$

where k_{total} and k are the total and current number of iterations, ω_{max} and ω_{min} are the upper and lower limits of inertia weight, and they are heuristically set at 0.9 and 0.4 by experiments..

4.3.2 Enhanced Particle Swarm Algorithm

Two new enhancements to the SPSO method are proposed here to form an EPSO with improved convergency and accuracy based on the following two strategies: 1) adopting different inertia weights for different groups of PSO particles; and 2) introducing a shrinking disturbance to the position of PSO particles.

1) Dynamic adjustment of inertia weight

The inertia weight ω is an important parameter of the PSO method. It controls the impact of previous velocities of particles on the current velocity, therefore directly influences the trade-off between global exploration and local exploitation ability. While a larger ω has better global searching capability to detect unexplored area, a smaller ω will facilitate local search ability to finely exploit the current search area [157]. A proper designed inertia weight can ensure a balance between global and local search capability. An improved PSO (IPSO) method with random dynamic inertia weight and linearly changed acceleration coefficients was presented in [115]. Different from a randomly changed initial weight in [115], the proposed EPSO method classified the particle into three groups according to its fitness, and then separately updated the inertia weight for particles in each group.

Let m be the size of the particle swarm, f_i be the fitness of particle X_i in iteration k, $fGBest$ be the global optimum of the swarm, $fAVg$ be the average fitness of the swarm, $f'AVg$ be the average fitness of the particles whose fitness are better than $fAVg$ with $\Delta = \left| fAVg - f'AVg \right|$, the inertia weight ω would be

adjusted as follows:

Group I: If f_i is better than $f'AVg$, the inertia weight is adjusted as:

$$\omega = 0.4 - \frac{1}{1 + k_1 \cdot \exp(k_2 \cdot \Delta)} \tag{4.20}$$

where k_1 and k_2 are empirically set to 2 and 5, respectively, by experiments. In case the particle distribution is widely dispersed, Δ would be larger, and larger ω would be resulted in (4.20) to enhance the exploration. When particles are gathered closely, Δ would be smaller and hence ω will be reduced as a result in (4.20) to enhance the local search ability.

Group II: If f_i is better than $fAVg$ but worse than $f'AVg$, particles are neither particularly well dispersed nor gathered, the regular linear adjustment following (4.19) would be adopted to update the inertia weight.

Group III: If f_i is worse than $fAVg$, particles are rangers in the swarm. They have better global search capability and helpful for new explorations, hence their inertia weight would be unchanged.

Through the well-tailored inertia weight for PSO particles in different groups, the proposed EPSO would balance the global and local search capabilities for searching high quality solutions.

2) Shrinking disturbance to PSO particle positions

Premature convergence is a common problem encountered by the PSO method. Many improvements have been proposed to handle this problem. In [113], a Hybrid PSO (HPSO) method introduced the mutation operation of GA to enhance the PSO search ability. A Modified PSO (MPSO) was proposed in [114] by combining the temperature judgment of simulated annealing algorithm for accepting partial bad particles to avoid the premature convergence. These methods enhanced the global search capability by adding new perturbations to PSO particles, such as by introducing GA mutation in HPSO or allowing partial bad particles in MPSO. As inspired by this observation, a Gaussian distributed

disturbance is introduced here for updating the EPSO particle positions so as to allow the particles to escape from the 'basin of attraction' of the local optimum. In addition, considered that the disturbance shall not influence the quality of final optimal solution, the disturbance is designed to nonlinearly shrink with iterations. Now the positions of EPSO particles are reinforced with a shrinking Gaussian distribution disturbance as follows:

$$R_i = (\frac{k_{total} - k}{k_{total}})^2 \cdot \rho \cdot PBest_i \cdot N(0,1) \tag{4.21}$$

where ρ is the coefficient of the neighbourhood radius which has been determined experimentally as 0.5, $PBest_i$ is the individual best position of ith particle, $N(0,1)$ is the Gaussian distribution whose mathematical expectation is zero and standard deviation is one. As shown in (4.21), the neighbourhood radius R_i decreases with iterations. In the beginning of the optimization, the radius of the area is large and hence a large disturbance will be resulted, and the algorithm will have a high probability to escape from a local optimum or move away from a plateau. As the number of iterations increase, EPSO moves gradually close to the optimum while the disturbance reduces to a negligible level. Through the above process, the dynamic adjustment of disturbance enhances the optimality of EPSO. Taking (4.21) into consideration, positions of EPSO particles are calculated as

$$\begin{cases} V_i^{k+1} = \omega V_i^k + c_1 \cdot Rand_1() \cdot (Pbest_i^k - X_i^k) + c_2 \cdot Rand_2() \cdot (Best_g^k - X_i^k) + R_i \\ X_i^{k+1} = X_i^k + V_i^{k+1} \quad i = 1, 2, ..., m \end{cases} \tag{4.22}$$

After the position is updated, a round operator is used to enforce the allowable discrete value for the discrete variables; then EPSO particles are evaluated and compared to find individual best and global best for next iteration.

4.3.3   Test on Mathematic MINLP Problem

A mathematic MINLP problem with a known global optimum is first selected

to test the proposed EPSO method. For MINLP problems, classical methods such as Outer Approximation with Equality-Relaxation (OA/ER), Benders Decomposition (BD), and B&B algorithm are often used [59]. The proposed EPSO method are therefore compared with these deterministic methods as well as different versions of published PSO methods, namely SPSO[112], HPSO[113], CPSO[44], MPSO[114] and IPSO[115]. The selected benchmark is a MINLP model of selecting reactors minimizing for the production cost in [59], which is described as

$$\text{Min COST} = 7.5y_1 + 5.5y_2 + 7v_1 + 6v_2 + 5x \qquad \text{(Model I)}$$

$$\text{s.t.} \quad z_1 - 0.9(1 - e^{-0.5v_1})x_1 = 0$$

$$z_2 - 0.8(1 - e^{-0.4v_2})x_2 = 0$$

$$x_1 + x_2 - x = 0$$

$$z_1 + z_2 = 10$$

$$v_1 - 10y_1 \leq 0$$

$$v_2 - 10y_2 \leq 0$$

$$x_1 - 20y_1 \leq 0$$

$$x_2 - 20y_2 \leq 0$$

$$y_1 + y_2 = 1$$

$$x_1, x_2, v_1, v_2, z_1, z_2 \geq 0$$

$$(y_1, y_2) \in \{0,1\}$$

where y_1 and y_2 are integer variables. The global optimal value of this MINLP problem is 99.24 with the solution at $(x_1, x_2, v_1, v_2, z_1, z_2, x, y_1, y_2) = (13.428, 0, 3.514, 0, 10, 0, 13.428, 1, 0)$. It was reported in [59] that OA/ER and BD obtained a suboptimal solution 107.376 with $(y_1, y_2) = (0, 1)$ as the initial point, while B&B found an optimal value of 99.24 with initial point $(y_1, y_2) = (1, 0)$ and 107.376 with initial point $(y_1, y_2) = (0, 1)$. It is clear that OA/ER and BD have found a suboptimal solution while the quality of B&B solution is dependent on the starting point and only a proper initial point would result in a global optimal

solution.

The SPSO, HPSO, CPSO, MPSO, IPSO and the proposed EPSO are implemented in Matlab 2011b and applied to solve this problem. The optimal variables coded in PSO particles are assumed as (y_1, z_1, x_1, x_2), while other variables (y_2, z_2, v_1, v_2, x) are solved from the equality constraints in the model. The inequality constraints are handled by the penalty method. The population size and iterations are fixed as 4 and 100; the penalty factor is 1000. The initial points of optimal variables for all the PSO methods are randomly generated within the corresponding boundary.

Table 4.1 Statistical results of various methods for MINLP Model I

Vars	SPSO [112]	HPSO [113]	CPSO [44]	MPSO [114]	IPSO [115]	EPSO	B&B[59] (y_1,y_2)	
							(1,0)	(0,1)
x_1	13.4122	13.4211	13.4381	13.4332	13.4265	13.4280	13.4280	0.0000
x_2	0.0000	0.0000	0.0000	0.0000	0.0000	0.0000	0.0000	14.9998
v_1	3.5256	3.5192	3.5070	3.5106	3.5153	3.5142	3.5142	0.0000
v_2	0.0000	0.0000	0.0000	0.0000	0.0000	0.0000	0.0000	4.4796
z_1	10.0000	10.0000	10.0000	10.0000	10.0000	10.0000	10.0000	0.0000
z_2	0.0000	0.0000	0.0000	0.0000	0.0000	0.0000	0.0000	10.0000
x	13.4122	13.4211	13.4381	13.4332	13.4265	13.4280	13.4280	14.9998
y_1	1.0000	1.0000	1.0000	1.0000	1.0000	1.0000	1.0000	0.0000
y_2	0.0000	0.0000	0.0000	0.0000	0.0000	0.0000	0.0000	1.0000
Best	99.2400	99.2397	99.2398	99.2397	99.2396	**99.2396**	**99.2396**	**107.3764**
Mean	112.5537	107.1383	103.2276	107.1290	105.1237	**99.2397**	-	-
Worst	193.1539	118.8530	118.8530	118.8530	118.8530	**99.2401**	-	-
Std. Dev.	29.4705	9.5803	8.2378	10.2916	9.4741	**0.0001**	-	-
CPU Time	0.40s	0.43s	0.41s	0.53s	0.42s	0.42s	0.30s	0.20s

Table 4.1 shows the statistical results including the mean, worst, best value and standard deviations of these methods for 50 independent runs. It is clear that all PSO methods could approach the optimal solution 99.24 at the expense of slightly higher average CPU time compared with B&B. Furthermore, the proposed EPSO has the lowest mean value with Standard Deviation (Std. Dev.)

as low as 0.0001. This means EPSO could nearly always approach the global optimal solution. In short, the proposed EPSO method has outperformed all other methods for the MINLP model as shown in Table 4.1.

When the MINLP problem has an objective with multiple minimums, B&B is even more likely to be trapped in suboptimal solutions and fails to escape from the basins of attraction around the local optimal solution. The proposed TSCOPF model is in fact one of such multimodal problems when the valve-point effects is considered in the fuel cost objective as formulated in (1). For the investigation on the impacts due to the valve-point effects, the benchmarking MINLP model (Model I) was modified with an additional sinusoidal term added in its objective to become Model II as follows.

$$\text{Min COST} = 7.5y_1 + 5.5y_2 + 7v_1 + 6v_2 + 5x + \left|10\sin(2\times(x-6))\right| \quad \text{(Model II)}$$

Table 4.2 Statistical results of various methods for MINLP model II

Vars	SPSO [112]	HPSO [113]	CPSO [44]	MPSO [114]	IPSO [115]	EPSO	B&B[59] (y_1, y_2)	
							(1,0)	(0,1)
x1	13.8539	13.8529	13.8542	13.8540	13.8405	13.8540	12.2818	0.0000
x2	0.0000	0.0000	0.0000	0.0000	0.0000	0.0000	0.0000	20.0000
v1	3.2392	3.2398	3.2390	3.2391	3.2470	3.2391	4.7010	0.0000
v2	0.0000	0.0000	0.0000	0.0000	0.0000	0.0000	0.0000	2.4521
z1	10.0000	10.0000	10.0000	10.0000	10.0000	10.0000	10.0000	0.0000
z2	0.0000	0.0000	0.0000	0.0000	0.0000	0.0000	0.0000	10.0000
x	13.8539	13.8529	13.8542	13.8540	13.8405	13.8540	12.2818	20.0000
y1	1.0000	1.0000	1.0000	1.0000	1.0000	1.0000	1.0000	0.0000
y2	0.0000	0.0000	0.0000	0.0000	0.0000	0.0000	0.0000	1.0000
Best	99.4446	99.4652	99.4477	99.4440	99.7020	**99.4439**	**101.8431**	**122.9214**
Mean	117.1390	111.5288	108.3631	99.6035	115.0278	**99.5701**	-	-
Worst	121.5621	121.5621	121.5621	100.1109	121.5621	**99.9554**	-	-
Std. Dev.	9.3247	10.6347	11.3617	0.2323	10.5213	**0.1597**	-	-
CPU Time	0.39s	0.44s	0.43s	0.52s	0.43s	0.43s	0.30s	0.20s

While B&B was re-run with initial points $(y_1, y_2) = (1, 0)$ and $(y_1, y_2) = (0, 1)$, the same parameters as before were used in SPSO, HPSO, CPSO, MPSO, IPSO

and EPSO. As shown in Table 4.2, B&B obtained suboptimal solutions of 101.84 and 122.92 for the two initial points while SPSO, HPSO, CPSO, MPSO, IPSO and EPSO all approached the global optimum 99.44. Furthermore, MPSO and EPSO have a better mean solution of 99.6 with small standard deviation of 0.23 and 0.16, respectively, therefore would be the best algorithms for this modified MINLP model. The success of MPSO and EPSO is mainly due to the insensitivity to initial points of the PSO method and the good balance of their exploration and exploitation capabilities.

4.4   Procedures of EPSO for TSCOPF

In applying the EPSO method to address the TSCOPF problem, the following screening strategy is adopted in the particle initialization to reduce the CPU time spending on non-convergent power flow [43]. If P_d is the total active power demand, P_S is the total generation sum excluding the slack bus, and $P_{slack}^{\min}$ and $P_{slack}^{\max}$ are the lower and upper generation limits at the slack bus, respectively; the individual will be re-initialized when one of the following two conditions is satisfied: i) $P_d > P_S + P_{slack}^{\max}$ which implies the power demand could never be met even with the maximum generation in the slack bus; ii) $P_d \times (1+10\%) < P_S + P_{slack}^{\min}$ which would be considered as a bad candidate as power loss over 10% would be considered as too large for a practical system.

The following are the main steps of EPSO in solving this TSCOPF problem.

Step 1: Input system data and contingency set C_i (*i=1,…, k*), specify EPSO parameters, control variables and the corresponding lower and upper boundaries.

Step 2: Randomly initialize the control variables within their lower and upper boundaries using the screening strategy described above.

Step 3: Run an unconstrained Newton-Raphson power flow for each particle to determine the static variables and the initial state values of the dynamic

differential equations. It should be noted that as the generation in the slack bus is obtained from the power flow calculation, it needs to be checked against its upper and lower limits for constraint (4) in *Step 5*.

Step 4: For each contingency C_i, solve the dynamic differential equations and obtain the transient angle and voltage performance in the simulation period. As a result, there will be k transient angle constraints and k transient voltage constraints derived and incorporated into the TSCOPF model for k contingencies.

Step 5: Evaluate the fitness of each particle with (19) by the penalty method.

Step 6: Find the best position of individual particle (*PBest$_i$*) by comparing the fitness between the current and previous iteration, then update the best position of the swarm (*Best$_g$*).

Step 7: If the maximum number of iterations is reached, go to *Step 10*; otherwise, increase the iteration number.

Step 8: Dynamic adjust the inertia weight with (21)-(22), and then update the velocity and position of each particle using (23)-(24) and check against their upper and lower limits.

Step 9: Return to *Step 3* to re-run the Newton-Raphson power flow.

Step 10: The last *Best$_g$* is the final optimal solution.

Remarks:

1) During the initialization in *Step 2*, if either condition i) or ii) is satisfied, particle X_i will be re-initialized as $X_i = X_L + \text{rand} \times (X_U - X_L)$, where X_U and X_L are the upper and lower limit of control variables; otherwise, unconstrained power flow calculation will be conducted. If the power flow is diverged, X_i will be re-initialized. The whole condition and divergence checking process will be repeated whenever the particle is re-initialized.

2) The time domain simulation in *Step 4* is the most calculation intensive part. Since one simulation will be required for each contingency, the run time for solving the TSCOPF will be increased linearly with the growing number of contingencies [44]. In order to reduce the total computation burden, contingency screening, ranking and filtering techniques [158, 159] shall therefore be used to identify the critical contingencies and thus reduced the number of contingencies in the TSCOPF optimization.

3) In *Step 6*, individual particles compete with each other to find the $PBest_i$ and $Best_g$. However, the fitness of particles obtained in *Step 5* may not be directly comparable since the definition of stability margin for normal unstable/stable and extreme unstable cases are different in *Step 4*. As a result, the following strategy is adopted to identify the better particle from two: If both particles are normal unstable/stable or extreme unstable, the one with a lower fitness value is better; otherwise, the normal unstable/stable one would be better.

4) In *Step 8*, the screening strategy for EPSO initialization is not considered again at each step of TSCOPF procedure. If an EPSO particle is identified as non-converged by the power flow calculation, it will be not considered for updating the best individual position $PBest_i$, thus will implicitly be abandoned in following iterations.

4.5   Discussion of TSCOPF Solutions for Power Systems

4.5.1   Case A : New England 10-generator 39-bus System

When factors such as FACTs devices, discrete control variables and valve point effects are considered, the TSCOPF model would become a complicated non-convex non-derivative MINLP-TSCOPF problem. So far there is no result published using any deterministic methods on this MINLP-TSCOPF problem, and comparisons in the following case studies are therefore made among different versions of PSO methods.

The New England 10-generator 39-bus system [160] tabulated in Appendix A was slightly modified by installing two SVCs at bus 3 and 26 with the following parameters: $T_1 = 0.65s$, $T_2 = 0.2s$, $K_B = 10$, $T_B = 0.05s$, $B_{svcmax} = 5pu$, $B_{svcmin} = -2pu$. The fuel cost coefficients a_i, b_i, c_i, of generators were extracted from [45] with valve-point effects considered as $e_i = 200$, $f_i = 0.35$ for $i = 1, 2,\ldots,5$ and $e_i = 300$, $f_i = 0.22$ for $i = 6, 7,\ldots,10$. The lower and upper limits of bus voltages were set to 0.95 and 1.1, respectively. The continuous control variables are the active power of the 10 generators while discrete control variables are the tap ratio of on-load tap changers 12-11, 12-13 and 19-20 (with range of 1.0-1.1 in discrete step of 0.01); the compensation capacitors at bus 5, 8, 9, 18, 21 and 25 (with size of 0-0.5 pu in discrete step of 0.05 pu). The contingency was a three-phase fault occurred at the end of line 15-16 near bus 15 and subsequently cleared by line tripping after 0.5 s. The simulation period was 2s with integration step of 0.01s. The penalty coefficient β_i in (19) for all PSO methods was set to 10^5.

First, EPSO method was executed for parameter sensitivity analysis. The effects of swarm size on the search performance and computation burden was investigated with swarm size varied from 10 to 40 when the iterations fixed at 100. As shown in Table 4.3, the quality of average solutions was improved greatly when the swarm size was increased from 10 to 20 while the quality of solutions was improved only slightly with larger swarm size. The best compromised swarm size was therefore set to 20. The corresponding total computation time was breakdown into CPU times for power flow (PF) calculation, Transient Simulation (TS), and Function evaluation and Position update (FP) in Table 4.3. It showed that the total CPU time increased linearly with the growing number of swarm size. Similar behaviour on the CPU time has also observed for varying the number of iterations as shown in Table 4.4. It was found that when the number of iterations was fixed at 100, EPSO had a good trade-off between the solution quality and the total computation time. Therefore, in this case study, swarm size and iteration number were fixed at 20 and 100,

respectively, for all PSO methods such that comparison among various PSO methods was on a basis of the same number of function evaluations while other parameters were directly cited from the corresponding references.

Table 4.3 CPU time and fuel cost against swarm sizes for Case A (Iterations=100)

Swarm size	CPU time (s)				Mean Fuel cost ($/h)
	PF (s)	TS (s)	FP (s)	Total	
10	4.86	437.55	19.18	461.59	62529.46
20	9.72	914.87	21.20	945.79	**62354.45**
30	14.10	1212.50	24.24	1350.84	62334.01
40	18.65	1773.30	27.07	1819.02	62319.70

Table 4.4 CPU time and fuel cost against iterations for Case A (swarm size=20)

Iterations	CPU time (s)				Fuel cost ($/h)
	PF	TS	FP	Total	
50	4.85	440.30	10.88	456.03	62725.81
100	9.72	914.87	21.20	945.79	62354.45
150	14.21	1295.34	32.66	1348.91	62322.28
200	19.41	1798.75	41.45	1859.60	62310.25

Table 4.5 Optimal solutions for New England system over 20 runs for Case A

Variables*	OPF	Generator outputs of TSCOPF					
		SPSO [112]	HPSO [113]	CPSO [44]	MPSO [114]	IPSO [115]	EPSO
G_1	242.6963	259.34	266.58	191.53	269.02	205.81	206.13
G_2	618.4651	501.88	538.97	565.17	574.56	574.46	565.51
G_3	593.6217	621.59	557.64	602.87	558.26	592.12	645.55
G_4	645.4233	564.93	565.36	629.47	570.67	591.95	493.74
G_5	430.9937	485.65	512.22	447.86	520.93	422.19	512.80
G_6	671.249	574.28	570.17	600.00	557.28	554.81	615.14
G_7	555.8852	487.92	470.20	442.51	472.24	499.81	483.00
G_8	511.6804	542.40	556.92	559.28	514.07	599.26	514.53
G_9	899.8187	900.00	900.00	900.00	900.00	898.65	900.00
G_{10}	971.5783	1200.00	1200.00	1200.00	1200.00	1200.00	1200.00
T_{12-11}	1.05	1.10	1.07	1.09	1.02	1.08	1.01
T_{12-13}	1.07	1.08	1.10	1.09	1.04	1.07	1.03
T_{19-20}	1.03	1.05	1.06	1.09	1.07	1.07	1.04
C_5	0.15	0.20	0.50	0.00	0.30	0.40	0.50
C_8	0.15	0.15	0.50	0.50	0.00	0.20	0.30

C_9	0.2	0.30	0.25	0.00	0.20	0.30	0.05
C_{18}	0.5	0.25	0.35	0.35	0.35	0.25	0.40
C_{21}	0.25	0.20	0.35	0.00	0.15	0.35	0.15
C_{25}	0.35	0.20	0.50	0.50	0.50	0.30	0.45
Best FC ($/h)	61619.21	62295.52	62093.18	62262.51	62099.37	62031.43	**62048.12**
Worst FC ($/h)	61956.81	62735.24	62744.52	62707.16	62608.70	62707.16	**62576.64**
Average FC ($/h)	61831.82	62485.84	62473.26	62486.58	62372.41	62463.32	**62354.45**
Std. Dev. FC ($/h)	100.0485	128.07	165.23	117.06	117.68	148.59	157.96
CPU time for PF (s)	13.35	9.89	9.71	10.36	9.79	11.14	9.72
CPU time for TS (s)	0.00	912.82	909.30	898.44	936.48	949.94	914.87
CPU time for FP (s)	19.85	22.18	19.18	21.61	23.47	24.35	21.20
Total CPU time (s)	33.20	944.89	938.20	930.41	969.74	985.43	945.79

* The units for generation, tap-ratio and capacitor are MW, per unit and per unit, respectively.

The optimal solutions of conventional OPF solved by EPSO and MINLP-TSCOPF solved by SPSO[112], HPSO[113], CPSO[44], MPSO[114], IPSO[115] and EPSO were detailed in Table 4.5. It is clear and expected that the fuel costs of MINLP-TSCOPF are higher than OPF without transient angle and voltage performance constraints as a compromise in cost for better system security. Furthermore, comparing the MINLP-TSCOPF solutions of different PSO methods, EPSO is capable to find a better solution with lower fuel cost than other PSO methods while the computation times are comparable among all. This clearly demonstrated that, with similar CPU time cost, the proposed EPSO does have superior performance in terms of solution quality.
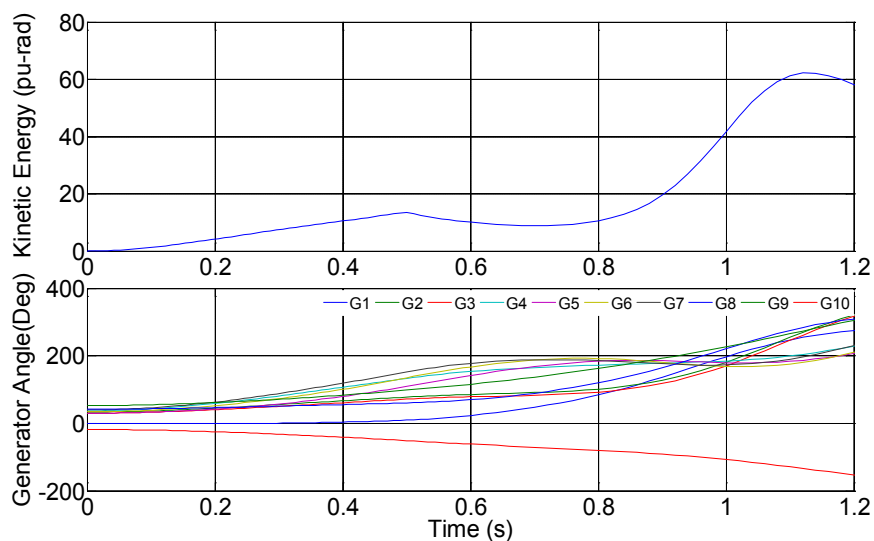
(a) Energy and angles with OPF
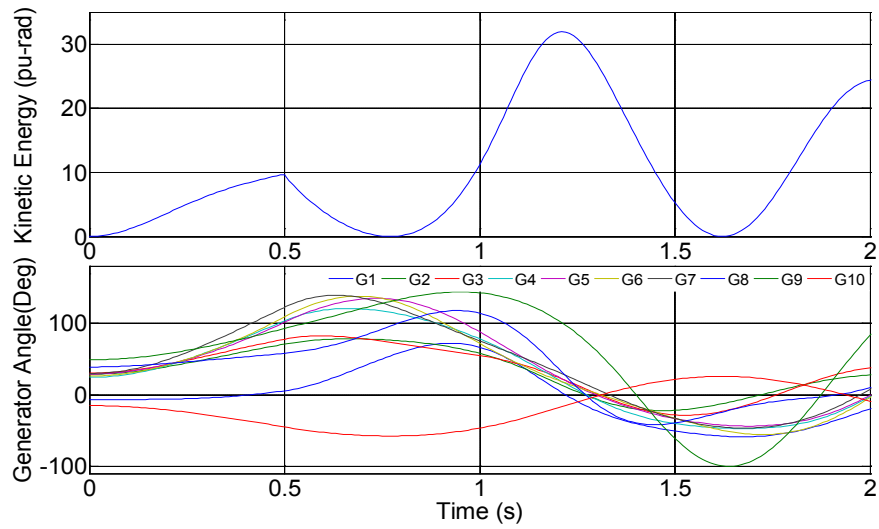
(b) Energy and angles with TSCOPF-EPSO
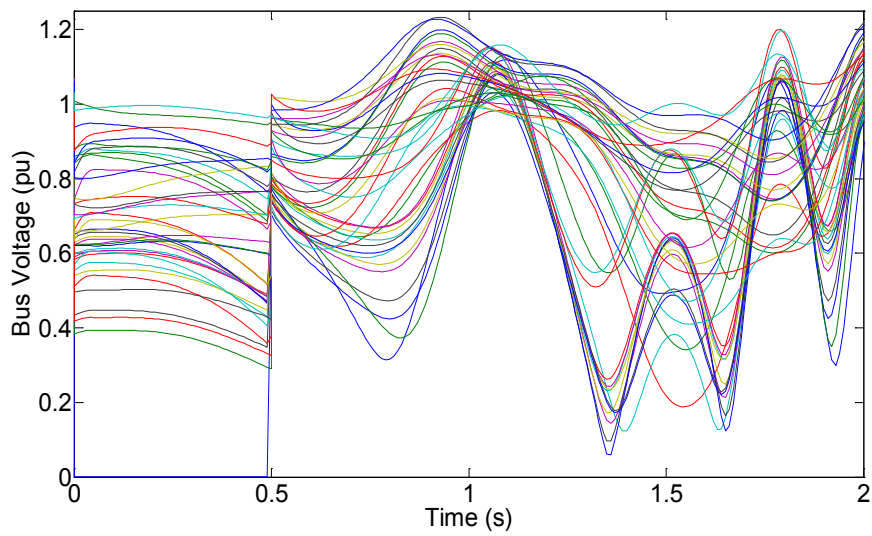
(c) Bus voltage plots with OPF
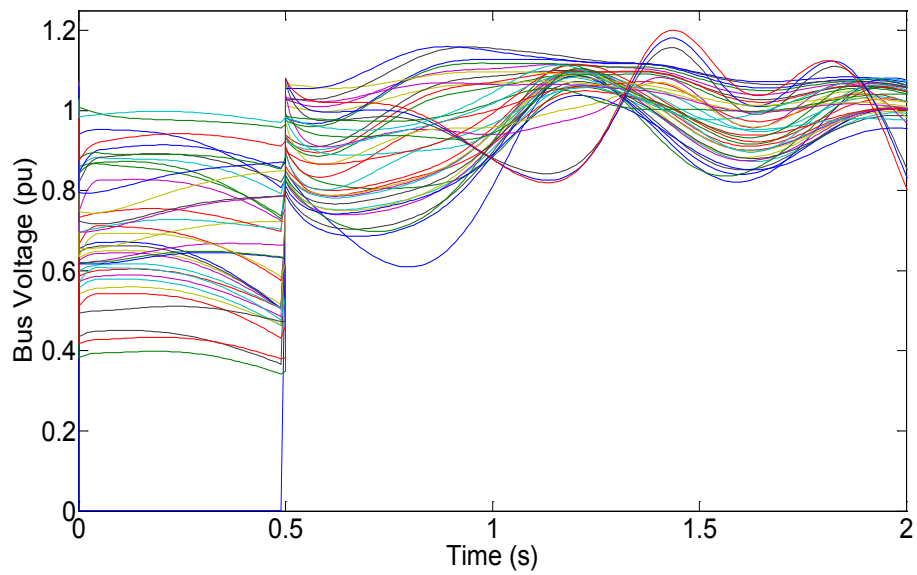
(d) Bus voltage plots with TSCOPF-EPSO
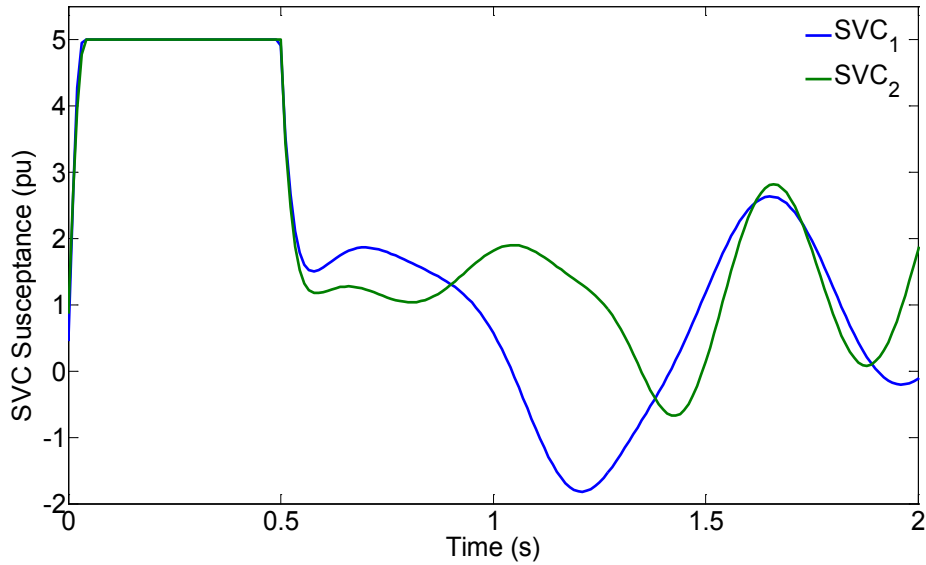
(e) SVC dynamic susceptance with TSCOPF-EPSO

Fig. 4.2 Transient energy, generator angle, bus voltage and SVC susceptance

profiles for New England system with OPF and TSCOPF-EPSO

Fig. 4.2 plotted the transient energies, generator rotor angles, and bus voltages for the solutions of OPF and MINLP-TSCOPF solved by EPSO. Though the fuel cost for the OPF solution is the lowest, it is transient unstable for the given contingency as shown in Fig. 4.2 (a) and (c). After the fault is cleared, the SIME kinetic energy of the system firstly decreases due to unbalance of mechanical and electrical power and then increases from a minima at 0.7s when ω_{AB} passes through the positive minimum value. The system loses its stability with TSM defined as the negative value of minimum SIME kinetic energy, i.e. -8.87 pu-rad. The instability can be seen from the generator rotor angle curves in Fig. 4.2(c) which became divergent. On the contrary, when the constraints of transient angle and voltage performance are considered, the resulted system is transient stable as shown in the plots of transient energies, generator rotor angles, and bus voltages in Fig. 4.2 (b) and (d). As shown in Fig. 4.2(b), the minima of SIME kinetic energy in the simulation period are always zero, which indicates that ω_{AB} have changed its sign twice. The system is stable in the simulation period with rotor angle peaked at 150 degrees and bus voltages fluctuated within

78

the predefined signal energy envelope as shown in Fig. 4.2 (d). Fig. 4.2 (e) also showed the dynamic behaviours of two SVCs.

Fig. 4.3 plotted the average convergence for 20 runs of different PSO methods. It is clear that TSCOPF-EPSO not only has a better convergence but also obtains a lower fuel cost.
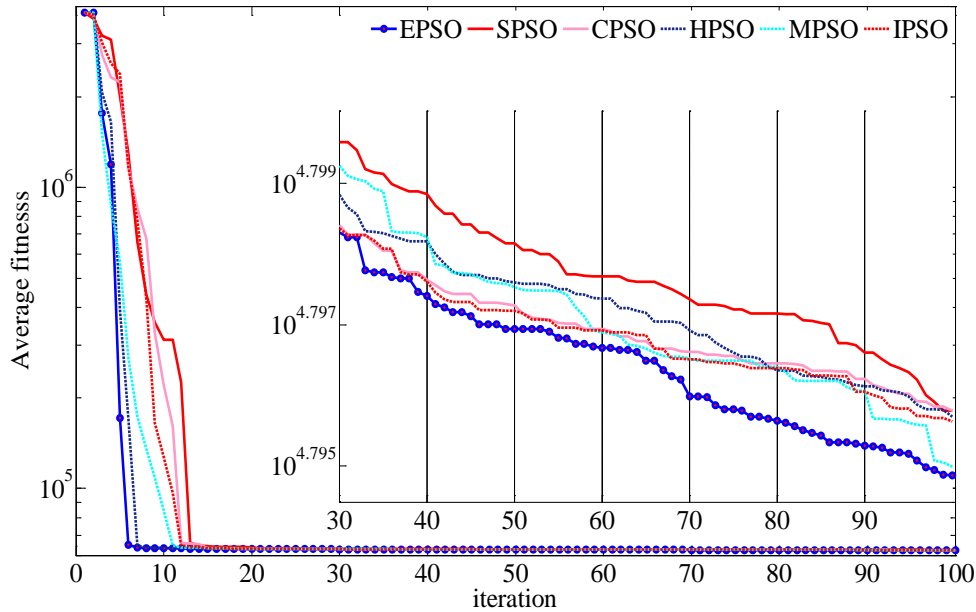
Fig. 4.3 Average convergence of various PSO methods for England system

4.5.2   Case B : IEEE 50-generator 145-bus System

The proposed EPSO method was further examined with the IEEE 50-generator 145-bus system including 4th order generators and AVR with parameters extracted from [150] and selectively listed in Table B.1. The system was slightly modified with three SVC devices installed at bus 18, 53 and 76, and a TCSC installed in line 58-57 to compensate 10% of its reactance in steady state. The lower and upper limits of bus voltage are 0.9 pu and 1.15 pu, respectively. The control variables are the active power of generators, the tap ratio of on-load tap changers at 17-59, 24-22, 22-83 and 24-76 (with range of 1.0-1.1 pu and discrete step of 0.01pu) and the compensation capacitors at bus 5, 15, 19, 35, 39 and 45 (with size of 0-0.5 pu in discrete step of 0.05 pu).

The parameter sensitivity strategy adopted in Case A was also used to study the impact of swarm size and iterations on the optimization solution quality and computation time. As shown in Table 4.6 and 4.7, the total CPU time increased linearly with the growing swarm size and increasing iteration number as in previous cases, and the best swarm size and iteration number were determined as 60 and 100 as a compromise between the computation time and solution quality. In the following comparisons, the penalty factor of PSO methods was set to 10^8 by experiments, and the following contingency was considered: a three-phase short-circuit occurred at the end of line 108-73 near bus 108, subsequently cleared by tripping the line after 0.26s. The transient stability simulation period was 2s with integration step 0.02s.

Table 4.6 CPU time and fuel cost against swarm sizes in Case B (Iterations=100)

Swarm size	CPU time (s)				Fuel cost ($/h)
	PF (s)	TS (s)	FP (s)	Total	
30	30.2	1205.3	33.2	1268.7	49305110.4
60	64.2	2252.3	36.1	2352.6	46858843.6
90	89.4	3351.2	39.1	3479.7	46504048.1
120	123.6	4506.8	41.5	4671.9	46325614.3

Table 4.7 CPU time and fuel cost against iterations in Case B (swarm size=60)

Iterations	CPU time (s)				Fuel cost ($/h)
	PF	TS	FP	Total	
50	31.5	1134.7	18.2	1184.4	51256372.4
100	64.2	2252.3	36.1	2352.6	46858843.6
150	95.6	3408.6	54.4	3558.6	46515532.3
200	126.1	4405.3	70.5	4601.9	46464048.1

Without any optimization, the system is unstable, as shown in the angle and bus voltage curves plotted in Fig. 4.4 (a) and (c), with total fuel cost of 63,314,317.12 $/h. The statistics solutions of TSCOPF optimized by SPSO [112], HPSO[113], CPSO[44], MPSO[114], IPSO[115] and EPSO method are detailed

and compared in Table 4.8. While solutions of all PSO methods are transient stable, EPSO outperforms other methods with better 'best fuel cost', lower 'worst fuel cost', smaller 'average fuel cost', similar 'variance' and comparable CPU time. Fig. 4.4 (b) and (d) plotted the corresponding transient energies, generator rotor angles, and bus voltages for the TSCOPF solution found by EPSO, and showed that the system is transient stable with maximum rotor angle close to 200° and bus voltages constrained within the acceptable range.
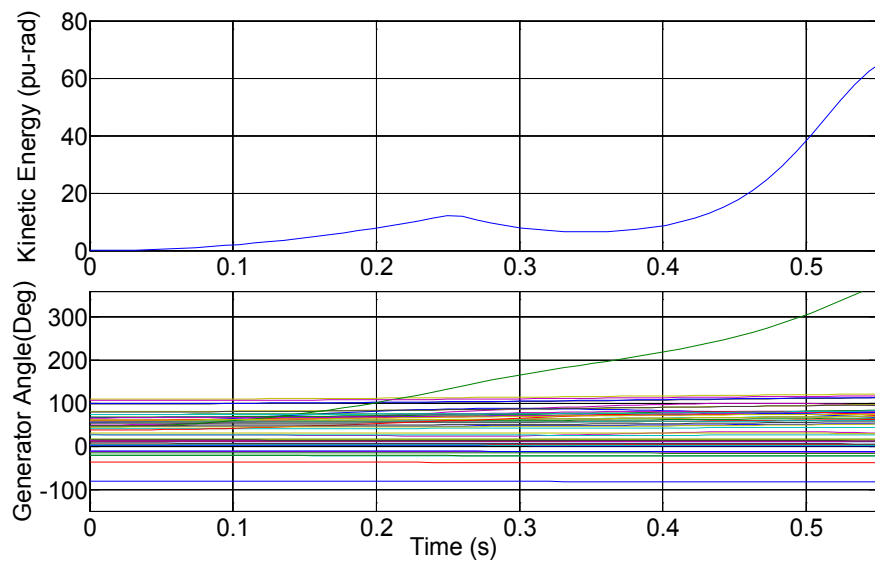
(a) Energy and angles without optimization
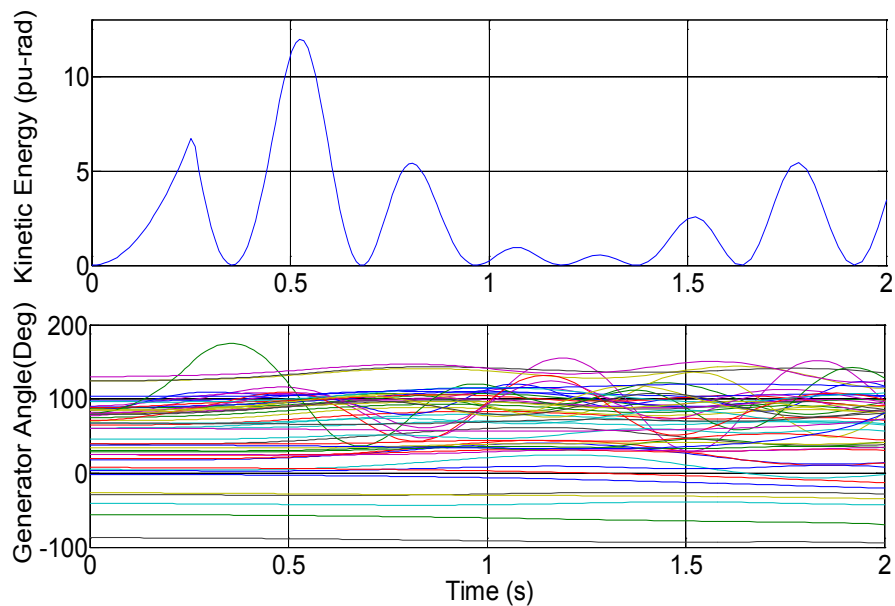
(b) Energy and angles with TSCOPF-EPSO
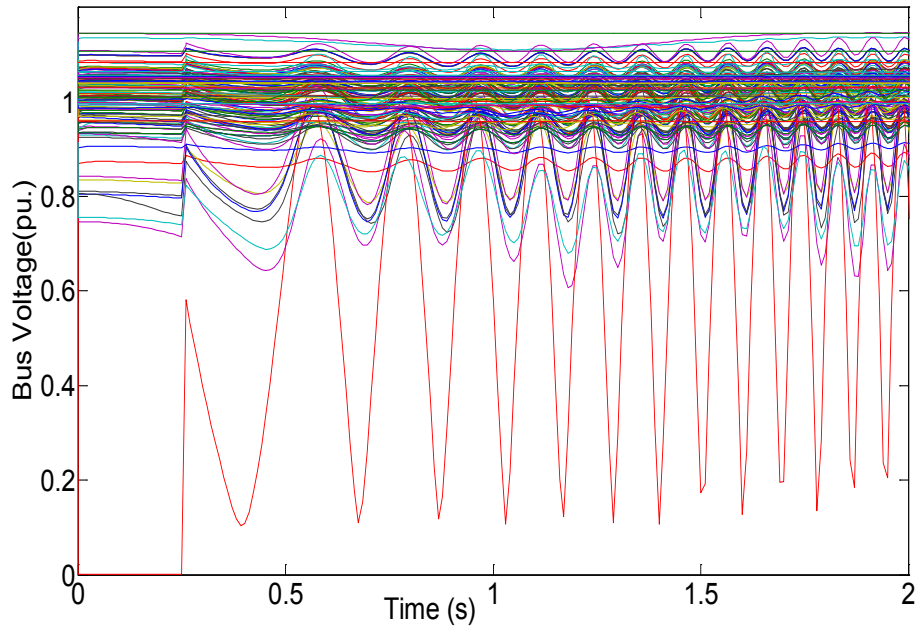
(c) Bus voltage plots without optimization
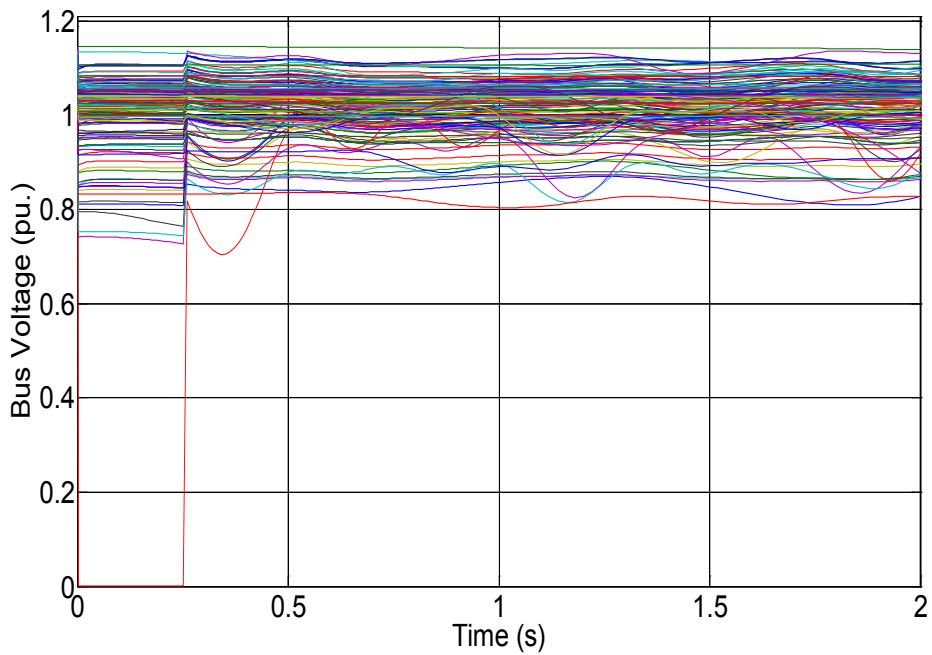
(d) Bus voltage plots with TSCOPF-EPSO

Fig. 4.4 Transient energy, generator angle and bus voltage profiles for IEEE 50-generator system without and with TSCOPF-EPSO method

Fig. 4.5 plotted the average convergence for 20 runs of different PSO methods and validated that the proposed EPSO had managed to consistently find a better solution with satisfied convergence rate.

Table 4.8 Optimal solutions for IEEE 50-generator system over 20 runs

Solutions	Generator outputs of TSCOPF					
	SPSO [112]	HPSO [113]	CPSO [44]	MPSO [114]	IPSO [115]	EPSO
Best FC ($/h)	47075681.1	50248845.9	51881827.6	47180529.2	47777960.1	45621431.8
Average FC ($/h)	48776956.9	52234796.4	52569842.1	48305108.4	48243209.4	46858843.6
Worst FC ($/h)	49800647.6	53662126.9	53465313.7	49449617.4	49264833.5	47755306.9
Std. Dev. FC ($/h)	767835.0	1399790.6	596230.4	966395.5	612024.6	893037.7
Total CPU time (s)	2399.1	2367.1	2406.0	2497.0	2388.6	2352.6
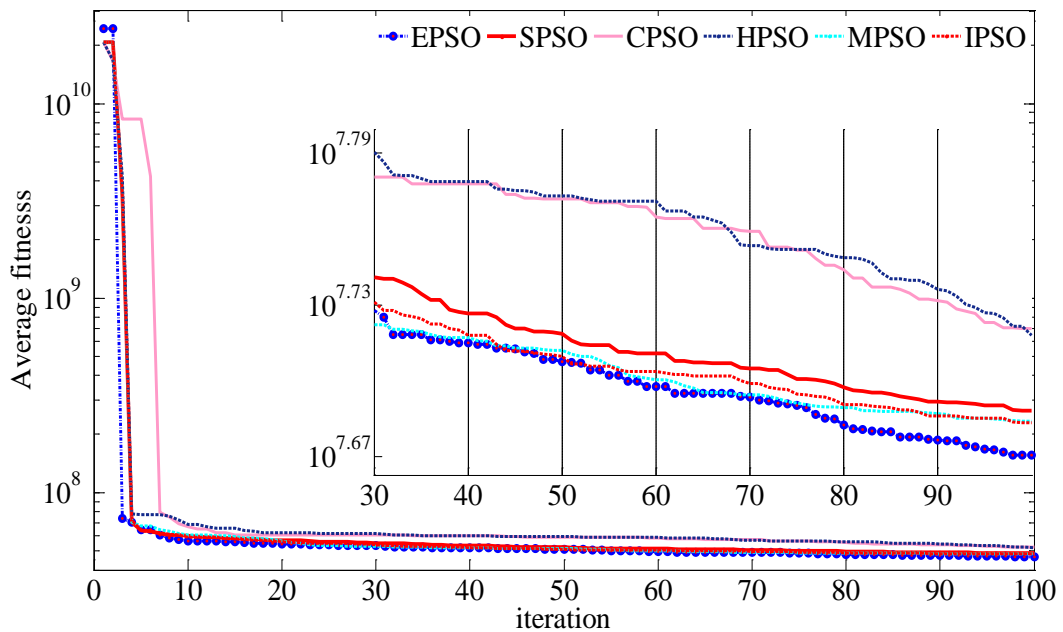
Fig. 4.5 Average convergence of various PSO methods for IEEE 50-gen system

4.6 Summary

A sophisticated TSCOPF model with valve-point effects and discrete control variables was first established as a hard MINLP problem, and a unified TSCOPF framework with consideration of both transient angle and voltage performance was conveniently formed. The proposed model is general and flexible, capable of supporting any complex dynamic power system models with valve point effects

and discrete control variables. An EPSO method with dynamic inertia weight and shrinking Gaussian distribution disturbance was then proposed to solve this MINLP-TSCOPF problem. The proposed model and solution methodology have been extensively studied and tested on the New England 10-generator 39-bus system and IEEE 50-generator 145-bus system with complex generator models and FACTS devices. Results of these case studies have confirmed the rationality of the non-convex MINLP-TSCOPF model and the promising performances of EPSO method for solving this problem.

Chapter V

An Improved Group Search Optimization Method for MINLP-TSCOPF with Detail Generator Model

5.1   Introduction

In Chapter IV, a very general and flexible MINLP-TSCOPF model has been proposed and primarily solved by an EPSO method. Since MINLP itself is a hard mathematical problem and TSCOPF problem with semi-infinite feature is also difficult to solve, TSCOPF with non-convex MINLP characteristic would be a huge challenge for any optimization methods. A specially designed method targeted to the discontinuity, non-convexity and multiple minima characteristics of MINLP-TSCOPF would therefore be highly desirable for solving this problem more effectively.

Artificial Intelligence algorithms (AIs) such as DE, GA and PSO, perform optimizations based on their population-based stochastic process, and they have potentials to comfortably handle non-derivative non-convex optimization problems. Most significantly, as a new breakthrough of AIs, the Group Search Optimization (GSO) method originated from [161, 162] has gained much attention recently due to its excellent global search ability, competitive accuracy and convergence speed. A co-operation evolutionary strategy based GSO algorithm was adopted in [163] to solve classical mechanical design problems. Since at least one feasible member is needed in the initialization, the method is inappropriate for solving hard optimization problems, as initializing a feasible solution is itself difficult. A Modified Group Search Optimization (MGSO) algorithm based on levy flight random step was proposed and validated using

simple mathematical benchmarks without constraints in [164]. Inspired by human social-network, a GSO with an Improved Small World topology (GSOISW) was also established to train the neural network for ammonia synthesis in [165]. [166] proposed an Opposition-based GSO method with Modified Differential Evolution strategy (OGSOMDE) for feed-forward networks training. Though the GSO method is a promising optimization approach with many engineering applications, so far it has not been applied to the TSCOPF problem. Furthermore, those previous algorithms have been designed and implemented only for rather simple optimization problems instead of, say, the proposed MINLP-TSCOPF model.

In this chapter, a newly Improved GSO (IGSO) method with improvements of backward searching strategy, Cauchy mutation and inheritance operator is specially designed as the best solver for this non-convex MINLP-TSCOPF problem. Simulations on four representative power systems and benchmarking with other AIs have validated the superior performance of IGSO method for solving MINLP-TSCOOPF problems.

5.2   Generation Prohibited Operation Zones for TSCOPF

In operation, generators may have certain Prohibited Operation Zones (POZs) due to physical operation limitations. Therefore, constraints (5.1) for generator output with POZs is included in TSCOPF model to substitute the continuous generation constraints (4.4) in Chapter IV.

The generation constraints with POZs restriction can be formulated as

$$P_{Gi} \in \begin{cases} P_{Gi,\min} \leq P_{Gi} \leq P_{Gi,1}^l & (i=1,2,......,n_G) \\ P_{Gi,j-1}^u \leq P_{Gi} \leq P_{Gi,j}^l & (i=1,2,......,n_G, j=2,3,...z_i) \\ P_{Gi,j}^u \leq P_{Gi} \leq P_{Gi,\max} & (i=1,2,......,n_G, j=z_i) \end{cases} \qquad (5.1)$$

where z_i is the total number of POZs, $P_{Gi,j}^l$ and $P_{Gi,j}^u$ are lower and upper bound of the jth POZ for generator i. Since the solution space of TSCOPF problem will

be partitioned into multiple discrete blocks by the POZs constraints, the solution will be very difficult to find.

The static equalities (4.1)-(4.9) and transient stability constraint (4.15) in Chapter IV plus the POZs constraints (5.1) constitute the MINLP-TSCOPF model in this chapter for validating the proposed IGSO in the following case studies.

5.3 Improved Group Search Optimization

GSO method is a population based optimization algorithm. Targeting to seek for optima in a bounded space of optimization problems, GSO employs the concept of resource searching behaviours of animals in nature and a producer–scrounger model to design the searching strategies [161, 162].

Based on the producer-scrounger model, each individual in GSO is classified either as a producer, scrounger or ranger based on its fitness [161, 162]. 1) Producer: it is the member with the best fitness for the current generation, and it will lead the searching directions of all members in next generation, thus has a profound influence on the optimization results; 2) Scroungers: besides the producer, usually 80% of the remaining members are randomly selected as scroungers to follow the producer to join its resource; 3) Rangers: the rest members in the GSO group are rangers responsible for discovering distributed resources in the search space by randomly walks. There is no restrict prohibition among the producer, scroungers and rangers, and they could switch from one to another according to their fitness evaluations.

5.3.1 Standard GSO Method

Suppose the ith member has a position $X_i^k = (x_1^k, x_2^k, ..., x_i^k, ...x_n^k) \in R^n$ and a head angle $\varphi_i^k = (\varphi_{i_1}^k, \varphi_{i_2}^k, ..., \varphi_{i_{(n-1)}}^k) \in R^{n-1}$, the search direction $D_i^k(\varphi_i^k) = (d_{i_1}^k, d_{i_2}^k, ..., d_{i_n}^k) \in R^n$ is calculated by sphere polar to Cartesian coordinate transformation as [161, 162]

$$d_{i_1}^k = \sum_{q=1}^{n-1} \cos(\varphi_{i_q}^k)$$

$$d_{i_j}^k = \sin(\varphi_{i_{(j-1)}}^k) \sum_{q=j}^{n-1} \cos(\varphi_{i_q}^k) \qquad (5.2)$$

$$d_{i_n}^k = \sin(\varphi_{i_{(n-1)}}^k)$$

1) *Producer:* The producer employs the scanning strategy to explore new solutions and the scanning field is represented by the maximum pursuit angle $\theta_{max} \in R^1$, the maximum pursuit distance $l_{max} \in R^1$ and producer's position X_p. At kth iteration, the producer will scan the hypercube search space by randomly selecting three points as [161, 162]

$$X_z = X_p^k + r_1 l_{max} D_p^k(\varphi^k) \qquad (5.3)$$

$$X_r = X_p^k + r_1 l_{max} D_p^k(\varphi^k + r_2 \theta_{max} / 2) \qquad (5.4)$$

$$X_l = X_p^k + r_1 l_{max} D_p^k(\varphi^k - r_2 \theta_{max} / 2) \qquad (5.5)$$

where $r_1 \in R^1$ is a normally distribution random number with mean 0 and standard deviation 1; $r_2 \in R^{n-1}$ is a uniform distributed random vector in range of [0,1]. The maximum pursuit distance l_{max} is

$$l_{max} = \|\boldsymbol{U} \cdot \boldsymbol{L}\| = \sqrt{\sum_{i=1}^{n}(U_i - L_i)^2} \qquad (5.6)$$

where U_i and L_i are the lower and upper bounds in the ith dimension of control variables.

Among the three randomly selected points by (5.3)-(5.5), the one having a better fitness than previous produce X_p will become the producer; otherwise, the producer will stay at its current position and turn its head angle to

$$\varphi^{k+1} = \varphi^k + r_2 \alpha_{max} \qquad (5.7)$$

where α_{max} is the maximum turning angle and equals $\theta_{max}/2$.

If the producer cannot find a better position within a iterations, it will turn its head angle at zero degree.

$$\varphi^{k+a} = \varphi^k \qquad (5.8)$$

where $a = round(\sqrt{n+1})$, n is the vector dimension of control variables.

2) *Scroungers:* At each generation, the positions of scroungers are updated by

$$X_i^{k+1} = X_i^k + r_3 \circ (X_p^k - X_i^k) \tag{5.9}$$

where $r_3 \in R^n$ is a uniform random vector in the range [0,1], and operator '$\circ$' is the entrywise product [161, 162].

3) *Rangers:* The rest members are rangers and they walk randomly to explore dispersed resources. At the *k*th iteration, it generates a random head angle φ_i by (5.7) and its position is update by [161, 162]

$$l_i = a \cdot r_1 l_{max} \tag{5.10}$$

$$X_i^{k+1} \varphi X_i^k + l_i D_i^k (\ _i^{k+1}) \tag{5.11}$$

where l_i is a random distance calculated from a normal distributed random number r_1 and constant *a*.

5.3.2 Improvements in the Proposed IGSO Method

1) Backward searching for producers

The position of producer updated via (5.3), (5.4) and (5.5) would search only forward for potential better solutions in the hypercube search space. This strategy would ignore the backward hypercube space even when there is a high possibility of good resources behind, thus enhancement on the back searching ability of producer is proposed here.

In the sphere polar coordinate, the backward searching is obtained by rotating the forward direction by π radian as shown in Fig. 5.1. Fig. 5.1(a) and (b) describe the backward searching point X_{Zs} of the producer X_Z in two and three dimensions, respectively. For *n* dimensions as a hypercube, the search cannot be visualized. However, when unfold the hypercube in a plane, the search direction of the *i*th member will be the length of a series of right angled triangles as shown in Fig. 5.1(c), and the backward searching point can be calculated by increasing the head angle by π radian. Thus, if the function $S_i^k(\varphi_i^k) = (s_{i_1}^k, s_{i_2}^k, ..., s_{i_n}^k) \in R^n$ is defined as

$$s_{i_1}^k = \cos(\varphi_{i_1}^k)\left|\sum_{q=2}^{n-1}\cos(\varphi_{i_q}^k)\right|$$

$$s_{i_j}^k = \sin(\varphi_{i_{(j-1)}}^k)\left|\sum_{q=j}^{n-1}\cos(\varphi_{i_q}^k)\right| \qquad (5.12)$$

$$s_{i_n}^k = \sin(\varphi_{i_{(n-1)}}^k)$$

and the three backward searching points can be calculated as

$$X_{zs} = \varphi X_p^k + r_1 l_{\max} S_p^k(\,^k + \pi) \qquad (5.13)$$

$$X_{rs} = \varphi X_p^k + r_1 l_{\max} S_p^k(\,^k + {}_2\theta_{\max}/2 + \pi) \qquad (5.14)$$

$$X_{ls} = \varphi X_p^k + r_1 l_{\max} S_p^k(\,^k - {}_2\theta_{\max}/2 + \pi) \qquad (5.15)$$
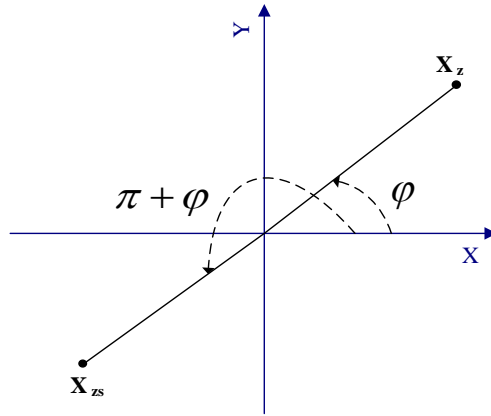
(a) Two dimensions
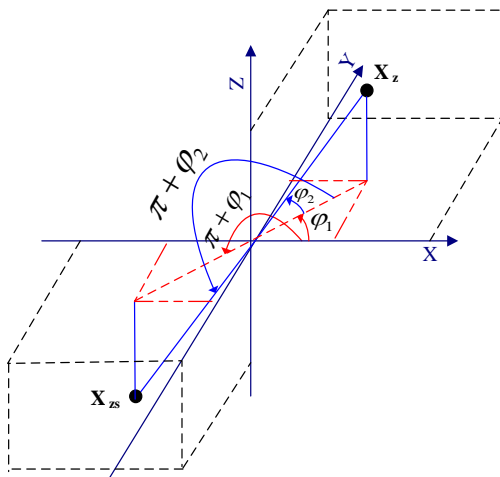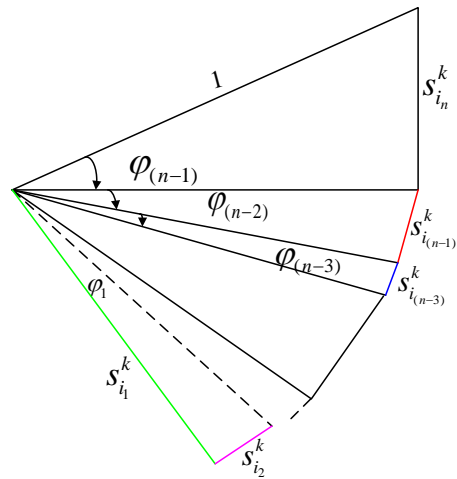
(b) Three dimensions   (c) *n* dimensions

Fig. 5.1 Backward searching strategy for IGSO method

Based on this backward searching strategy, previously ignored searching space will be covered and the new producer would derive from six scanning points by (5.3)-(5.5) and (5.13)-(5.15) in both forward and backward directions simultaneously.

2) Cauchy mutation disturbance for scroungers

The scroungers, as the dominated type (80%) of GSO individuals, are influenced only by the producer via (5.9), and premature problem is often resulted. Since the mutation operator in heuristic methods could improve the solution performance [167] and Cauchy mutation is capable to generate a larger jumps compared with other mutations such as Gaussian mutation [168], Cauchy mutation is adopted for the GSO scroungers in the proposed IGSO method to escape from a local optimum or jump out a plateau, and increase the diversity of the GSO individuals. In addition, considered that the mutation disturbance shall not have any negative effects on the quality of the final solution, the disturbance should be reduced to a negligible level at later stage, a self-adaptive Cauchy mutation is formulated as (5.16) in which a large deviation would be resulted in the beginning to reduce the impact of producer on scroungers while at later stage the deviation will become small and the producer would have dominant influence on scroungers for fine searching.

$$X_i^{k+1} = X_i^k + r_3 \circ (X_p^k - X_i^k) + X_i^k \times \rho \times (\frac{k_{total} - k}{k_{total}})^2 \times Cauchy(0,1) \tag{5.16}$$

where $r_3 \in R^n$ is a uniform random vector in the range [0, 1]; k and k_{total} are the current and total iteration number, respectively; $Cauchy(0, 1)$ stands for the standard Cauchy distribution with the probability density function $Cauchy(0,1)=1/(\pi(1+x^2))$ [168]; ρ is the coefficient of Cauchy mutation. According to (5.16), the Cauchy mutation space will dynamically shrink with increasing iteration number, and the last term of (5.16) will therefore have more influence on the position updating of scroungers in the beginning while less impact at the later stage in optimization process. The head angles of scroungers

are also updated by (5.7).

3) Inheritance operator for GSO individuals

For the position updated via (5.9) or (5.11), it is uncertain if there is any good attributes inherited from one generation to another. For instance, after updating the position of ith member via (5.9) or (5.11), if the previous member X_i^k has better fitness than X_i^{k+1}, X_i^{k+1} will be retrogressive compared with X_i^k, and some of the good attributes of previous members would be lost in the new generation as a result. In fact, good attributes of previous generation could be inherited to next generation by comparing the fitness of X_i^k and X_i^{k+1} and retaining the better one as (5.17).

$$X_i^{k+1} = X_i^k \times \langle f(X_i^k) < f(X_i^{k+1}) \rangle + X_i^{k+1} \times \langle f(X_i^{k+1}) < f(X_i^k) \rangle \tag{5.17}$$

where $f(X_i^k)$ is the fitness evaluation; symbol $\langle x < y \rangle$ is the Boolean calculation, namely if $x < y$, $\langle x < y \rangle$ equals one, otherwise zero. Considering that $f(X_i^k)$ and $f(X_i^{k+1})$ have already been evaluated, this strategy maintains the useful information for the IGSO individuals in next generation only by simple comparisons without heavy computation but with high cost-performance gain.

5.3.3 Procedures of IGSO for Solving TSCOPF Problem

In the proposed IGSO method, the external penalty method [44, 156] is adopted to deal with the inequality and equality constraints of the MINLP-TSCOPF model. The following are the main steps of IGSO method in solving the TSCOPF problem.

Step 1: Input system data and contingency set C_i ($i=1,\ldots, k$), specify IGSO parameters and randomly initialize IGSO individuals for the control variables within their lower and upper boundaries.

Step 2: For each contingency C_i, run an unconstrained Newton-Raphson power flow and time domain simulation for each individual to determine the static variables and transient stability margin, then evaluate the fitness of

these initialized points by the penalty method.

Step 3: Find the IGSO producer X_p and perform producing strategy, i.e. the producer searches points forward by (5.3)-(5.5) and backward by (5.13)-(5.15). If any one of the scanning points has a better fitness than the producer, the producer will fly to that point; otherwise the producer will stay at the current position and update its head angle by (5.7), or by (5.8) if the producer cannot find a better point in *a* iterations.

Step 4: Randomly select 80% members to perform scrounging strategy using (5.16).

Step 5: Rest of the members are scroungers to perform dispersing strategy by (5.10) and (5.11).

Step 6: For each contingency C_i, run an unconstrained Newton-Raphson power flow and time domain simulation for IGSO members to determine the static variables and transient stability margin and evaluate their fitness by the penalty method.

Step 7: Compare previous generation fitness $f(X_i^k)$ with current generation fitness $f(X_i^{k+1})$, then update X_i^{k+1} by the inheritance operator using (5.17).

Step 8: If the number of iterations reach maximum, go to next step; otherwise, increase the iteration number and go to *Step 3*.

Step 9: The individual with best fitness of the last generation is the final optimal solution.

Remarks:

1) Since the proposed TSCOPF problem has discontinuous control variables due to the POZs of generations considered in (5.1), a well-designed round operation as follows is needed to properly handle the discontinuity.

$$P_{Gi} = P_{Gi,j-1}^{u} + (P_{Gi,j}^{l} - P_{Gi,j-1}^{u}) \times \left[\frac{x_i - P_{Gi,j-1}^{u}}{P_{Gi,j}^{l} - P_{Gi,j-1}^{u}} \right] \tag{5.18}$$

$$if \quad x_i \in (P_{Gi,j-1}^{u} \quad P_{Gi,j}^{l})(i = 1, 2, ..., n_G, j = 2, 3, ... z_i)$$

where [*] stands for the round operation, x_i is the control variable and $x_i \in X$. It is clear that, if the control variable for generation is located in POZs, the generation output will be confined to either $P_{Gi,j-1}^{u}$ or $P_{Gi,j}^{l}$.

2) Targeted to the specific characteristics of proposed discontinuous non-convex TSCOPF model with many minima, the IGSO method is tailored in the following aspects: 1) the round operator (5.18) can effectively deal with the discontinuous variables stemmed from generation POZs; 2) the Cauchy mutation disturbance is specially designed to allow escape from the local optimum plateau of the optimization problem with many minima; 3) the backward searching strategy and inheritance operator enhance and refine the search capability of IGSO in solving the TSCOPF problem.
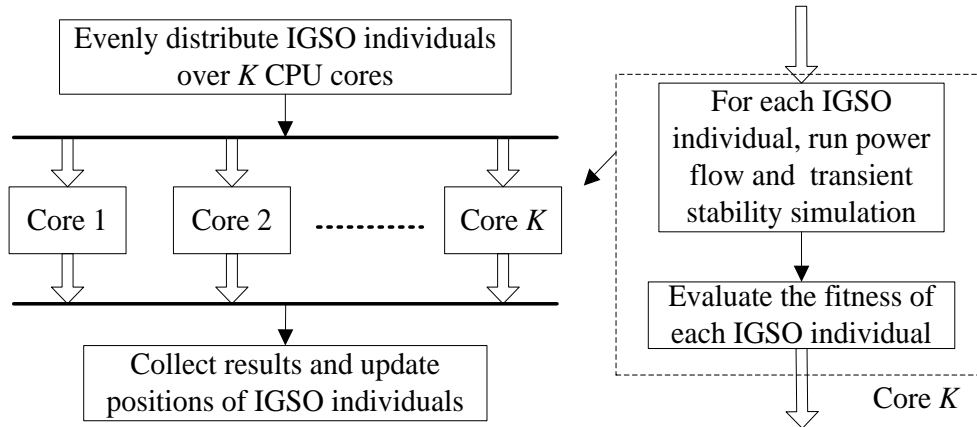
Fig. 5.2 Parallel IGSO implementation for TSCOPF problem

3) When large-scale power system is considered, the computation time of TSCOPF optimization would increase rapidly. However, due to the intrinsic independent characteristic of GSO members, TSCOPF optimization can be readily parallelized. A distributed platform with a master and slave architecture has been established to conduct the parallel TSCOPF optimization as shown in Fig. 5.2, in which the master is responsible for

94

distributing IGSO individuals, collecting results and updating the positions of IGSO members while slave CPU cores are responsible for fitness evaluation including the power flow calculation and transient stability analysis.

5.4   Validation of IGSO Method in Power Systems

The prowess of proposed IGSO method to solve the discontinuous non-convex TSCOPF problem has been fully tested with following four case studies using the WSCC 3-machine 9-bus system, New England 10-machine 39-bus system, and IEEE 50-machine 145-bus system. In all studies, loads are modelled as constant impedances in the time domain simulation with a time period of 5s. A distributed computing platform with 16 nodes, each equipped with a 3.2GHz Intel Core 2 Quad processor and 8GB RAM, has been built with MATLAB Distributed Computing Server 5.2 and Parallel Computing Toolbox 5.2 for conducting the parallel TSCOPF optimization. Furthermore, the following seven representative AIs have also been implemented for benchmarking the performance of the proposed IGSO method: DE [43], GA [60], GSO[162], MGSO[164], GSOISW[165], OGSOMDE[166] and EPSO in Chapter IV.

5.4.1   Case A : 3-machine 9-bus System

The widely used WSCC 3-machine 9-bus system was firstly tested. The system network and load data are taken from [169], and the generation ratings and fuel cost coefficients are cited from [45]. The generation valve-point effects and POZs are not considered for benchmarking of results from published papers. All bus voltages are limited to [0.95, 1.05]. A three-phase ground fault at the end of line 7-5 near bus 7 is applied at t=0ms and subsequently cleared by tripping line 7-5 at t=350ms.

The parameters of GA and EPSO method are cited from [60] and Chapter IV, respectively. For various GSO variants including IGSO, the initial head angle φ^0

of individuals is set to ($\pi/4$ … $\pi/4$); the constant a is given by *round(*$\sqrt{n+1}$*)* and the maximum search angle θ_{max} is π/a^2; the maximum turning angle α_{max} is set to $\theta_{max}/2$. For the IGSO method, the coefficient of the Cauchy mutation ρ is set to *0.005*. In order to have fair comparisons with the same number of function evaluations for each method, the population size of IGSO is set to 10 since the producer of IGSO method would scan extra 5 points in each iteration; similarly, the population size of GSO, GSOISW and OGSOMDE are set to 13 since their producer would explore extra 2 points in each iteration, while the population size of GA, EPSO and MGSO were 15. The maximum iterations of all methods are fixed at 100.

For the given contingency, two published solutions are also collected from [40] and [43] for benchmarking with the results obtained from the proposed IGSO method and the seven representative AIs as tabulated in Table 5.1. While DE approached a quite expensive stable solution with fuel cost of 1,140.06 \$/hr in [43] and 1,137.31 \$/hr here, the TSB and ANN method in [40] found a better stable solution with fuel cost of 1,134.2 \$/hr. It is clear that all AIs including the EPSO proposed in Chapter IV manage to find a satisfactory best solution compared with [40] and [43] with comparable CPU time. Compared with the other AIs, IGSO is capable of finding the best stable solution with the lowest fuel cost of 1,133.96 \$/hr, average, worst, and standard deviation as highlighted in bold in Table 5.1. This shows that the proposed IGSO method is the best solution approach for this case study.

Fig. 5.3 plots the generator angle and kinetic energy curve for the solutions of IGSO method, and validates the system stability with maximum rotor angle close to 135° and SIME kinetic energy varied from zero to 2 pu-rad.
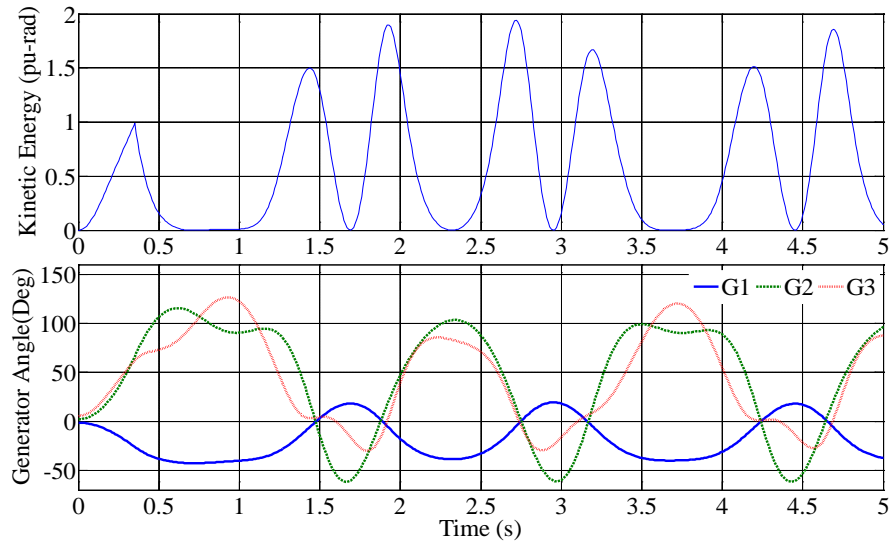
Fig. 5.3 Angle and energy curves of 9-bus system with classical model after

optimization

Table 5.1 Optimal solutions of different methods for 9-bus system in Case A

Variables	Generator optimal outputs										
	{ANN [40]}*	{DE [43]}*	DE [43]	GA [60]	GSO [162]	MGSO [164]	GSOISW [165]	OGSOM DE [166]	EPSO in Chapter IV	IGSO	(IGSO)*
G_1 (MW)	{119.75}*	{130.94}*	127.65	120.12	119.87	118.21	118.10	118.25	118.55	118.04	(133.66)*
G_2 (MW)	{106.35}*	{94.46}*	100.37	105.27	101.89	103.93	103.87	103.31	104.22	103.51	(96.36)*
G_3 (MW)	{91.81}*	{93.09}*	89.82	92.55	96.28	95.84	96.05	96.41	95.19	96.43	(88.11)*
V_1 (pu)	{1.05}*	{0.959}*	1.049	1.050	1.040	1.047	1.045	1.050	1.048	1.045	(0.994)*
V_2 (pu)	{1.05}*	{1.014}*	1.037	1.043	1.025	1.040	1.027	1.047	1.045	1.048	(1.046)*
V_3 (pu)	{1.04}*	{1.047}*	1.037	1.037	1.025	1.043	1.046	1.040	1.041	1.041	(1.050)*
Fuel cost ($/hr)	{1134.2}*	{1140.06}*	1137.31	1134.37	1134.85	1133.98	1134.09	1133.99	1133.99	**1133.96**	(1141.63)*
Mean ($/hr)	-	{1140.65}*	1139.68	1136.21	1135.89	1134.55	1135.63	1134.71	1134.61	**1134.12**	(1141.77)*
Worst ($/hr)	-	{1141.57}*	1140.76	1141.82	1137.24	1135.66	1138.49	1136.38	1135.67	**1134.52**	(1142.11)*
Std. Dev. ($/hr)	-	{0.456}*	0.67	2.00	0.69	0.59	1.13	0.69	0.65	**0.14**	(0.14)*
Time cost (s)	-	-	39.62	49.3	47.4	45.2	46.1	55.4	42.51	46.1	47.2

Note: { }* are published results, and ( )* are solutions of TSCOPF with complex power system models.

For the investigation of the impacts of complex power system models on TSCOPF solution, Table 5.1 also includes the IGSO optimal solution for TSCOPF with 4th order generator model and IEEE Type 1 exciters in the last column. The best fuel cost obtained is 1,141.63 $/hr which is also better than the

counterpart in [40] with fuel cost of 1,143.42 $/hr. Compared with the solutions with classical model, the fuel cost is increased by about 1% but with quite different generator outputs as well as generator angle and kinetic energy as plotted in Fig. 5.3 and Fig. 5.4. This indicates that complex power system models are necessary in practice for accurate representation of the system dynamics of TSCOPF problem.
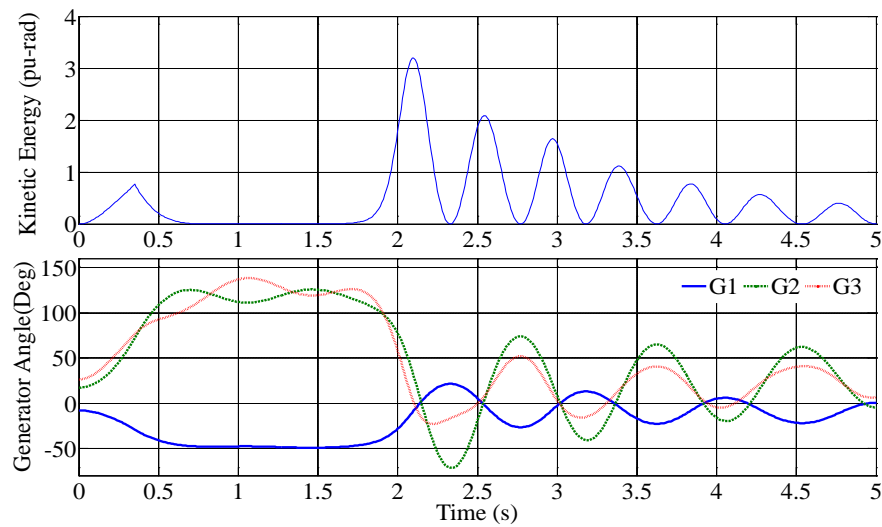
Fig. 5.4 Angle and energy curves of 9-bus system with complex model after optimization

5.4.2   Case B : 10-generator 39-bus System

The New England 10-generator 39-bus system [149] was used as the second test system to evaluate the effectiveness of the proposed IGSO method. The fuel cost coefficients for the quadratic polynomial objective of TSCOPF are extracted from [45] for benchmarking with [42, 43] without considering any valve-point effects and POZs. The contingency is a fault occurred at 21-16 near bus 21 and cleared by line tripping after 0.16 s.

The parameter settings for all the AIs are the same as in Case A except for the population size which is fixed as following: 40 individuals for GA, EPSO and MGSO, 38 for GSO, GSOISW and OGSOMDE, 35 for the proposed IGSO method, such that the total number of function evaluations for each method

remains the same.

As shown in Table 5.2, DE stabilized the system with a fuel cost of 60,988.25 $/hr in [43] and CPU time of 91.86s running on a computer with Intel Pentium IV 2.66GHz CPU and 512M RAM. In [42], the OMIB equivalent method found a stable solution with fuel cost of 60,937.85 $/hr and a normalized CPU time of 57.39 p.u. for one OPF without stability constraints plus one time-domain simulation. Table 5.2 also lists the statistical results obtained with all the AIs including the proposed IGSO method running on the MATLAB distributed computing platform. It is clear that all AIs including the EPSO proposed in Chapter IV approach an excellent optimal solution with comparable CPU time while the proposed IGSO method has the most economic solution 60,925.21 $/hr with lowest mean fuel cost and smallest standard deviation compared with others.

Table 5.2 Optimal solutions of different methods for New England system in

Case B

Variables	Generator optimal outputs (MW)									
	{OMIB [42]}*	{DE [43]}*	DE [43]	GA [60]	GSO [162]	MGSO [164]	GSO-SW [165]	OGSO-DE [166]	EPSO in Chapter IV	IGSO
G30	{245.94}*	{237.06}*	244.16	247.24	242.61	244.18	249.06	245.67	244.48	244.37
G31	{572.56}*	{587.35}*	568.53	569.85	568.50	567.55	569.65	568.15	569.44	568.11
G32	{648.11}*	{668.64}*	647.41	640.85	644.02	642.45	638.56	645.41	643.15	646.15
G33	{627.56}*	{634.92}*	614.33	630.69	629.50	632.39	628.39	631.39	621.98	631.84
G34	{505.91}*	{493.77}*	524.35	503.68	513.75	511.38	505.50	507.22	506.53	504.78
G35	{628.12}*	{619.79}*	609.94	648.05	644.79	648.67	645.90	645.40	650.53	641.96
G36	{539.01}*	{514.00}*	567.23	557.54	555.76	550.32	556.26	552.97	563.52	556.93
G37	{539.94}*	{542.87}*	550.60	530.29	530.81	539.51	534.15	533.26	537.12	533.40
G38	{833.38}*	{837.03}*	820.67	825.64	823.72	818.42	827.35	831.82	824.71	827.87
G39	{998.56}*	{1003.93}*	992.99	985.65	986.50	984.75	985.50	978.79	978.15	984.07
Best FC ($/h)	{60937.85}*	{60988.25}*	60965.70	60928.57	60935.42	60930.12	60940.82	60930.48	60925.53	**60925.21**
Mean FC($/h)	-	{61027.57}*	61010.60	60943.79	60969.37	60946.41	60962.92	60936.94	60939.55	**60932.99**
Worst FC($/h)	-	{61068.87}*	61078.12	60985.34	61078.12	61030.32	60993.02	60998.67	60983.91	**60936.94**
Std. Dev. ($/h)	-	{24.41}*	37.77	13.24	31.90	25.87	19.29	14.70	17.79	**2.98**
CPU time (s)	{57.39 p.u.}*	{91.86}*	53.38	63.27	54.16	56.37	57.27	63.99	58.46	57.82

Note: { }* are published results.

5.4.3 Case C : 10-generator 39-bus System with POZs

The third case study was also conducted on the New England 10-machine 39-bus system but with 4th order dynamic generator model [160] and Type 1 exciter with parameters listed in appendix A and Table C.1. The generation valve point effects and POZs are also considered in this study. The coefficients of fuel cost with valve-point effects consist of a_i, b_i, c_i, from [45] plus e_i=200, f_i,=0.35 for i=1, 2…5 and e_i=300, f_i=0.22 for i=6, 7…10 with generation rating given in [45]. The POZs are set to an interval of 10% of the generation range in the middle of the original operation zone for each generator. The control variables include 9 active power outputs and 10 generator terminal voltages. The static constraints are the same as the ones provided in Matpower [170] and the node voltage range is [0.94, 1.06]. The contingency is a three-phase earth fault at line 4-5 near bus 4 and subsequently cleared by tripping line 4-5 at 300ms. The population size for DE, GA, EPSO and MGSO methods are 40; GSO, GSOISW and OGSOMDE methods have 38 individuals while IGSO has a population size of 35.
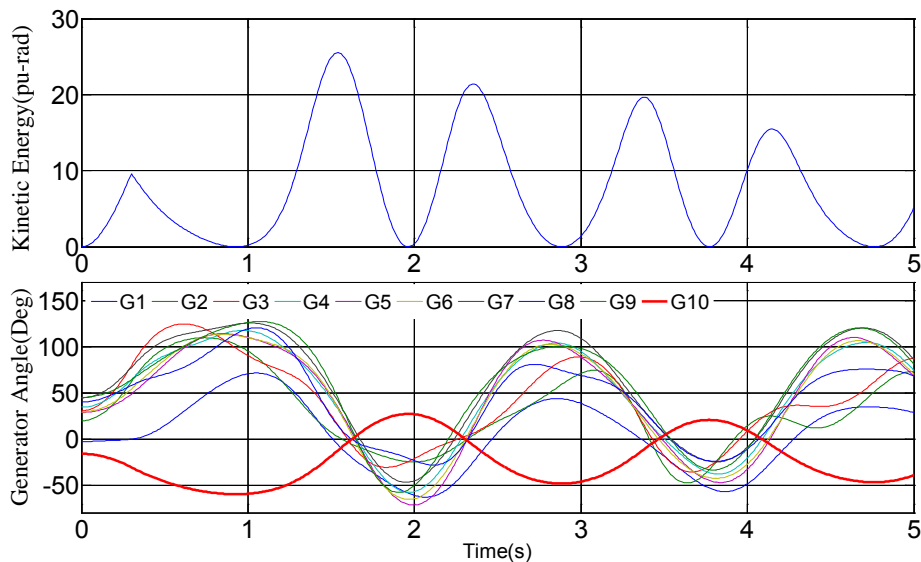
Fig. 5.5 Angle and energy of New England system after optimization in Case C

Table 5.3 shows the best solution of DE[43], GA[60], GSO[162], MGSO[164], GSOISW[165], OGSOMDE[166], EPSO and IGSO with the corresponding best fuel costs of 62,986.22 $/h, 61,299.60 $/h, 61,350.17 $/h, 61,404.71 $/h,

61,411.45 \$/h, 61,299.13 \$/h, 61,314.37 \$/h and 61,250.64 \$/h, respectively. While all the solutions are stable without violating any generation and voltage limits, the one from IGSO method is the most economic. Fig. 5.5 plots the 10 generator angles and kinetic energy curves for the best solution of IGSO method and shows that the system is indeed stable with maximum generator angle reached 140°.

Further comparison of the statistical results among all the AIs for 20 independent runs showed that the proposed IGSO method has the lowest mean fuel cost 61,488.55 \$/h, the smallest worst fuel cost 61,783.59 \$/h, and the lowest standard deviation 135.63 \$/h while the CPU time of various AIs are comparable. This verified that the proposed IGSO method indeed outperformed the other AIs including EPSO in terms of both solution quality and consistency. Fig. 5.6 plots the average convergence curve of all the AIs. It is evident that IGSO is able to find the lowest mean fuel cost with good convergence.

Table 5.3 Optimal solutions of different AIs for New England system in Case C

Variables	Generator optimal outputs							
	DE [43]	GA [60]	GSO [162]	MGSO [164]	GSO-ISW [165]	OGSO-MDE [166]	EPSO in Chapter IV	IGSO
G_1 (MW)	157.50	251.34	251.35	252.09	250.91	260.20	269.31	242.56
G_2 (MW)	448.50	422.25	439.82	466.75	457.77	457.77	484.70	484.66
G_3 (MW)	537.56	664.14	647.98	637.50	636.21	637.31	637.51	646.37
G_4 (MW)	660.56	637.31	637.38	628.92	628.32	619.21	628.61	601.15
G_5 (MW)	591.36	511.69	511.57	511.81	502.96	511.54	466.00	493.79
G_6 (MW)	643.11	642.64	656.91	642.69	656.47	641.15	685.05	656.85
G_7 (MW)	629.21	571.21	571.20	571.34	570.85	571.64	499.91	599.59
G_8 (MW)	547.40	556.95	556.96	557.35	556.38	557.04	556.92	571.30
G_9 (MW)	789.65	856.90	841.47	842.65	856.34	842.94	856.30	756.83
G_{10} (MW)	1140.72	1028.80	1028.22	1030.66	1027.28	1042.54	1056.72	1085.23
V_1 (pu)	1.058	1.049	1.048	1.048	1.045	1.046	1.038	1.045
V_2 (pu)	1.012	0.981	0.981	0.984	0.976	0.988	0.968	0.997
V_3 (pu)	1.009	0.985	0.984	0.999	0.979	0.985	0.990	0.984

V_4 (pu)	0.979	0.997	0.998	1.004	0.990	1.009	1.001	0.999
V_5 (pu)	0.941	1.011	1.012	1.015	1.006	1.009	1.010	1.011
V_6 (pu)	1.008	1.059	1.048	1.049	1.045	1.049	1.040	1.055
V_7 (pu)	1.052	1.060	1.058	1.058	1.051	1.057	1.055	1.047
V_8 (pu)	1.029	1.030	1.027	1.029	1.022	1.029	1.034	1.025
V_9 (pu)	1.023	1.027	1.024	1.028	1.021	1.033	1.029	1.003
V_{10} (pu)	0.969	1.031	1.029	1.026	1.023	1.025	0.969	1.020
Best FC ($/h)	62986.22	61299.60	61350.17	61404.71	61411.45	61299.13	61314.37	**61250.64**
Mean FC ($/h)	63636.10	61768.18	61634.89	61602.52	61583.88	61546.36	61575.29	**61488.55**
Worst FC ($/h)	65146.48	62383.60	61906.64	61894.65	61971.97	61959.06	61929.91	**61783.59**
Std. Dev. ($/h)	534.22	282.64	164.45	144.33	144.98	165.48	161.48	**135.63**
CPU time (s)	65.70	73.89	68.99	69.62	71.23	74.87	64.79	70.09
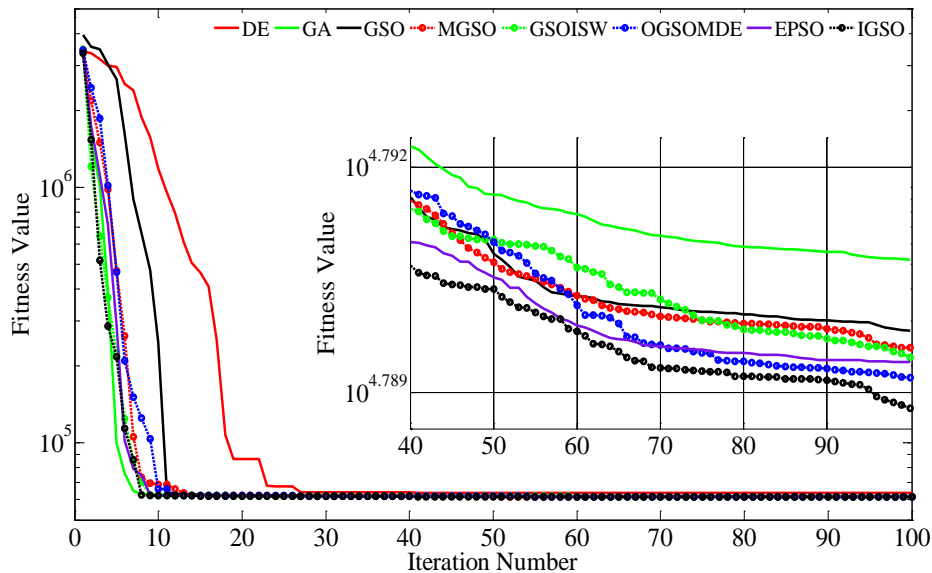
Fig. 5.6 Convergence of different methods for New England system in Case C

5.4.4 Case D : 50-generator 145-bus System with POZs

The IEEE 50-generator 145-bus system was tested as the fourth case study for validating the IGSO method on a larger power grid. The control variables consist of the active power outputs of 49 generators and the terminal voltage of 50 generators, thus there are 99 optimal variables in total. The dynamic data is obtained from [150], in which all the generators are modelled as classical model except those at bus 93,104, 105, 106, 110 and 111 which use a 4th order model,

i.e. G_9, G_{20}, G_{21}, G_{22}, G_{25}, G_{26} in Table 5.4, with IEEE Type 1 exciter and its parameters listed in Table C.1. The optimal range of generation is [0, 1.4×P_{rating}], where P_{rating} is the generator rating. All bus voltages are limited in the range [0.9, 1.15]. Coefficients of fuel cost with valve-point effects are: *a=0.01, b=0.3, c=0.2, e=100, f=8.4* for G_1 to G_{30}; *a=0.006, b=0.3, c=0.2, e=150, f=6.3* for G_{31} to G_{50}. The POZs are set to an interval of 10% of the generation range in the middle of the original operation zone for each generator. The population size of DE, GA, EPSO and MGSO are 100, and 98 for MGSO, GSOISW and OGSOMDE, while IGSO has a population size of 95.
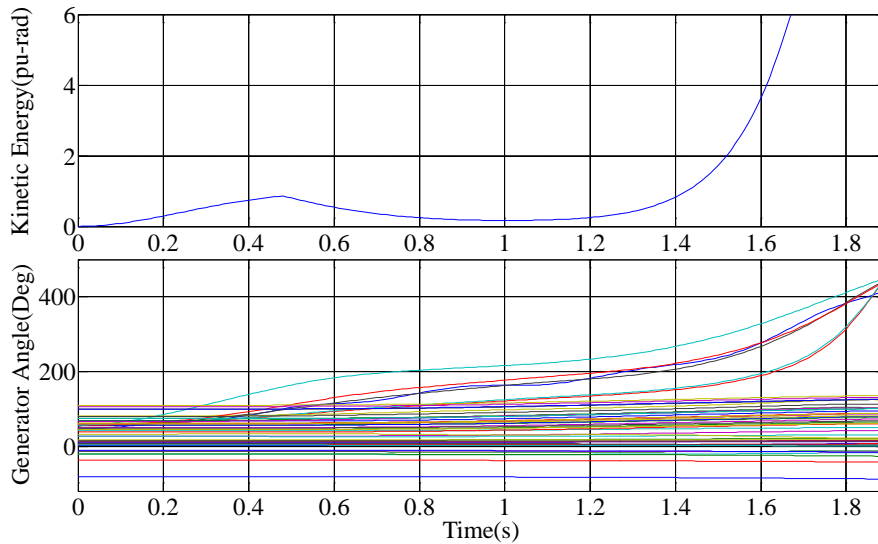
Fig. 5.7 Angle and energy of IEEE 50-gen system before optimization in Case D

The contingency is a three-phase ground fault occurred at the end of line 138-95 near bus 138, and subsequently cleared by tripping line 138-95 at 500ms. The system is unstable with the default generation setting. Fig. 5.7 plots the generator angle and energy curves and shows that G_1, G_3, G_4, G_7, G_{10} and G_{11} are the critical machines while the rest are non-critical machines.

With 20 runs of the proposed IGSO method, Table 5.4 shows the best solution with fuel cost 46,043,271.01 \$/h without violating any constraints. The effects of POZs constraints can be observed from the generation of G_1, G_{19}, G_{21}, G_{38} and G_{42} being bounded at the upper limit of POZs while G_2 was bounded at lower

limit of POZs. Fig. 5.8 plots the corresponding generator angle and system kinetic energy curves and clearly shows that the system is stable with maximum rotor angle close to 180° which is significantly larger than the empirical threshold of 100° in [11, 13], 120° in [18, 19, 29], or $4\pi/5$ radian in [17].

Table 5.4 Optimal solution of IGSO method for IEEE 50-gen system in Case D

Variables	IGSO				
$G_1(V_1)$	**39.27**	1.0988	$G_{26}(V_{26})$	1665.46	0.9981
$G_2(V_2)$	*936.18*	1.1050	$G_{27}(V_{27})$	245.64	0.9559
$G_3(V_3)$	307.37	1.1408	$G_{28}(V_{28})$	2252.40	1.1128
$G_4(V_4)$	45.95	1.1411	$G_{29}(V_{29})$	3798.20	1.1107
$G_5(V_5)$	43.52	0.9098	$G_{30}(V_{30})$	2122.38	1.0383
$G_6(V_6)$	767.88	1.1027	$G_{31}(V_{31})$	3840.20	1.0294
$G_7(V_7)$	26.86	0.9607	$G_{32}(V_{32})$	9904.95	1.1029
$G_8(V_8)$	23.89	0.9000	$G_{33}(V_{33})$	3404.67	1.0802
$P_9(V_9)$	692.88	1.0120	$G_{34}(V_{34})$	1058.86	1.0578
$G_{10}(V_{10})$	247.37	1.0333	$G_{35}(V_{35})$	4207.00	1.0093
$G_{11}(V_{11})$	109.23	1.0227	$G_{36}(V_{36})$	14249.05	1.0400
$G_{12}(V_{12})$	60.45	1.0486	$G_{37}(V_{37})$	8280.49	1.1219
$G_{13}(V_{13})$	130.51	0.9621	$G_{38}(V_{38})$	**21791.00**	1.0970
$G_{14}(V_{14})$	587.28	0.9797	$G_{39}(V_{39})$	4333.00	0.9808
$G_{15}(V_{15})$	192.30	1.0497	$G_{40}(V_{40})$	27232.82	1.1194
$G_{16}(V_{16})$	205.32	1.0881	$G_{41}(V_{41})$	8374.41	1.1246
$G_{17}(V_{17})$	250.46	1.0192	$G_{42}(V_{42})$	**40001.50**	1.0552
$G_{18}(V_{18})$	2059.41	0.9773	$G_{43}(V_{43})$	14306.98	1.0682
$G_{19}(V_{19})$	**103.95**	0.9669	$G_{44}(V_{44})$	32195.66	1.1164
$G_{20}(V_{20})$	930.77	1.0894	$G_{45}(V_{45})$	27431.87	0.9733
$G_{21}(V_{21})$	**1247.40**	1.0370	$G_{46}(V_{46})$	29211.03	1.0379
$G_{22}(V_{22})$	873.11	0.9524	$G_{47}(V_{47})$	25321.20	1.1459
$G_{23}(V_{23})$	979.25	1.0538	$G_{48}(V_{48})$	7219.72	1.0046
$G_{24}(V_{24})$	72.77	0.9146	$G_{49}(V_{49})$	15955.80	1.0000
$G_{25}(V_{25})$	759.11	0.9664	$G_{50}(V_{50})$	21834.87	1.1063
Cost	46043271.01($/h)				

Note: The units for generation and voltage are MW and per unit.
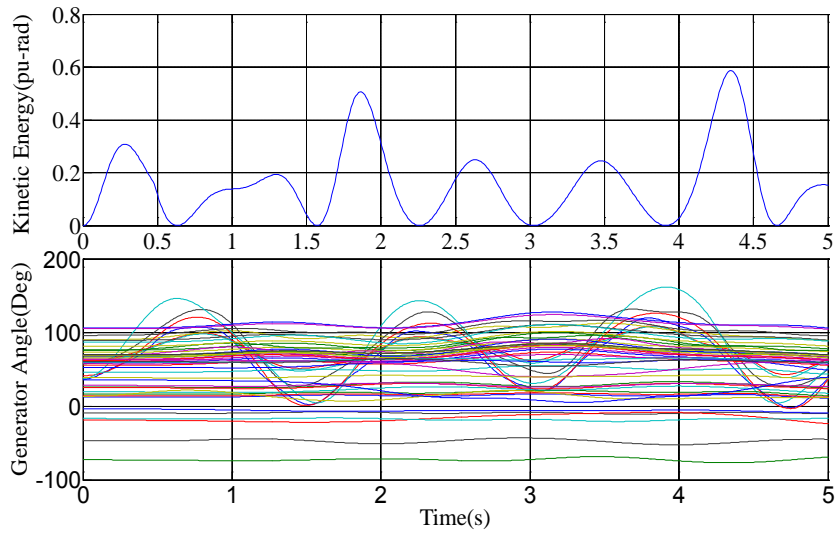
Fig. 5.8 Angle and energy of IEEE 50-gen system after optimization in Case D
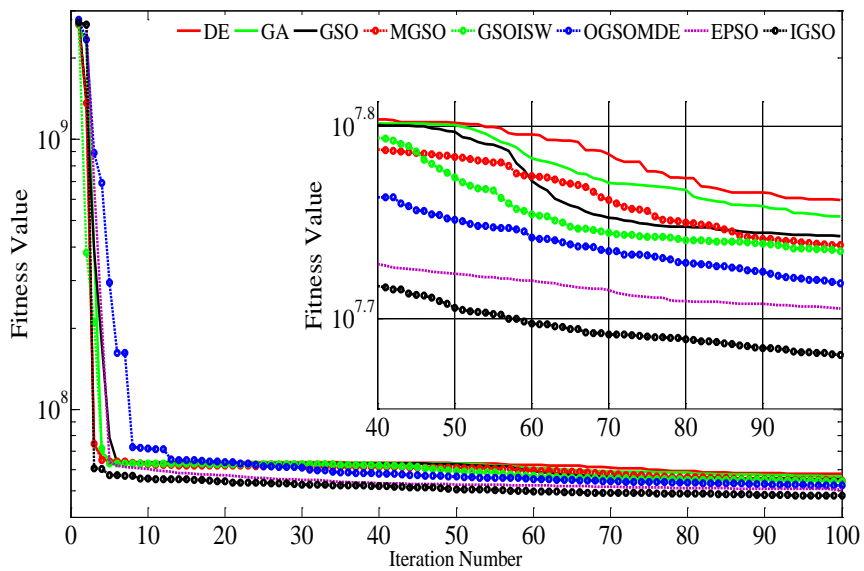
Fig. 5.9 Convergence of different methods for IEEE 50-gen system in Case D

Table 5.5 Comparisons of different AIs for IEEE 50-gen system in Case D

Fuel Cost	DE [43]	GA [60]	GSO [162]	MGSO [164]	GSO-ISW [165]	OGSO-MDE [166]	EPSO in Chapter IV	IGSO
Best ($/hr)	55032371.54	53920751.33	52386874.34	53466038.74	52216875.00	49739707.81	49212273.27	**46043271.01**
Mean ($/h)	57783502.58	56622866.91	55317901.43	54727309.22	54315216.66	52296503.87	50717998.90	**47984385.80**
Worst $/h)	61363637.67	59692039.35	59547554.79	56342188.82	58827847.14	57153966.81	52101561.24	**49410461.11**
Std. ($/h)	1805766.28	1590076.79	1860467.10	952195.23	2089197.63	2134928.66	964491.61	1062587.63
Std. Dev. (%)	3.1%	2.8%	3.4%	1.7%	3.8%	4.1%	112.68	2.2%
CPU Time (s)	100.21	114.35	107.12	111.47	117.76	122.60	49212273.27	116.94

Fig. 5.9 plots the average convergence of all the AIs after 20 runs. It is obviously that the proposed IGSO method does have the best convergence and obtained the most economic solution. Details of the statistical results are given in Table 5.5. The average fuel cost of IGSO is 47,984,385.80 $/hr, which was reduced by 17%, 15%, 13%, 12%, 11%, 8% and 5% compared with the counterpart of DE [43], GA [60], GSO[162], MGSO[164], GSOISW[165], OGSOMDE[166] and EPSO in Chapter IV, respectively. Also, in terms of the best and worst value, IGSO is the best one for this IEEE 50-generator 145-bus system with comparable standard deviation.

5.5   Summary

The practical operation limitations caused by generation prohibited operation zones is considered and incorporated into the formulation of the TSCOPF model. A tailor-made solution method IGSO is proposed based on the GSO with new enhancement features including backward searching strategy, Cauchy mutation and inheritance operator. Four comprehensive case studies on the WSCC 9-bus system, New England 39-bus system, and IEEE 145-bus system with complex power system models have verified the superiority of the proposed IGSO method with results benchmarked and compared against seven representative artificial intelligence algorithms including the EPSO proposed in Chapter IV.

Chapter VI

Optimization of Probabilistic TSCOPF with Renewable Energy Uncertainties

6.1   Introduction

In Chapter III to V, the deterministic TSCOPF problem is comprehensively investigated to find an optimal point for power systems operation with predefined parameters, while the uncertainties in practical power systems such as the uncertain loads injections or fault clearing time etc. are not considered. With the increasing concerns on environment and energy conservation, the high penetration of renewable energy generation would surely bring even more uncertainties to power systems and challenge the safe operation of power grid. Therefore, a probabilistic TSCOPF (P-TSCOPF) model capable of coordinating the economics, transient stability and uncertainties would be timely and desirable for the new generation of power system preventive control. However, so far there is still no satisfactory solution method published for such P-TSCOPF model yet.

In this chapter, a novel P-TSCOPF model is first proposed to consider generation and operation uncertainties in TSCOPF for power system preventive control. In the proposed P-TSCOPF, the wind generation systems are dynamically modelled with rotor flux magnitude and angle control (FMAC) while stochastic loads injections, fault clearing time, and wind generations are all considered with their individual correlations handled effectively by the $2m+1$ PE method with Cholesky decomposition. Furthermore, a new IGSO-PE solution approach is developed using the IGSO algorithm and PE method to efficiently solve the P-TSCOPF problem. The validity of the proposed P-TSCOPF model

and the effectiveness of the IGSO-PE method have been thoroughly tested and evaluated on a modified New England system.

6.2 Model of Wind Generations

In the proposed P-TSCOPF model, the wind generation system used for transient stability analysis consists of a dynamic wind turbine (WT) model with two lumped-mass shaft as described in (6.1)-(6.2) [48], and a Doubly Fed Induction Generator (DFIG) model with partial scale frequency converter as shown in Fig. 6.1 [171].

$$\frac{d\theta_{tw}}{dt} = \omega_b \left(\omega_t - \omega_r \right) \tag{6.1}$$

$$\frac{d\omega_t}{dt} = \frac{1}{2H_t} \left[\frac{P_m}{\omega_t} - K_{tw}\theta_{tw} - D_{tw} \left(\omega_t - \omega_r \right) \right] \tag{6.2}$$

where ω_t, ω_r and ω_b are the turbine speed, rotor speed and system base speed, respectively; θ_{tw} (rad) is the shaft twist angle; K_{tw} (p.u./rad) and D_{tw} are the shaft stiffness and mechanical damping coefficients; H_t (s) is wind turbine inertia constant; P_m is the mechanical power extracted from the wind.
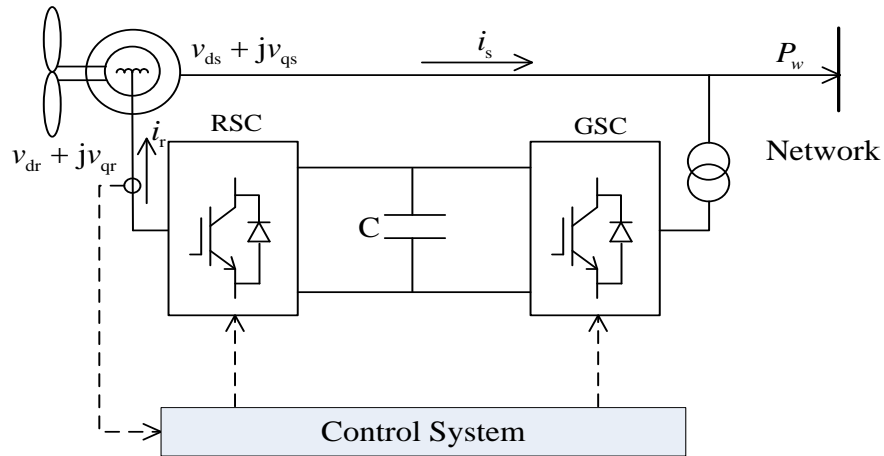
Fig. 6.1 Structure of Doubly Fed Induction Generators

Fig. 6.1 shows the schematic diagram of the DFIG generator widely used for stability analysis in which 1) the dynamics of the DC capacitor can be neglected, and 2) the active powers on the rotor side converter (RSC) and grid side

converter (GSC) are considered as equal. Moreover, GSC is assumed ideal that there is no reactive power exchanged with the grid during the transient and the total reactive power is supported only by the stator [171]. By ignoring the dynamics of the stator current, the DFIG model is derived as

$$\frac{1}{\omega_b}\frac{de_d}{dt} = -\frac{1}{T_0}\Big[e_d - (X - X')i_{qs}\Big] + s\omega_s e_q - \omega_s \frac{L_m}{L_r + L_m}v_{qr} \tag{6.3}$$

$$\frac{1}{\omega_b}\frac{de_q}{dt} = -\frac{1}{T_0}\Big[e_q + (X - X')i_{ds}\Big] - s\omega_s e_d + \omega_s \frac{L_m}{L_r + L_m}v_{dr} \tag{6.4}$$

$$\frac{d\omega_r}{dt} = \frac{1}{2H_g}\Big[K_{tw}\theta_{tw} + D_{tw}(\omega_t - \omega_r) - (e_d i_{ds} + e_q i_{qs})\Big] \tag{6.5}$$

$$v_{ds} = -r_s i_{ds} + X' i_{qs} + e_d \tag{6.6}$$

$$v_{qs} = -r_s i_{qs} - X' i_{ds} + e_q \tag{6.7}$$

$$P_w = v_{ds}i_{ds} + v_{qs}i_{qs} - v_{dr}i_{dr} - v_{qr}i_{qr} \tag{6.8}$$

$$Q_w = v_{qs}i_{ds} - v_{ds}i_{qs} \tag{6.9}$$

where e_d and e_q are d and q components of internal voltage; P_w and Q_w are active and reactive power of DFIG absorbed by network; X and X' are open-circuit and short-circuit reactance; T_0 is the transient open-circuit time constant; H_g is the generator inertia constant.
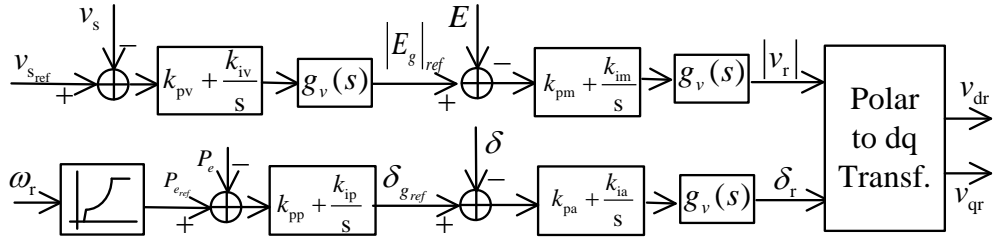
Fig. 6.2 Block diagram of FMAC controller

Fig. 6.2 shows the FMAC structure with two control loops, one for the terminal voltage and the other for the power output of DFIG [171]. It controls the generator terminal voltage and power by adjusting the magnitude and angle of the rotor flux vector, and has the advantage of 1) providing low interaction between the power and voltage control loop, and 2) enhancing voltage recovery after faults.

6.3   General Form of Proposed P-TSCOPF Model

Inspired by the chance constrained programming problems for power system optimization in [172-175], the general formation of the P-TSCOPF model is proposed as

$$\text{Minimize} \quad E\{F(\mathbf{x}^{t_0}, \mathbf{y}^{t_0}, \mathbf{u},)\} \tag{6.10}$$

$$\text{Subject to} \quad \mathbf{G}(\mathbf{x}^{t_0}, \mathbf{y}^{t_0}, \mathbf{u},) = 0 \tag{6.11}$$

$$P\{h_j(\mathbf{x}^{t_0}, \mathbf{y}^{t_0}, \mathbf{u},) \leq \} \geq \beta_j \tag{6.12}$$

$$\begin{cases} \dfrac{d\mathbf{x}}{dt} = \mathbf{H}(\mathbf{x}(t), \mathbf{y}(t), \mathbf{u},) \\ \mathbf{G}(\mathbf{x}(t), \mathbf{y}(t), \mathbf{u},) = 0 \quad t \in (t_0, t_{end}] \\ \mathbf{x}(t_0) = \mathbf{x}^{t_0}, \mathbf{y}(t_0) = \mathbf{y}^{t_0} \end{cases} \tag{6.13}$$

$$P\{\eta(\mathbf{x}(t), \mathbf{y}(t), \mathbf{u},) > 0\} \geq \beta_r \tag{6.14}$$

where symbol E stands for the mathematic expectation calculation; ε is the uncertain variables; u is the control variables with lower and upper limits, such as the traditional generator active power and terminal voltage; $\mathbf{x}(t)$ and $\mathbf{y}(t)$ are the state and algebraic variables during the transient period with initial value as $\mathbf{x}^t_0$ and $\mathbf{y}^t_{0;}$ η is the transient stability margin. Since the objective function would depend on the uncertain variables, its expectation is adopted as the P-TSCOPF objective in (6.10). Equality constraint (6.11) stands for steady-state power flow equation. Constraint (6.12) requires the chance constraints for steady-state variables, such as node voltage magnitudes and transmission line thermal limits, above a fixed security level β_j. (6.13) describes the dynamics of the power system during the transient period, including complex generator models with AVR and dynamic wind generator models. (6.14) is the probabilistic transient stability constraint with an acceptable security level β_r.

The proposed P-TSCOPF model can be interpreted as follows: an optimal solution u is to be searched for power system preventive control such that the expectation of its objective is minimized while the inequality constraints are satisfied with a predefined probability for the optimal solution u. Fig. 6.3 shows

the probability density functions of constraint $h(x,y,\varepsilon,u)$ which has two different control variables u_1 and u_2 with diverse objective expectation $E\{f(x,y,\varepsilon,u)\}$ in solving P-TSCOPF. As the best compromise for smaller probability of constraints violation or higher security level, the proposed P-TSCOPF model would search for the best control u with minimal expected value above a satisfactory security level.
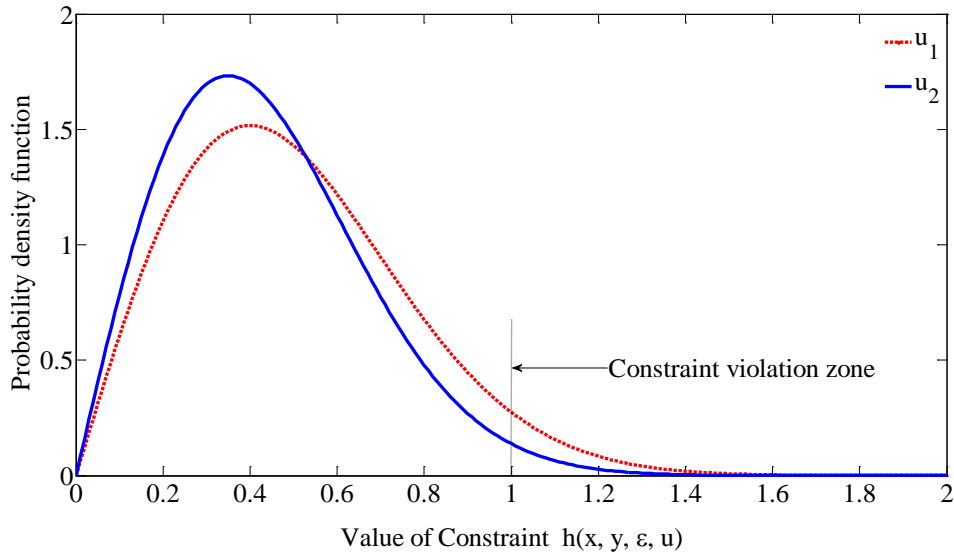
Fig. 6.3 Constraint violations for different control variables

For simplicity, only the following three uncertain variables are considered here in the case study: load injections, wind generations, and fault clearing time, while other uncertain factors, such as fault occurrence, fault type and fault location, could be tackled similarly using the conditional probability approach in [48, 122-124, 176].

1) Probabilistic model of load injection

The continuous varying load injection is an important factor contributing to uncertainties in real power system. Normal distribution is commonly adopted to model the uncertainties of active load injections as [120, 177]

$$f(P_{D_i}) = \frac{1}{\sqrt{2\pi}\sigma_p} e^{-(P_{D_i}-\mu_p)^2/(2\sigma_p^2)} \tag{6.15}$$

where μ_p and σ_p are the mean and standard deviation of probabilistic load active

power. As load power consumption usually has related or dependent patterns in different conditions such as in holiday, in evening or in cold days, the correlations of active load injections in different conditions should therefore be considered and are described here using the correlation coefficients C_{pd} while the reactive load injection is modelled as a variable with a constant ratio to its corresponding active load.

2) Probabilistic model of wind generations

The popular Weibull distribution with shape parameter λ and scale parameter k is used for modelling the probabilistic wind speed as follows [178, 179]

$$f(v_w, \lambda, k) = \frac{k}{\lambda}(\frac{v_w}{\lambda})^{k-1} e^{-(\frac{v_w}{\lambda})^k} \tag{6.16}$$

where v_w is the wind speed. Similarly, the correlation of wind speeds for wind farms at different locations is represented with a correlation coefficient C_v. The wind power output is determined from the linear speed-power curve characteristic of wind turbine [179].

$$P_m = \begin{cases} 0, & (v_w < v_{ci}, \ v_w > v_{ct}) \\ P_{rated} \cdot (\dfrac{v_w - v_{ci}}{v_{rd} - v_{ci}}), & (v_{ci} \le v_w \le v_{rd}) \\ P_{rated}, & (v_{rd} < v_w < v_{ct}) \end{cases} \tag{6.17}$$

where P_{rated} is the rated power; v_{ci}, v_{rd} and v_{ct} are the cut-in, rated and cut-out wind speed, respectively. The distribution of wind generations can be calculated from (6.17) using the wind speed samples based on its probabilistic model (6.16).

3) Probabilistic model of fault clearing time

The fault clearing time t_{cl} used for transient stability analysis here is not a deterministic value, and its probabilistic model is assumed as a normal distribution [123]

$$f(t_{cl}) = \frac{1}{\sqrt{2\pi}\sigma_t} e^{-(t_{cl}-\mu_t)^2/2\sigma_t^2} \tag{6.18}$$

where μ_t and σ_t are mean and standard deviations of t_{cl}.

6.4 Proposed P-TSCOPF Problem: Explicit Formulation

Based on the general form of P-TSCOPF model described in Section 6.3, a representative P-TSCOPF model is constructed here for further investigation and studying in Section 6.6.

1) Objective function

Usually, slack bus generator is used to keep the power balance in the system. However, the uncertainties of random variables would cause the slack bus generation become probabilistic too. As a result, the system total generation fuel cost will be probabilistic, and its expected value shall be adopted as the objective of the proposed P-TSCOPF model as (6.19)

$$F_G = E\{\sum_{i=1}^{n_G}(a_i P_{Gi}^2 + b_i P_{Gi} + c_i)\} \tag{6.19}$$

where P_G is the active power of traditional generators, n_G is the total generator number.

2) Static equality constraints

The static constraints (6.11) for the P-TSCOPF problem are explicitly described by the following power flow equations.

$$\begin{cases} 0 = P_{Gi} + P_w - P_{Di} - V_i \sum_{j=1}^{n_b} V_j (G_{ij} \cos\theta_{ij} + B_{ij} \sin\theta_{ij}) \\ 0 = Q_{Gi} + Q_w - Q_{Di} - V_i \sum_{j=1}^{n_b} V_j (G_{ij} \sin\theta_{ij} - B_{ij} \cos\theta_{ij}) \end{cases} \tag{6.20}$$

where $i=1,2,\ldots,n_b$; n_b is the total number of nodes; P_{Di} is the active load; Q_{Gi} and Q_{Di} are the generator reactive output and the reactive load; V_i and V_j are the voltage magnitude of node i and j; θ_{ij} is the angle difference between node i and j. These active and reactive power balance constraints are enforced in initialization and subsequent time domain simulations for transient stability analysis.

3) Static probabilistic inequality constraints

The static constraints (6.12) explicitly include the probabilistic constraints for

generator reactive power, node voltage and transmission line thermal limit as

$$P\{Q_{Gi\,\min} \le Q_{Gi} \le Q_{Gi\,\max}\} > \beta_Q \quad (i = 1, 2, \ldots\ldots, n_G) \tag{6.21}$$

$$P\{V_{i\,\min} \le V_i \le V_{i\,\max}\} > \beta_V \quad (i = 1, 2, \ldots\ldots, n_b) \tag{6.22}$$

$$P\{S_{l_i} \le S_{l_i\,\max}\} > \beta_S \quad (i = 1, 2, \ldots.. n_l) \tag{6.23}$$

where n_l is the index of branches and S_{li} is the apparent power in the ith branch. These probabilistic constraints ensure that bus voltage, generator reactive power and power flow of transmission line are bounded in the required ranges with an acceptable security level.

4) Dynamic equality constraint

Equality constrains (6.13) are a set of differential algebraic equations (DAEs) describing the dynamic behaviours of power system components including the traditional and wind generators. In this chapter, a four-order dynamic model with IEEE Type 1 exciter [169] is adopted for presenting the traditional generators while the dynamic WT and DFIG model presented in Section 6.2 is used to model the wind generators.

5) Probabilistic transient stability constraint

The SIME method has been an effective strategy for transient stability assessment [93, 94] and TSCOPF problem [42, 66]. With the transient stability margin η calculated by the SIME method in Chapter III, the probabilistic stability constraint (6.14) of the proposed P-TSCOPF model could be expressed as

$$P\{\eta > 0\} \ge \beta_r \tag{6.24}$$

In other words, the proposed explicit P-TSCOPF model would consists of objective (6.19), power balance equality constraint (6.20), DAEs for the wind generator model (6.1)-(6.9) and four-order traditional generators with IEEE Type 1 exciters, probabilistic static inequality constraints (6.21)-(6.23), and probabilistic transient stability constraints (6.24). The challenge for solving this model is how the probabilistic constraints (6.21)-(6.24) could be effectively evaluated.

6.5   Methodology

The new IGSO-PE method proposed here uses a two-stage approach for solving the P-TSCOPF model. In the first stage, the PE method is used to calculate the probability of concerned output variables. The IGSO algorithm in Chapter V is then used in the second stage to search for the optimal generation outputs that would minimize the expected total fuel cost as well as satisfy all the probabilistic security constraints.

6.5.1   Point Estimated Method

$2m+1$ PE method concentrates the statistical information provided by the first four central moments on three points for each variable [120, 121]. Based on these concentrations and the function relating input and output variables, the uncertain properties of outputs can be estimated.

The uncertain input variables in the proposed model, denoted as (z_1, z_2,..., z_l,... ,z_m), include the stochastic load injections, uncertain wind generations and the normal distributed fault clearing time. Based on probability theory [120, 121], the $2m+1$ PE method would generate three concentrations for each uncertain variable as follows: the uncertain variable z_l is replaced with three locations $z_{l,k}$ (k=1,2,3), while the remaining m-1 uncertain variables are fixed at their mean value μ_{z1}, μ_{z2},..., μ_{zm}, thus three vectors, referred as concentrations of PE, would be formed in terms of (μ_{z1}, μ_{z2},... $z_{l,k}$,..., μ_{zm}). Similarly, in total $3m$ concentrations (μ_{z1}, μ_{z2},... $z_{l,k}$,..., μ_{zm}) (k=1,2,3, l=1,2,…,m) would be generated for the uncertain vector (z_1, z_2,..., z_l,... ,z_m) with m random variables. The location $z_{l,k}$ is expressed as

$$z_{l,k} = \mu_{zl} + \varepsilon_{l,k} \cdot \sigma_{zl} \quad k = 1, 2, 3 \tag{6.25}$$

where l=1,…,m; $\varepsilon_{l,k}$ is the standard location, μ_{zl} and σ_{zl} are the mean and standard deviation of the variable z_l. The standard location $\varepsilon_{l,k}$ and weight $\omega_{l,k}$ are obtained by Hong's method [121]

$$\varepsilon_{l,k} = \frac{\lambda_{l,3}}{2} + (-1)^{3-k}\sqrt{\lambda_{l,4} - \frac{3\lambda_{l,3}^2}{4}} \quad k = 1,2$$
$$\varepsilon_{l,3} = 0 \qquad\qquad\qquad\qquad\qquad k = 3 \tag{6.26}$$

$$\omega_{l,k} = \frac{(-1)^{3-k}}{\varepsilon_{l,k}(\varepsilon_{l,1} - \varepsilon_{l,2})} \quad k = 1,2$$
$$\omega_{l,3} = \frac{1}{m} - \frac{1}{\lambda_{l,4} - \lambda_{l,3}^2} \quad k = 3 \tag{6.27}$$

where $\lambda_{l,3}$ and $\lambda_{l,4}$ are the skewness and kurtosis of variable z_l. In (6.26), the setting $\varepsilon_{l,3}=0$ yields $z_{l,k}=\mu_{zl}$ in (6.25), thus m of the concentrations are the same as $(\mu_{z1}, \mu_{z2},..., \mu_{zl},... ,\mu_{zm})$, and the total number of concentrations would reduce from $3m$ to $2m+1$.

With the known concentrations, which are a set of deterministic scenarios standing for the uncertain variables, the conventional power flow and transient stability analysis are conducted at each concentration to calculate the concerned outputs, say the slack bus generation, the reactive power of each generator, node voltages, transmission line power flows and the transient stability margin η. Here the relationship between these outputs S and the concentration $(\mu_{z1}, \mu_{z2},... z_{l,k},..., \mu_{zm})$ is denoted by function F as

$$S_{l,k} = F(\mu_{z1},\mu_{z2},\ldots, z_{l,k},\ldots,\mu_{zm}) \tag{6.28}$$

where $S_{l,k}$ is a vector of concerned outputs obtained by deterministic power flow and transient stability analysis at concentration $(\mu_{z1}, \mu_{z2},... z_{l,k},..., \mu_{zm})$. Then, by using $S_{l,k}$ with its weights $\omega_{l,k}$, the jth raw moment m_j of outputs S is calculated as

$$m_j = E(S^j) = \sum_{l=1}^{m}\sum_{k=1}^{3}\omega_{l,k}\cdot(S_{l.k})^j = \sum_{l=1}^{m}\sum_{k=1}^{2}\omega_{l,k}\cdot(S_{l.k})^j$$
$$+\sum_{l=1}^{m}\omega_{l,3}\cdot[F(\mu_{z1},\mu_{z2},\ldots,\mu_{zl},\ldots,\mu_{zm})]^j \tag{6.29}$$

Once various order of raw moments of outputs S are obtained, their cumulative distribution functions (CDFs) $F(x)$ can be estimated as (6.30) by using the Gram-Charlier expansion [141].

$$F(x) = \int_{-\infty}^{\tilde{x}} N(u)du - N(\tilde{x})[\frac{K_3}{3!\sigma^3}(\tilde{x}^2 - 1) + \frac{K_4}{4!\sigma^4}(\tilde{x}^3 - 3\tilde{x}) + \frac{K_5}{5!\sigma^5}(\tilde{x}^4 - 6\tilde{x}^2 + 3)] \tag{6.30}$$

where $\tilde{x} = (x - \mu)/\sigma$ is the standardized variable, μ and σ are the mean value and the standard deviation of S; $N(*)$ is the standard normal distribution function; K_j are the jth order cumulant derived from the central moment M_j as

$$
\begin{aligned}
K_3 &= M_3 \\
K_4 &= M_4 - 3(M_2)^2 \\
K_5 &= M_5 - 10M_3M_2
\end{aligned}
\tag{6.31}
$$

where M_j is calculated from raw moment m_j in (6.29) as

$$
\begin{aligned}
M_2 &= m_2 - (m_1)^2 \\
M_3 &= m_3 - 3m_1m_2 + 2(m_1)^3 \\
M_4 &= m_4 - 4m_1m_3 + 6\ m()^2 m_2 - 3(m_1)^4 \\
M_5 &= m_5 - 5m_1m_4 + 10(m_1)^2 m_3 - 10(m_1)^3 m_2 + 4(m_1)^5
\end{aligned}
\tag{6.32}
$$

Once the CDFs for the random outputs, including the generation of slack bus generator, reactive powers of all generators, node voltages, transmission line power flows, stability margin, etc., are obtained by (6.30), the probabilistic constraints in (6.21)-(6.24) and the system total fuel cost expectation (6.19) could be easily evaluated from the CDFs.

6.5.2 Cholesky Decomposition for Handing Correlations

As mentioned in Section 6.3, random variables are often correlated to each other and these correlations should be considered in the probabilistic analysis [180]. The $2m+1$ PE method with Cholesky decomposition in [181] is adopted here to handle the correlated uncertainties in P-TSCOPF. The correlated input variables are first converted to uncorrelated variables by Cholesky decomposition; then the concentration points for these uncorrelated variables are worked out and inversed to find the corresponding correlated input variables.

The following briefly summarizes how the probabilistic correlated input variables are handled using the $2m+1$ PE method with Cholesky decomposition.

1) Based on the probabilistic model given in Section 6.3 for each random input with correlation coefficients, calculate the mean value μ_x, covariance matrix

C_x, skewness coefficients $\lambda_{l,3}$ and kurtosis coefficients $\lambda_{l,4}$ ($l=1,2,...,m$), then obtain the matrix L using the Cholesky decomposition $C_x = LL^T$ where L is an inferior triangular matrix.

2) Transform the mean value, covariance, skewness and kurtosis coefficients to the independent space using the following transformation.

$$
\begin{aligned}
\mu_x' &= L^{-1}\mu_x \\
C_x' &= L^{-1}C_x \\
\lambda_{l,3}' &= \sum_{r=1}^{m}(L_{l,r}^{-1})^3\lambda_{l,3}\sigma_r^3 \\
\lambda_{l,4}' &= \sum_{r=1}^{m}(L_{l,r}^{-1})^4\lambda_{l,4}\sigma_r^4
\end{aligned}
\tag{6.33}
$$

where $L_{l,r}^{-1}$ represents the element at the lth row and r^{th} column of the inverse of matrix L.

3) Calculated the $2m+1$ transformed concentration points as $x' = (\mu_{z1}', \mu_{z2}',..., z_{l,k}',..., \mu_{zm}')$ with corresponding weights $\omega_{l,k}$ by (6.25)-(6.27).

4) Transform the concentration points x' back to the original space by applying the inverse transformation $x = Lx'$.

5) Solve a deterministic power flow and transient stability analysis for each concentration point obtained in Step 4 so as to obtain the solution $S_{l,k}$ in (6.28).

6) Calculate the jth order raw moment m_j by (6.29) and the CDFs of output random variables using Gram-Charlier expansion by (6.30); thus, the fuel cost expectation, the probabilistic inequality constraints (6.21)-(6.23) and probabilistic transient stability constraint (6.24) can be easily evaluated.

6.5.3 Group Search Optimization Method

GSO is an effective global optimization method based on producer-scrounger model developed in [162, 182]. It is initialized with random individuals and approaches the optimal solution by updating the positions of its producer, scroungers and ranger.

In Chapter V, the IGSO has been proposed and successfully applied to solve discontinuous non-convex TSCOPF problems with complex system model. Here, this IGSO method is adopted as the optimization engine for solving the proposed P-TSCOPF model (6.10)-(6.14) which consists of 1) equality constraints, formed by the power flow equations (6.20) and DAEs for the traditional and wind generators, which are implicitly handled by the power flow calculation and time domain simulation embedded within the $2m+1$ PE method, and 2) probabilistic inequality constraints (6.21)-(6.24), evaluated by the $2m+1$ PE method with Cholesky decomposition. The penalty function method [44] is adopted to transform the constrained P-TSCOPF problem to an unconstrained one like (6.34) such that it could be readily optimized using the IGSO method.

$$
\begin{aligned}
Min\ F(x,u) = F_G &+ p_j \max(0, \beta_j - P\{h_j(\mathbf{x}^{t_0}, \mathbf{y}^{t_0}, \mathbf{u},\ )\}) \\
&+ p_r \max(0, \beta_r - P\{\eta(\mathbf{x}(t), \mathbf{y}(t), \mathbf{u},\ )\})
\end{aligned}
\tag{6.34}
$$

where p_j and p_r are the penalty factors to produce large discrimination if any probabilistic constraints in (6.21)-(6.24) are violated.

The following are the main procedures of the proposed IGSO-PE method for solving the P-TSCOPF problem with the flowchart shown in Fig. 6.4.

Step 1: Input system data, specify IGSO parameters and randomly initialize the IGSO particles for control variables within the lower and upper limits;

Step 2: The CDFs of steady-state variables in (6.21)-(6.23), the stability margin in (6.24) and fuel cost are calculated by $2m+1$ PE approach with Cholesky decomposition, then the probabilistic constraint and fuel cost expectation can be evaluated from the corresponding CDFs;

Step 3: Evaluate the fitness of each particle by (6.34);

Step 4: Find the best fitness value among all particles, and determine whether the maximum number of iterations is reached , if yes, go to *Step 6*; otherwise, go to *Step 5*;

Step 5: Increase iteration number and update control variables by IGSO method,

then go to *Step 2*;

Step 6: Output the optimal solutions of P-TSCOPF model.
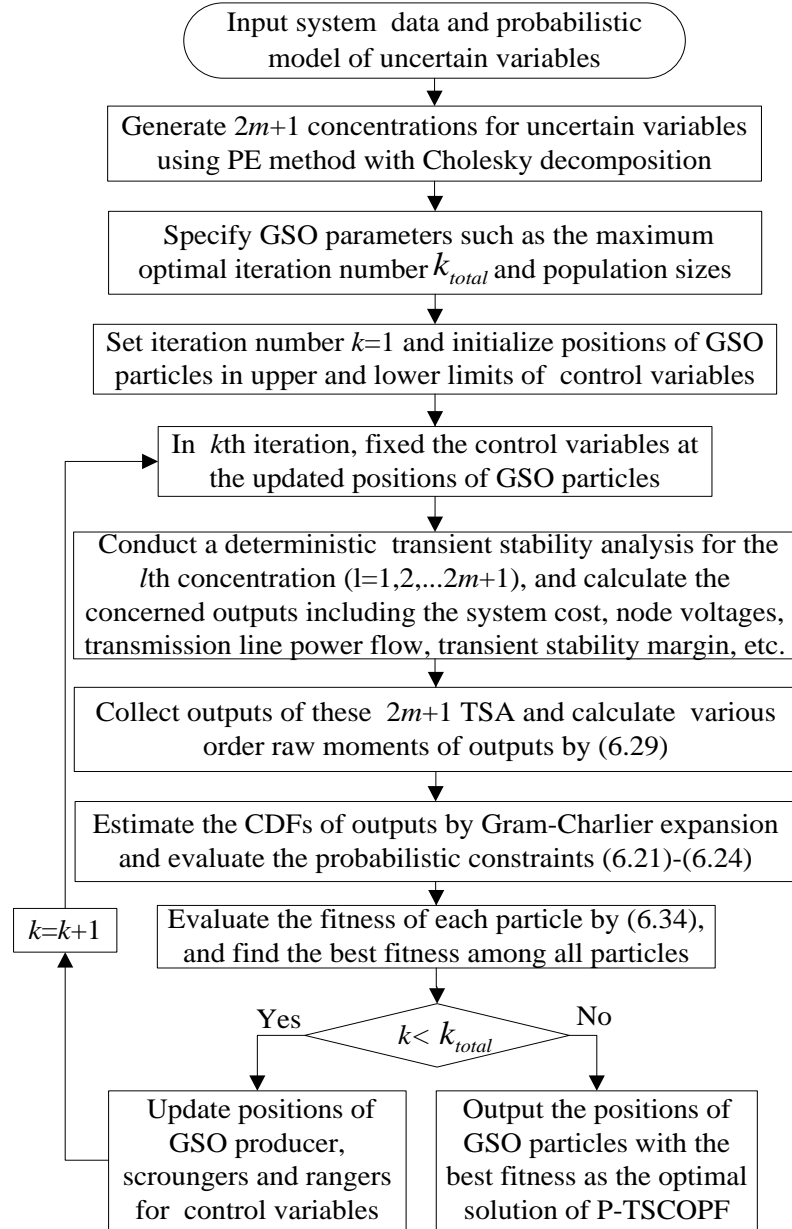
Fig. 6.4 Flowchart of IGSO-PE for solving P-TSCOPF model

6.6   Case Study

For evaluating the proposed P-TSCOPF model and IGSO-PE solution approach, a modified New England 39-bus system with four correlated wind farms (WFs) as shown in Fig. 6.5 is prepared.

The fuel cost coefficients of generators at bus 30 to 39 are cited from [45], and their dynamic model for transient stability analysis are 4th order with data cited from [160], and equipped with IEEE Type 1 exciter with data given in Table C.1. For WFs, an aggregated model is sufficient for investigating its impact on the system transient stability [183]. Specifically, a total number of 100 DFIGs with rated power 2 MW each and parameters cited from [171] are aggregated to form a WF with wind turbine parameters: K_{tw} =0.6p.u./rad, D_{tw}=0.45 and H_t=3.8s.

Fig. 6.5 Modified New England System with four WFs

The contingency considered in transient stability analysis is a three-phase earth fault occurred at the end of line 15-16 near bus 15 at t=0ms, and subsequently cleared by tripping line 15-16 at time t_{cl}. Generator reactive power limits and transmission line thermal limits are cited from Matpower [170]; the node voltages of PQ bus are required to be in the range [0.97, 1.06]. The threshold of all probabilistic constraints (i.e. β_Q, β_V, β_S, and β_r) are assumed as 0.95, which means when all the left hand side of probabilistic constraints (6.21)-(6.24) are not smaller than 0.95, the corresponding operation point is considered as acceptable in the view of security risk.

The following are the uncertain parameter settings for the random variables.

1) The base load given in [170] is assumed as the mean value of the normal distributed load injection with the standard deviation is fixed as 10% of the mean value. There are totally 21 correlated loads with correlations assumed as 0.15.

2) The shape and scale parameters of wind speed are set as $\lambda=2$ and $k=12$ with correlations of 0.3, while the cut-in, cut-out and rated wind speed for WTs are $v_{ci}=3$m/s, $v_{ct}=25$m/s and $v_{rd}=12$ m/s [184], respectively.

3) The normal distribution parameters for the fault clearing time are set as μ_t =350ms, σ_t =0.1 μ_t.

6.6.1 Benchmarking and Comparisons of Results

For evaluating the accuracy and efficiency of the proposed IGSO-PE method, the widely used MC method is also deployed for benchmarking. Both the MC and PE methods run on a PC with a 3.0GHz Intel Core2Quad CPU and 4GB RAM under MATLAB R2010b. The required number of samples in MC is estimated as 5,000 based on the convergence theory [185-187]. The performance of IGSO-PE is compared with MC using the mean and standard deviation (SD) error ε_μ^x and ε_σ^x .

$$\varepsilon_\mu^x = 100(|\mu_{MC} - \mu_{PE}|)/\mu_{MC}[\%] \tag{6.35}$$

$$\varepsilon_\sigma^x = 100(|\sigma_{MC} - \sigma_{PE}|)/\sigma_{MC}[\%] \tag{6.36}$$

where μ_{MC}, σ_{MC}, μ_{PE} and σ_{PE} are the mean value and SD of output random variables calculated by MC and PE method, respectively. The Average Root Mean Square (ARMS) [141] error of output random variables resulted from the PE method is measured by an accuracy index as

$$\text{ARMS} = \frac{\sqrt{\sum_{i=1}^{N}(F_{MC_i} - F_{PE_i})^2}}{N} \tag{6.37}$$

where F_{MCi} and F_{PEi} are the values on the CDF curve solved by MC and PE method, respectively. Here, N is set as 10 for the range of CDF curve with

confident level [2%, 98%].

6.6.2   Investigations on Original Operating Point

The proposed P-TSCOPF model is first checked with the base operating conditions that consists of original generations and slack bus voltage in [160], as detailed in Table 6.1. At this operation point, the probabilistic output of generator at slack bus by the PE method is shown in Fig. 6.6 and the expectation of total fuel cost is relatively low as 57486.97 $/h. However, not all the probabilistic constraints are satisfied with the acceptable security level at this operating point. For example, the probability of voltage profile for bus 4 in range [0.97, 1.06] is only 0.19 as shown in Fig. 6.7, which means the probabilistic voltage constraint (6.22) cannot be fulfilled with the required 0.95 security level. Similarly, the probabilistic constraint for transmission line 6-11 is also violated as shown in Fig. 6.8. With its thermal limit being 6 p.u., the probability of over-loading line 6-11 is 0.5, which considerably violates the limit that probability of line over-loading shall not be larger than 0.05. Moreover, the probabilistic transient stability margin for stable case (η>0) is 0.53 as shown in Fig. 6.9, which indicates that the system would lose transient stability with a probability of 0.47; therefore, the system cannot maintain the transient stability with a satisfactory security level.
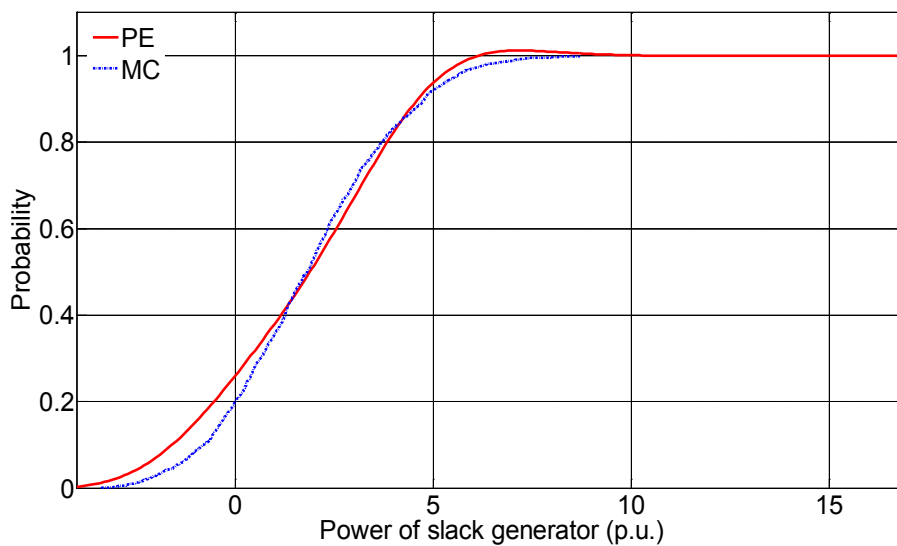
Fig. 6.6 Generation of slack bus without P-TSCOPF
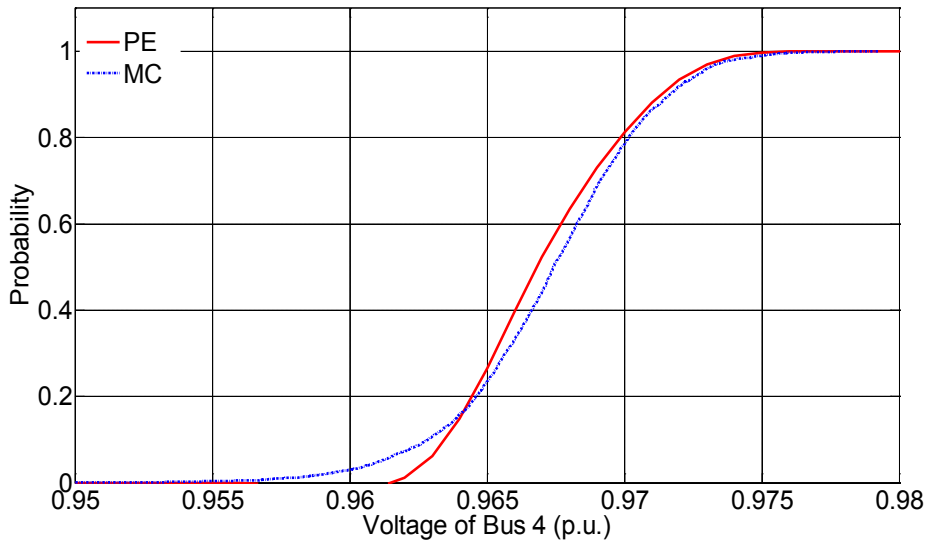
Fig. 6.7 Voltage probability of bus 4 without P-TSCOPF

Fig. 6.8 Power probability of line 6-11 without P-TSCOPF
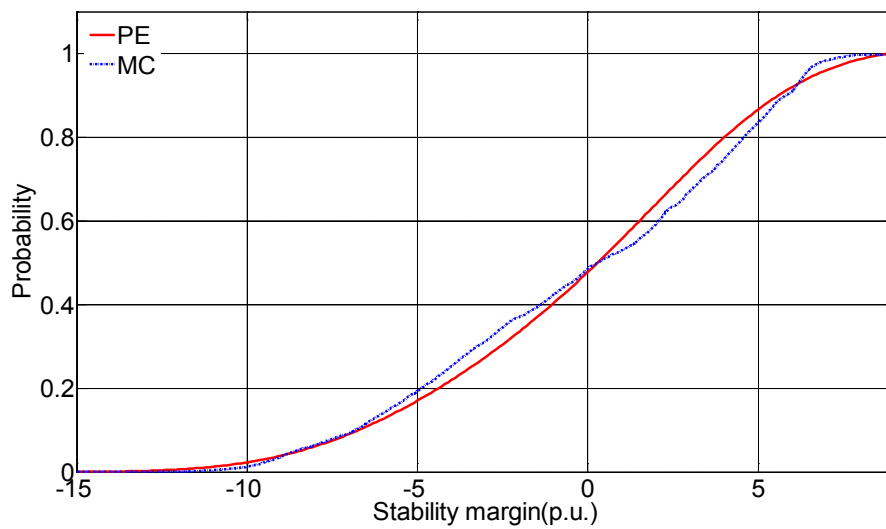
Fig. 6.9 Probability of stability margin without P-TSCOPF

Table 6.1 Comparisons of the base case and P-TSCOPF solution

Control Variables	Original point	P-TSCOPF solution
G_{30} (MW)	250	281
G_{32} (MW)	650	476
G_{33} (MW)	632	652
G_{34} (MW)	508	536
G_{35} (MW)	650	411
G_{36} (MW)	560	241
G_{37} (MW)	540	485
G_{38} (MW)	830	869
G_{39} (MW)	1000	1199
V_{31} (p.u.)	0.982	1.095
Are All Constraints Satisfied?	No	Yes
Cost Expectation ($/h)	57486.97	59008.96

Table 6.2 Error comparisons for the base case

Variable	MC (Mean, SD)	PE (Mean, SD)	Error (%)		
			ε_{μ}^{x}	ε_{σ}^{x}	ARMS
V_4	(0.9686,0.0012)	(0.9684,0.0013)	0.02	3.63	0.09
$P_{6\text{-}11}$	(5.9911,1.0510)	(6.1421,1.0799)	2.52	2.76	0.08
TSM	(-0.1594,4.8406)	(-0.1758,4.5155)	10.28	6.72	0.08
P_{slack}	(1.7826,2.1355)	(1.6453,2.2283)	7.70	4.35	0.05

The MC method with 5,000 samples is also conducted for benchmarking the performance of the $2m+1$ PE method. The total computation time taken by the MC method is 2,236s, which is almost 2 orders of magnitude slower than the proposed $2m+1$ PE method whose computation time is only 24s. Compared with

the large number of time domain simulations required by the MC method, the $2m+1$ PE method only needs to perform a small fraction of time domain simulations and is therefore significantly more efficient. For instance, only 53 time domain simulations would be needed with $m=26$ as in this case study. Furthermore, the accuracy of the PE method is diligently validated by qualitatively comparing the probability curves of slack bus generation (P_{slack}), voltage in bus 4 (V_4), power flow in line 6-11 (P_{6-11}), and transient stability margin (SM) obtained by the PE and MC methods as plotted in Fig. 6.6-6.9. The results of this comparison study are concisely summarized in Table 6.2. As is evidenced by the small mean and SD errors (<10.3% and <6.8%, respectively) as well as small ARMS errors (<0.2%) found in all the four variables in concern, the accuracy of the PE method is acceptable for its application in P-TSCOPF.

6.6.3 Investigations on Optimal Solutions of P-TSCOPF Model

As shown in Section 6.6.2, the base case does pose a high risk of system instability, a new operating point, which shall be secure and economic, is therefore desirable and can be found using the proposed IGSO-PE method as demonstrated in the following case study which contains 10 control variables consisting of 9 generator active powers and a slack bus voltage within the range of [0.95, 1.1]. The swarm size of IGSO is set to 15 and the total number of iterations is fixed at 30. Parameters for initializing IGSO individuals are the same as in Chapter V. The penalty factors p_j and p_r in (6.34) are set to 10^7 to introduce sufficient discrimination for any constraint violations in the P-TSCOPF model.

Fig. 6.10 plots the convergence of the proposed IGSO-PE optimization applied to solve this P-TSCOPF problem. The convergence is good and the total CPU time taken for the whole optimization process is 2,647s which is comparable to a single run of MC for assessing one IGSO individual.
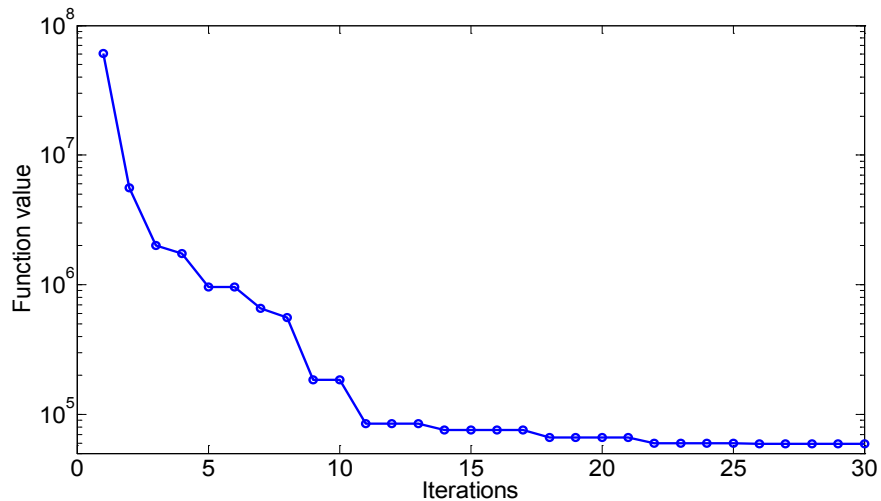
Fig. 6.10 Convergence of IGSO-PE approach for New England system

After P-TSCOPF optimization, the system has a slightly higher total fuel cost expectation of 59,008.96 $/h, which is increased by 2.6% compared to the base case as a small price to pay to mitigate the risk of instability. The optimized solution given in Table 6.1 is probabilistically transient stable and all the static probabilistic constraints are satisfied. For example, as shown in Fig. 6.11, the voltage CDF of bus 4 at threshold 0.97 is zero, thus the probability of voltage in the range of [0.97, 1.06] is 1 which is higher than the required security level 0.95. In Fig. 6.12, the probability of line flow 6-11 below the thermal limit 6 p.u. is 0.97 which is also higher than the required security level 0.95. In other words, this line is statistically unlikely to be overloaded. Moreover, the probability plot of stability margin in Fig. 6.13 indicates that the system is stable with a high probability as 1 with the given uncertainties. Meanwhile, the probability curves of bus 4 voltage, line flow 6-11 and transient stability margin obtained using the MC method are also given in Fig. 6.11-6.13 to show the good match of results between the PE and MC methods.

When compare the fuel cost expectation before and after P-TSCOPF optimization in Table 6.1, the fuel cost expectation of optimal solution increases 2.6 percent compared with the fuel cost expectation 57486.97 $/h of the base case. It is reasonable to sacrifice a small amount economic benefit for considerably mitigating the risk of instability for the stressed power system.
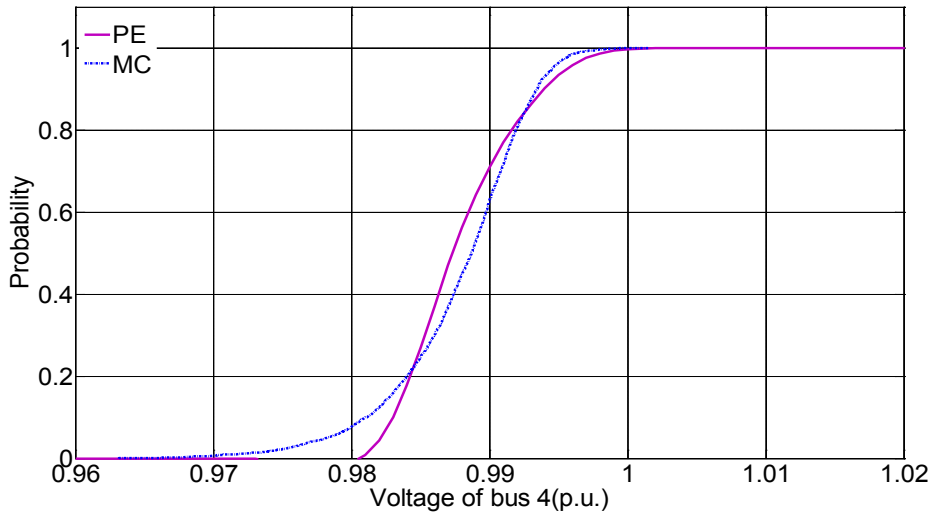
Fig. 6.11 Voltage probability of bus 4 with P-TSCOPF

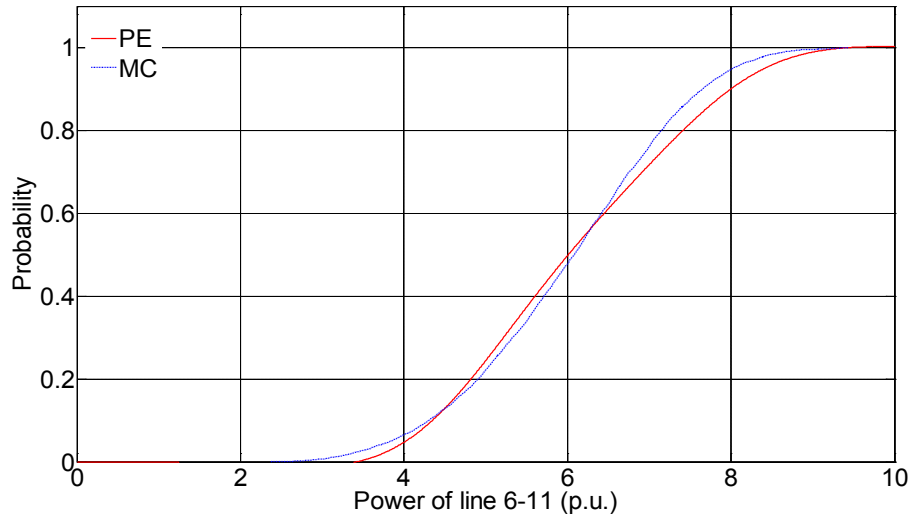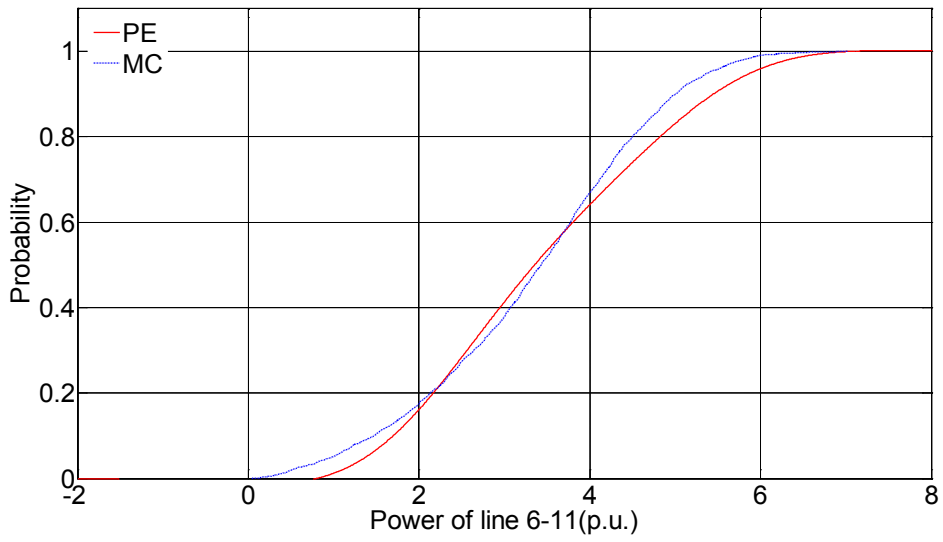
Fig. 6.12 Power probability of line 6-11 with P-TSCOPF
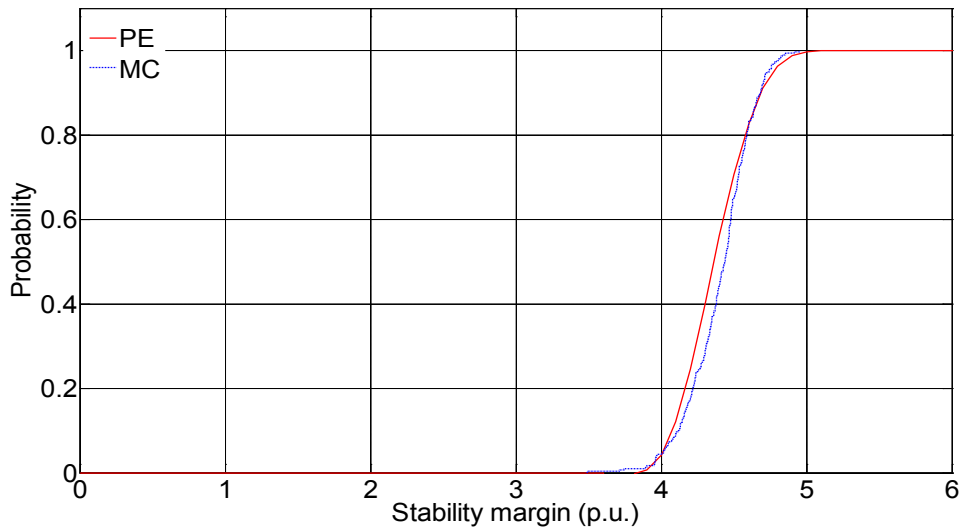
Fig. 6.13 Probability of stability margin with P-TSCOPF

Table 6.3 compares the results obtained from the PE and MC methods for the optimized solution found by the proposed IGSO-PE method. Again, the mean, SD, and ARMS errors are small (<2.8%, <4.8%, and <0.6%, respectively), and the PE method can indeed be used as the fast alterative of the MC method with acceptable accuracy.

Table 6.3 Error comparisons for the optimal solution

Variable	MC (Mean, SD)	PE (Mean, SD)	Error (%)		
			ε_μ^x	ε_σ^x	ARMS
V_4	(0.9876,0.0042)	(0.9880,0.0040)	0.04	4.76	0.45
P_{6-11}	(3.4174,1.3011)	(3.5041,1.3485)	2.53	3.64	0.15
SM	(4.4237,0.2289)	(4.3737,0.2271)	1.13	0.78	0.60
P_{slack}	(6.5295,3.4782)	(6.3513,3.5012)	2.73	0.66	0.16

The fuel cost expectations at different security levels for β_Q, β_V, β_S, and β_r are also investigated. As shown in Table 6.4, the fuel cost expectation is relative small when the security level is low. With a higher security level, the fuel cost expectation increased as expected since the system has to pay a higher expected fuel cost to establish a more secure operation state. Results presented in Table 6.4 also provide qualitative information to power system operators for making decisions in selecting the best compromised operation point with low expected fuel cost and acceptable system security level.

Table 6.4 Fuel cost expectations at different security level

Confident Level	0.80	0.85	0.90	0.95	0.98
Fuel Cost($/h)	57189	57420	57876	59009	59885

6.7   Summary

In this chapter, a novel probabilistic transient stability constrained optimal power flow (P-TSCOPF) model is presented for the first time to simultaneously consider the transient stability and uncertainties stemming from, for instance, correlated uncertain loads, uncertain fault clearing time and multiple correlated wind generations, etc. for power system preventive control. A new IGSO-PE approach based on the point-estimated method and IGSO algorithm has been established to efficiently solve the P-TSCOPF model. Tests and analysis on the modified New England 39-bus system with four correlated uncertain WFs have demonstrated the validity of the proposed P-TSCOPF model and the effectiveness of IGSO-PE method. Compared with the widely used MC method, the proposed IGSO-PE method is orders of magnitude faster while the solution quality is generally comparable.

Chapter VII

Conclusions and Future Work

7.1　Conclusions

With worldwide increasing concerns on the forthcoming energy crisis, OPF has regained its vital force due to its capability of approaching the best power system economic operation point and saving energy for power industries. However, the endless pursuit of economic benefits would continuously push modern power systems to operate with deteriorated stability margin or even instability when contingencies occur. Moreover, under the sustainable and smart grid paradigm, there is a continuous surge of wind power generations in power grids. Operation uncertainties coupled with the intermittent nature of wind power have brought new challenges and problems to power system security. A powerful schedule tool capable of simultaneously reconciling the economics, stability and uncertainties would be urgently needed for the much stressed power grids, and TSCOPF is such tool. In this thesis, various TSCOPF models and their effective solution methods are studied and investigated, and the uncertainties in operation and generation are further considered and handled in the P-TSCOPF model. Specifically, the following are the primary conclusions drawn from this research.

1) An all-round analytical approach capable of effectively handling multi-swing unstable, normal unstable or extreme unstable cases with multi-contingency and over-stabilization is proposed for TSCOPF problems.

Based on the SIME theory, a single stability constraint derived from the minimum accelerating power distance is proposed to handle the extreme unstable TSCOPF cases. Since only one stability constraint is introduced for each

contingency, the dimension of TSCOPF is greatly reduced to be comparable to traditional OPF and hence make solution approach scalable for large power systems. Also, the problem of over-stabilization in the TSCOPF optimization process is overcome by guiding the solution gradually across the stability boundary. As a result, an all-round approach is established for the first time to effectively solve all types of TSCOPF problems with multi-swing, normal or extreme unstable conditions, multi-contingency and over-stabilization.

2) *A general and flexible MINLP-TSCOPF model with consideration of valve-point effects and discrete control variables as well as transient angle and voltage performance is proposed and solved by a novel EPSO method.*

With consideration of the practical power system operation characteristics such as generation valve-point effects and discrete control variables, a non-convex discrete TSCOPF model with many minima is proposed and formulated as a general MINLP optimization problem. The reliable SIME-based *TSM* and signal energy are introduced to establish the constraints for transient angle stability and transient voltage performance, respectively, so as to conveniently form a unified MINLP-TSCOPF framework with transient angle and voltage performance taken into account. Furthermore, an EPSO with dynamic inertia weight and shrinking Gaussian distribution disturbance is proposed for solving this MINLP-TSCOPF. While the proposed MINLP-TSCOPF model is general and flexible to support any complex dynamic power system components, valve point effects and discrete control variables, the proposed EPSO is verified to be capable of finding effective MINLP-TSCOPF solutions.

3) *A novel IGSO method with backward searching strategy, Cauchy mutation and inheritance operator is specially designed as the best solver for MINLP-TSCOPF problems compared with other AI methods.*

A novel IGSO algorithm is specially developed for solving the non-convex MINLP-TSCOPF model with many minima. While backward searching strategy

and inheritance operator are adopted to enhance its search capability, Cauchy mutation disturbance is introduced to allow solutions to escape from the local optimum plateau during the optimization. The performance of IGSO method is fully investigated using four comprehensive case studies and benchmarked with variants of PSO, GA, GSO and DE methods, etc. to demonstrate its superiority in solving the MINLP-TSCOPF problem with generation POZs.

4) For the first time, a probabilistic transient stability constrained optimal power flow model with consideration of correlated wind power generation and operation uncertainties is established and efficiently solved by the proposed hybrid IGSO-PE approach.

An original P-TSCOPF model is proposed to consider both transient stability and uncertainties for power system preventive control. Typical uncertainties including uncertain load injections, probabilistic fault clearing time and multiple correlated stochastic wind generations are considered in this P-TSCOPF model. A hybrid approach, consisting of IGSO optimization and PE strategy with Cholesky decomposition, is established for solving the proposed P-TSCOPF model effectively. Case study on a modified New England 39-bus system with four correlated uncertain WFs has confirmed the validity of the proposed P-TSCOPF model and demonstrated the effectiveness of IGSO-PE solution method with fast computation speed and good accuracy compared with Monte Carlo simulations.

7.2 Future Work

The thesis has first developed an efficient and all-round analytical approach to solve the traditional TSCOPF problem, then proposed a general and flexible MINLP-TSCOPF model solved by specially designed heuristic solution methods, and finally established a P-TSCOPF model with consideration of generation and operation uncertainties for power system preventive control. With the endeavour

to solve the P-TSCOPF model more effectively, the following on-going work is worth to continue in the follow-up research.

1) Large-scale parallel computation should be adopted to reduce the CPU time of IGSO-PE method in solving P-TSCOPF problems.

The dominated execution in solving the P-TSCOPF problem by IGSO-PE method is to calculate the transient stability index for each PE concentration using time domain simulations. As these time domain simulations are independent of each other, large-scale parallel computation strategy can therefore be used to efficiently speed up the IGSO-PE optimization process.

2) The principal component analysis strategy can be used to identify the key uncertain factors among all uncertain input variables, thus reduce the number of concentrations required for time domain simulations.

When the PE strategy is used to approximate the probabilistic distribution of concerned outputs, a few concentrations shall be selected based on the probability theory for time domain simulations. As the number of concentrations required is dependent on the number of uncertain factors, identifying the key uncertain factors so as to decrease the number of concentrations would reduce the time cost for solving the P-TSCOPF problem. The principal component analysis is a promising strategy which could be used to screen out the main uncertain factors from non-significant uncertainties.

3) An analytical method based on power system dynamic security region and convolution calculation could be developed to address the P-TSCOPF problem more efficiently.

The major key in solving the P-TSCOPF problem is how the probabilistic distribution of concerned random output variables can be determined effectively, in particular the probabilistic transient stability margin which is always coupled with solutions of power system DAEs. With the linear relationship between

concerned outputs and uncertain inputs provided, the analytical method using convolution computation could approximate the probability of random outputs. As a result, an analytical approach based on power system dynamic security region [188] targeting to estimating the linear relationship between the transient stability index and uncertain inputs by perturbations, could be formed to compute the probabilistic distribution of transient stability margin, and hence the P-TSCOPF problem could be solved more efficiently in an analytical manner.

4) *Besides the wind power generations, uncertainties and dynamic models of many other intermittent renewable generations shall also be investigated such that a complete P-TSCOPF model accommodating various renewable energies could be formed and analysed in the future.*

Since only multiple correlated wind generations is considered as one typical renewable generation in this thesis, many other common intermittent renewables such as photovoltaic power generations and electric vehicle aggregators could also be introduced in the P-TSCOPF problem. The full models of photovoltaic power generations and electric vehicle aggregators shall be properly developed for describing their dynamic behaviours in P-TSCOPF for bulk power systems, such that an all-sided P-TSCOPF model including all types of renewables could be established and investigated.

Appendices

A. Data of New England 10-Generator 39-Bus Power System

Note: If not specified, all data in per unit are given based on power rating of 100 MW.

Table A.1 Generation cost coefficients of New England system

Gen No.	Bus No.	a_i ($/(MW^2·h))	b_i ($/(MW·h))	c_i ($/h)	d_i	e_i ($/(MW·h))	Rating (MW)
G1	30	0.0193	6.9	0	200	0.35	350
G2	31	0.0111	3.7	0	200	0.35	650
G3	32	0.0104	2.8	0	200	0.35	800
G4	33	0.0088	4.7	0	200	0.35	750
G5	34	0.0128	2.8	0	200	0.35	650
G6	35	0.0094	3.7	0	300	0.22	750
G7	36	0.0099	4.8	0	300	0.22	750
G8	37	0.0113	3.6	0	300	0.22	700
G9	38	0.0071	3.7	0	300	0.22	900
G10	39	0.0064	3.9	0	300	0.22	1200

Table A.2 Machine data of New England system

Gen No.	H	X_d'	X_q'	X_d	X_q	T'_{d0} (s)	T'_{q0} (s)
G1	42	0.004	0.004	0.2	0.196	5.7	0.5
G2	30.3	0.0647	0.0647	0.295	0.282	6.56	1.5
G3	35.8	0.0531	0.0531	0.2495	0.237	5.7	1.5
G4	28.6	0.0436	0.0436	0.262	0.258	5.69	1.5
G5	26	0.066	0.066	0.33	0.31	5.4	0.44
G6	34.8	0.05	0.05	0.254	0.241	7.3	0.4
G7	26.4	0.049	0.049	0.295	0.292	5.66	1.5
G8	24.3	0.057	0.057	0.29	0.28	6.7	0.41
G9	34.5	0.057	0.057	0.2106	0.205	4.79	1.96
G10	500	0.006	0.006	0.02	0.019	6	0.7

Table A.3 Transmission line data of New England system

Line No.	From bus	To bus	Resistance (pu)	Reactance (pu)	Susceptance (pu)	Ratio	Rating (MVA)
1	2	1	0.0035	0.0411	0.6987	1	600
2	39	1	0.001	0.025	0.75	1	1000
3	3	2	0.0013	0.0151	0.2572	1	500
4	25	2	0.007	0.0086	0.146	1	500
5	4	3	0.0013	0.0213	0.2214	1	500
6	18	3	0.0011	0.0133	0.2138	1	500
7	5	4	0.0008	0.0129	0.1382	1	600
8	14	4	0.0008	0.0128	0.1342	1	500
9	6	5	0.0002	0.0026	0.0434	1	1200
10	8	5	0.0008	0.0112	0.1476	1	900
11	7	6	0.0006	0.0092	0.113	1	900
12	11	6	0.0007	0.0082	0.1389	1	600
13	8	7	0.0004	0.0046	0.078	1	900
14	9	8	0.0023	0.0363	0.3804	1	900
15	39	9	0.001	0.025	1.2	1	900
16	11	10	0.0004	0.0043	0.0729	1	600
17	13	10	0.0004	0.0043	0.0729	1	600
18	14	13	0.0009	0.0101	0.1723	1	600
19	15	14	0.0018	0.0217	0.366	1	600
20	16	15	0.0009	0.0094	0.171	1	600
21	17	16	0.0007	0.0089	0.1342	1	600
22	19	16	0.0016	0.0195	0.304	1	600
23	21	16	0.0008	0.0135	0.2548	1	600
24	24	16	0.0003	0.0059	0.068	1	600
25	18	17	0.0007	0.0082	0.1319	1	600
26	27	17	0.0013	0.0173	0.3216	1	600
27	22	21	0.0008	0.014	0.2565	1	900
28	23	22	0.0006	0.0096	0.1846	1	600
29	24	23	0.0022	0.035	0.361	1	600
30	26	25	0.0032	0.0323	0.513	1	600
31	27	26	0.0014	0.0147	0.2396	1	600
32	28	26	0.0043	0.0474	0.7802	1	600
33	29	26	0.0057	0.0625	1.029	1	600
34	29	28	0.0014	0.0151	0.249	1	600

35	12	11	0.0016	0.0435	0	1.006	500
36	12	13	0.0016	0.0435	0	1.006	500
37	6	31	0	0.025	0	1.07	1800
38	10	32	0	0.02	0	1.07	900
39	19	33	0.0007	0.0142	0	1.07	900
40	20	34	0.0009	0.018	0	1.009	900
41	22	35	0	0.0143	0	1.025	900
42	23	36	0.0005	0.0272	0	1	900
43	25	37	0.0006	0.0232	0	1.025	900
44	2	30	0	0.0181	0	1.025	900
45	29	38	0.0008	0.0156	0	1.025	1200
46	19	20	0.0007	0.0138	0	1.06	900

Table A.4 Load demand data of New England system

Bus No.	P_{Di} (pu)	Q_{Di} (pu)
3	3.22	0.024
4	5	1.84
7	2.338	0.84
8	5.22	1.76
12	0.075	0.88
15	3.2	1.53
16	3.294	0.323
18	1.58	0.3
20	6.28	1.03
21	2.74	1.15
23	2.475	0.8466
24	3.086	-0.922
25	2.24	0.472
26	1.39	0.17
27	2.81	0.755
28	2.06	0.276
29	2.835	0.269
31	0.092	0.046
39	11.04	2.5

B. Data of IEEE 50-Generator 145-Bus Power System

Note: If not specified, all data in per unit are calculated on the basis of power rating of 100 MW.

Table B.1 Machine data of IEEE 50-generator system

Gen No.	Bus No.	H	$X_d{'}$	$X_q{'}$	X_d	X_q	T'_{d0} (s)	T'_{q0} (s)
G1	60	1.41	0.4769					
G2	67	52.1796	0.0213					
G3	79	6.65	0.1292					
G4	80	1.2857	0.6648					
G5	82	2.115	0.5291					
G6	89	20.5602	0.0585					
G7	90	0.7628	1.6					
G8	91	1.6848	0.3718					
G9	93	115.037	0.024	0.03655	0.09842	0.09673	8.5	1.24
G10	94	17.3424	0.0839					
G11	95	5.4662	0.1619					
G12	96	2.1216	0.4824					
G13	97	5.4912	0.2125					
G14	98	13.96	0.0795					
G15	99	17.108	0.1146					
G16	100	7.56	0.1386					
G17	101	12.2844	0.0924					
G18	102	78.4366	0.0135					
G19	103	8.16	0.1063					
G20	104	73.8528	0.0122	0.0144	0.1016	0.0982	10	1.5
G21	105	84.3915	0.0208	0.03149	0.1144	0.1092	6.61	1.5
G22	106	56.261	0.03118	0.0472	0.17165	0.16377	6.61	1.5
G23	108	30.432	0.0248					
G24	109	2.6622	0.2029					
G25	110	115.05	0.024	0.0365	0.09842	0.09673	8.5	1.24
G26	111	73.8528	0.0122	0.0144	0.1016	0.0982	10	1.5

G27	112	12.2844	0.0924					
G28	115	97.33	0.0024					
G29	116	105.5	0.0022					
G30	117	102.16	0.0017					
G31	118	162.74	0.0014					
G32	119	348.22	0.0002					
G33	121	116.54	0.0017					
G34	122	39.24	0.0089					
G35	124	116.86	0.0017					
G36	128	503.87	0.0001					
G37	130	230.9	0.001					
G38	131	1101.72	0.0001					
G39	132	120.35	0.0016					
G40	134	802.12	0.0003					
G41	135	232.63	0.0008					
G42	136	2018.17	0.0001					
G43	137	469.32	0.0004					
G44	139	2210.2	0.0001					
G45	140	899.19	0.0003					
G46	141	1474.22	0.0001					
G47	142	950.8	0.0003					
G48	143	204.3	0.0023					
G49	144	443.22	0.0004					
G50	145	518.08	0.0018					

C. Data of Excitation System for 4th Order Generators

Note: If not specified, all data in per unit are calculated on the basis of power rating of 100 MW.

Table C.1 Excitation System parameters for 4th order generators

Systems	Gen No.	K_A	$T_A(s)$	K_E	$T_E(s)$	$K_F(s)$	$T_F(s)$	A_{ex}	B_{ex}	V_{rmin}	V_{rmax}
New England 10-gen system	All generators	20	0.055	0.36	0.05	0.125	1.8	0.0056	1.075	-10	10
IEEE 50-gen system	G9	20	0.055	0.36	0.05	0.125	1.8	0.0056	1.075	-10	10
	G20	20	0.055	0.36	0.05	0.125	1.8	0.0056	1.075	-10	10
	G21	20	0.055	0.36	0.05	0.125	1.8	0.0056	1.075	-10	10
	G22	20	0.055	0.36	0.05	0.125	1.8	0.0056	1.075	-10	10
	G25	20	0.055	0.36	0.05	0.125	1.8	0.0056	1.075	-10	10
	G26	20	0.055	0.36	0.05	0.125	1.8	0.0056	1.075	-10	10

References

[1]   J. A. Momoh, R. Adapa, and M. E. El-Hawary, "A review of selected optimal power flow literature to 1993. I. Nonlinear and quadratic programming approaches," *IEEE Trans. Power Syst.,* vol. 14, no. 1, pp. 96-104, Feb. 1999.

[2]   J. A. Momoh, M. E. El-Hawary, and R. Adapa, "A review of selected optimal power flow literature to 1993. II. Newton, linear programming and interior point methods," *IEEE Trans. Power Syst.,* vol. 14, no. 1, pp. 105-111, Feb. 1999.

[3]   Y. C. Li, Y. L. Wang, and B. Li, "A hybrid artificial bee colony assisted differential evolution algorithm for optimal reactive power flow," *Int. J. Elect. Power Energy Syst.,* vol. 52, pp. 25-33, Nov. 2013.

[4]   T. Nireekshana, G. Kesava Rao, and S. Siva Naga Raju, "Enhancement of ATC with FACTS devices using Real-code Genetic Algorithm," *Int. J. Elect. Power Energy Syst.,* vol. 43, no. 1, pp. 1276-1284, Dec. 2012.

[5]   S. Sivasubramani and K. S. Swarup, "Multi-objective harmony search algorithm for optimal power flow problem," *Int. J. Elect. Power Energy Syst.,* vol. 33, no. 3, pp. 745-752, Mar. 2011.

[6]   P. Dehghanian, S. H. Hosseini, and M. Moeini-Aghtaie, et al., "Optimal siting of DG units in power systems from a probabilistic multi-objective optimization perspective," *Int. J. Elect. Power Energy Syst.,* vol. 51, pp. 14-26, Oct. 2013.

[7]   S. Kumar and D. K. Chaturvedi, "Optimal power flow solution using fuzzy evolutionary and swarm optimization," *Int. J. Elect. Power Energy Syst.,* vol. 47, pp. 416-423, May 2013.

[8]   D. ThanhLong, J. Yao, and T. VietAnh, "A new method for secured optimal power flow under normal and network contingencies via optimal location of TCSC," *Int. J. Elect. Power Energy Syst.,* vol. 52, pp. 68-80, Nov. 2013.

[9]   K. Shanmukha Sundar and H. M. Ravikumar, "Selection of TCSC location for secured optimal power flow under normal and network contingencies," *Int. J. Elect. Power Energy Syst.,* vol. 34, no. 1, pp. 29-37, Jan. 2012.

[10]   W. J. Zhang, F. X. Li, and L. M. Tolbert, "Review of reactive power planning: objectives, constraints, and algorithms," *IEEE Trans. Power Syst.,* vol. 22, no. 4, pp. 2177-2186, Nov. 2007.

[11]   H. Wei, H. Sasaki, and J. Kubokawa, et al., "An interior point nonlinear programming for optimal power flow problems with a novel data structure," *IEEE Trans. Power Syst.,* vol. 13, no. 3, pp. 870-877, Aug. 1998.

[12]   F. W. Felix, G. Gross, and J. F. Luini, et al.,"A two-stage approach to solving large-scale optimal power flows*," in Proc. Power Industry Computer Applications Conference, IEEE Service Center*, 1979, pp. 126-136.

[13]   S. Frank, I. Steponavice, and S. Rebennack, "Optimal power flow: a bibliographic survey I," *Energy Systems,* vol. 3, no. 3, pp. 221-258, 2012.

[14]   S. Frank, I. Steponavice, and S. Rebennack, "Optimal power flow: a bibliographic survey II," *Energy Systems,* vol. 3, no. 3, pp. 259-289, 2012.

[15]   M. Huneault and F. D. Galiana, "A survey of the optimal power flow literature," *IEEE Trans. Power Syst.,* vol. 6, no. 2, pp. 762-770, May 1991.

[16]   S. Sivasubramani and K. S. Swarup, "Sequential quadratic programming based differential evolution algorithm for optimal power flow problem," *IET Gener. Transm. Distrib.,* vol. 5, no. 11, pp. 1149-1154, Nov. 2011.

[17]   X. Bai, H. Wei, and K. Fujisawa, et al., "Semidefinite programming for optimal power flow problems," *Int. J. Elect. Power Energy Syst.,* vol. 30, no. 6–7, pp. 383-392, Jul. 2008.

[18] Y. Chang, T. Lee, and C. Chen, et al., "Optimal power flow of a wind-thermal generation system," *Int. J. Elect. Power Energy Syst.,* vol. 55, pp. 312-320, Feb. 2014.

[19] I. Szuvovivski, T. S. P. Fernandes, and A. R. Aoki, "Simultaneous allocation of capacitors and voltage regulators at distribution networks using Genetic Algorithms and Optimal Power Flow," *Int. J. Elect. Power Energy Syst.,* vol. 40, no. 1, pp. 62-69, Sep. 2012.

[20] Q. Kang, M. Zhou, and J. An, et al., "Swarm intelligence approaches to optimal power flow problem with distributed generator failures in power networks," *IEEE Trans. Automation Science and Engineering,* vol. 10, no. 2, pp. 343-353, Apr. 2013.

[21] B. Mahdad, K. Srairi, and T. Bouktir, "Optimal power flow for large-scale power system with shunt FACTS using efficient parallel GA," *Int. J. Elect. Power Energy Syst.,* vol. 32, no. 5, pp. 507-517, Jun. 2010.

[22] P. Siano and G. Mokryani, "Assessing wind turbines placement in a distribution market environment by using Particle Swarm Optimization," *IEEE Trans. Power Syst.,* vol. 28, no. 4, pp. 3852-3864, Nov. 2013.

[23] P. Dzung and J. Kalagnanam, "Some efficient optimization methods for solving the security-constrained optimal power flow problem," *IEEE Trans. Power Syst.,* vol. 29, no. 2, pp. 863-872, Mar. 2014.

[24] Q. Wang, J. D. McCalley, and T. Zheng, et al., "A computational strategy to solve preventive risk-based security-constrained OPF," *IEEE Trans. Power Syst.,* vol. 28, no. 2, pp. 1666-1675, May 2013.

[25] T. Niknam, R. Azizipanah-Abarghooee, and M. R. Narimani, "Reserve constrained dynamic optimal power flow subject to valve-point effects, prohibited zones and multi-fuel constraints," *Energy,* vol. 47, no. 1, pp. 451-464, Nov. 2012.

[26] T. Niknam, R. Azizipanah-Abarghooee, and J. Aghaei, "A new modified Teaching-Learning algorithm for reserve constrained dynamic economic dispatch," *IEEE Trans. Power Syst.,* vol. 28, no. 2, pp. 749-763, May 2013.

[27] X. Bai and H. Wei, "Semi-definite programming-based method for security-constrained unit commitment with operational and optimal power flow constraints," *IET Gener. Transm. Distrib.,* vol. 3, no. 2, pp. 182-197, Feb. 2009.

[28] D. Gayme and U. Topcu, "Optimal power flow with large-scale storage integration," *IEEE Trans. Power Syst.,* vol. 2, no. 28, pp. 709-717, May 2013.

[29] C. Y. Chung, Y. Wei, and L. Fang, "Decomposed predictor-corrector Interior Point Method for dynamic optimal power flow," *IEEE Trans. Power Syst.,* vol. 26, no. 3, pp. 1030-1039, Aug. 2011.

[30] A. Berizzi,"The Italian 2003 blackout*," in Proc. Power Engineering Society General Meeting*, Denver, CO, Jun. 2004, pp. 1673-1679.

[31] G. Andersson, P. Donalek, and R. Farmer, et al., "Causes of the 2003 major grid blackouts in North America and Europe, and recommended means to improve system dynamic performance," *IEEE Trans. Power Syst.,* vol. 20, no. 4, pp. 1922-1928, Nov. 2005.

[32] S. Larsson and A. Danell,"The black-out in southern Sweden and eastern Denmark, September 23, 2003*.," in Proc. 2006 IEEE PES Power Systems Conference and Exposition*, Atlanta, GA, Nov. 2006, pp. 309-313.

[33] R. F. Yan and T. K. Saha, "Investigation of voltage stability for residential customers due to high photovoltaic penetrations," *IEEE Trans. Power Syst.,* vol. 27, no. 2, pp. 651-662, May 2012.

[34] M. Esmaili, E. C. Firozjaee, and H. A. Shayanfar, "Optimal placement of distributed generations considering voltage stability and power losses with observing voltage-related constraints," *App. Energy,* vol. 113, pp. 1252-1260, Jan. 2014.

[35] G. Y. Wu, C. Y. Chung, and K. P. Wong, et al., "Voltage stability constrained optimal dispatch in deregulated power systems," *IET Gener. Transm. Distrib.,* vol. 1, no. 5, pp. 761-768, Sep. 2007.

[36] R. S. Al Abri, E. F. El-Saadany, and Y. M. Atwa, "Optimal placement and sizing method to improve the voltage stability margin in a distribution system using distributed generation," *IEEE Trans. Power Syst.,* vol. 28, no. 1, pp. 326-334, Feb. 2013.

[37] P. J. Li, H. Wei, and B. Li, et al., "Eigenvalue-optimisation-based optimal power flow with small-signal stability constraints," *IET Gener. Transm. Distrib.,* vol. 7, no. 5, pp. 440-450, May 2013.

[38] J. Condren and T. W. Gedra, "Expected-security-cost optimal power flow with small signal stability constraints," *IEEE Trans. Power Syst.,* vol. 21, no. 4, pp. 1736-1743, Nov. 2006.

[39] R. Zarate-Minano, F. Milano, and A. Conejo, "An OPF methodology to ensure small signal stability," *IEEE Trans. Power Syst.,* vol. 26, no. 3, pp. 1050-1061, Aug. 2011.

[40] H. Ahmadi, H. Ghasemi, and A. M. Haddadi, et al., "Two approaches to transient stability-constrained optimal power flow," *Int. J. Elect. Power Energy Syst.,* vol. 47, pp. 181-192, May. 2013.

[41] A. Pizano-Martinez, C. R. Fuerte-Esquivel, and D. Ruiz-Vega,"Global transient stability constrained optimal power flow using SIME sensitivity analysis*," in Proc. Power and Energy Society General Meeting*, Minneapolis, MN, Jul. 2010, pp. 1-8.

[42] R. Zarate-Minano, T. Van Cutsem, and F. Milano, et al., "Securing transient stability using time-domain simulations within an optimal power flow," *IEEE Trans. Power Syst.,* vol. 25, no. 1, pp. 243-253, Feb. 2010.

[43] H. R. Cai, C. Y. Chung, and K. P. Wong, "Application of differential evolution algorithm for transient stability constrained optimal power flow," *IEEE Trans. Power Syst.,* vol. 23, no. 2, pp. 719-728, May 2008.

[44] N. Mo, Z. Y. Zou, and K. W. Chan, et al., "Transient stability constrained optimal power flow using particle swarm optimisation," *IET Gener. Transm. Distrib.,* vol. 1, no. 3, pp. 476-483, May 2007.

[45] T. B. Nguyen and M. A. Pai, "Dynamic security-constrained rescheduling of power systems using trajectory sensitivities," *IEEE Trans. Power Syst.,* vol. 18, no. 2, pp. 848- 854, May 2003.

[46] P. Kundur, J. Paserba, and V. Ajjarapu, et al., "Definition and classification of power system stability IEEE/CIGRE joint task force on stability terms and definitions," *IEEE Trans. Power Syst.,* vol. 19, no. 3, pp. 1387- 1401, Aug. 2004.

[47] D. Gautam, V. Vittal, and T. Harbour, "Impact of increased penetration of DFIG-based wind turbine generators on transient and small signal stability of power systems," *IEEE Trans. Power Syst.,* vol. 24, no. 3, pp. 1426-1434, Aug. 2009.

[48] S. O. Faried, R. Billinton, and S. Aboreshaid, "Probabilistic evaluation of transient stability of a wind farm," *IEEE Trans. on Energy Conversion,* vol. 24, no. 3, pp. 733-739, Sep. 2009.

[49] X. F. Bai, T. Jiang, and Z. Z. Guo, et al., "A unified approach for processing unbalanced conditions in transient stability calculations," *IEEE Trans. Power Syst.,* vol. 21, no. 1, pp. 85- 90, Feb. 2006.

[50] S. M. Muyeen, R. Takahashi, and M. H. Ali, et al., "Transient stability augmentation of power system including wind farms by using ECS," *IEEE Trans. Power Syst.,* vol. 23, no. 3, pp. 1179-1187, Aug. 2008.

[51] A. A. Fouad and J. Tong, "Stability constrained optimal rescheduling of generation," *IEEE Trans. Power Syst.,* vol. 8, no. 1, pp. 105-112, Feb. 1993.

[52] K. N. Shubhanga and A. M. Kulkarni, "Stability-constrained generation rescheduling using energy margin sensitivities," *IEEE Trans. Power Syst.,* vol. 19, no. 3, pp. 1402- 1413, Aug. 2004.

[53] D. Gan, R. J. Thomas, and R. D. Zimmerman, "Stability-constrained optimal power flow," *IEEE Trans. Power Syst.,* vol. 15, no. 2, pp. 535-540, May 2000.

[54] S. Bruno, E. De Tuglie, and M. La Scala, "Transient security dispatch for the concurrent optimization of plural postulated contingencies," *IEEE Trans. Power Syst.,* vol. 17, no. 3, pp. 707- 714, Aug. 2002.

[55] Y. Yue, J. Kubokawa, and H. Sasaki, "A solution of optimal power flow with multicontingency transient stability constraints," *IEEE Trans. Power Syst.,* vol. 18, no. 3, pp. 1094- 1102, Aug. 2003.

[56] H. Xin, D. Gan, and Z. Huang, et al., "Applications of stability-constrained optimal power flow in the East China system," *IEEE Trans. Power Syst.,* vol. 25, no. 3, pp. 1423-1433, Aug. 2010.

[57] T. A. A. Victoire and A. E. Jeyakumar, "Reserve constrained dynamic dispatch of units with valve-point effects," *IEEE Trans. Power Syst.,* vol. 20, no. 3, pp. 1273- 1282, Aug. 2005.

[58] C. Chao-Lung, "Improved genetic algorithm for power economic dispatch of units with valve-point effects and multiple fuels," *IEEE Trans. Power Syst.,* vol. 20, no. 4, pp. 1690- 1699, Nov. 2005.

[59] G. R. Kocis and I. E. Grossmann, "A modelling and decomposition strategy for the minlp optimization of process flowsheets," *Comput Chem Eng,* vol. 13, no. 7, pp. 797-819, Jul. 1989.

[60] K. Y. Chan, S. H. Ling, and K. W. Chan, et al.,"Solving multi-contingency transient stability constrained optimal power flow problems with an improved GA*," in Proc. IEEE Congress on Evolutionary Computation*, Singapore, Sep. 2007, pp. 2901-2908.

[61] D. H. Wolpert and W. G. Macready, "No free lunch theorems for optimization," *IEEE Trans. Evol. Comput.,* vol. 1, no. 1, pp. 67-82, Apr. 1997.

[62] Q. Jiang, B. Zhou, and M. Zhang, "Parallel Augment Lagrangian Relaxation method for transient stability constrained unit commitment," *IEEE Trans. Power Syst.,* vol. 28, no. 2, pp. 1140-1148, May 2013.

[63] Y. Xu, Z. Y. Dong, and K. Meng, et al., "A hybrid method for transient stability-constrained optimal power flow computation," *IEEE Trans. Power Syst.,* vol. 27, no. 4, pp. 1769-1777, Nov. 2012.

[64] A. Pizano-Martinez, C. R. Fuerte-Esquivel, and D. Ruiz-Vega, "A new practical approach to transient stability-constrained optimal power flow," *IEEE Trans. Power Syst.,* vol. 26, no. 3, pp. 1686-1696, Aug. 2011.

[65] Y. Xia and K. W. Chan, "Dynamic constrained optimal power flow using semi-infinite programming," *IEEE Trans. Power Syst.,* vol. 21, no. 3, pp. 1455-1457, Aug. 2006.

[66] A. Pizano-Martianez, C. R. Fuerte-Esquivel, and D. Ruiz-Vega, "Global transient stability-constrained optimal power flow using an OMIB reference trajectory," *IEEE Trans. Power Syst.,* vol. 25, no. 1, pp. 392-403, Feb. 2010.

[67] A. Togelou, G. Sideratos, and N. D. Hatziargyriou, "Wind power forecasting in the absence of historical data," *IEEE Trans. Sustain. Energy,* vol. 3, no. 3, pp. 416-421, Jul. 2012.

[68] P. Meibom, R. Barth, and B. Hasche, et al., "Stochastic optimization model to study the operational impacts of high wind penetrations in Ireland," *IEEE Trans. Power Syst.,* vol. 26, no. 3, pp. 1367-1379, Aug. 2011.

[69] P. Kundur, *Power System Stability and Control*. New York: McGraw-Hill, 1994.

[70] M. Celik and L. T. Oileggi, "Simulation of lossy multiconductor transmission lines using backward Euler integration," *IEEE Trans. Circuits Syst.,* vol. 45, no. 3, pp. 238-243, Mar. 1998.

[71] Z. Yuan and V. Ajjarapu, "A novel approach to trace time-domain trajectories of power systems in multiple time scales," *IEEE Trans. Power Syst.,* vol. 20, no. 1, pp. 149- 155, Feb. 2005.

[72] C. K. Tang, C. E. Graham, and M. El-Kady, et al., "Transient stability index from conventional time domain simulation," *IEEE Trans. Power Syst.,* vol. 9, no. 3, pp. 1524-1530, Aug. 1994.

[73] Y. Zhang, L. Wehenkel, and P. Rousseaux, et al., "SIME: A hybrid approach to fast transient stability assessment and contingency selection," *Int. J. Elect. Power Energy Syst.,* vol. 19, no. 3, pp. 195-208, Mar. 1997.

[74] M. La Scala, G. Sblendorio, and R. Sbrizzai, "Parallel-in-time implementation of transient stability simulations on a transputer network," *IEEE Trans. Power Syst.,* vol. 9, no. 2, pp. 1117-1125, May 1994.

[75] I. C. Decker, D. M. Falcao, and E. Kaszkurewicz, "Conjugate gradient methods for power system dynamic simulation on parallel computers," *IEEE Trans. Power Syst.,* vol. 11, no. 3, pp. 1218-1227, Aug. 1996.

[76] Y. Li, X. Zhou, and Z. Wu, et al.,"Parallel algorithms for transient stability simulation on PC cluster*," in Proc. International Conf. on Power System Technology*, Jan. 2002, pp. 1592- 1596.

[77] J. W. Shu, W. Xue, and W. M. Zheng, "A parallel transient stability simulation for power systems," *IEEE Trans. Power Syst.,* vol. 20, no. 4, pp. 1709- 1717, Nov. 2005.

[78] Y. Chen, C. Shen, and J. Wang, "Distributed transient stability simulation of power systems based on a Jacobian-free Newton-GMRES method," *IEEE Trans. Power Syst.,* vol. 24, no. 1, pp. 146-156, Feb. 2009.

[79] J. A. Hollman and J. R. Marti, "Real time network simulation with PC-cluster," *IEEE Trans. Power Syst.,* vol. 18, no. 2, pp. 563- 569, May 2003.

[80] S. Furuya, "Fast transient stability solution using Taylor expansion and energy function," *Trans. IEEE of Japan,* vol. 3, no. 105, pp. 123-130, 1985.

[81] M. H. Haque and A. H. M. A. Rahim, "An efficient method of identifying coherent generators using Taylor series expansion," *IEEE Trans. Power Syst.,* vol. 3, no. 3, pp. 1112-1118, Aug. 1988.

[82] M. H. Haque and A. H. M. A. Rahim, "Determination of first swing stability limit of multimachine power systems through Taylor series expansions," *IEE Proc. Gener. Transm. Distrib.,* vol. 136, no. 6, pp. 373-380, Nov. 1989.

[83] Z. Y. Wang and Z. Z. Guo,"A fast method for transient stability assessment based on Taylor series expansion*," in Proc. IEEE/PES Transmission and Distribution Conference and Exhibition: Asia and Pacific*, Dalian, Jan. 2005, pp. 1-5.

[84] Z. Z. Guo and Z. Liu, "Fast transient stability simulation by higher order Taylor series expansions," *Proceedings of the CSEE,* vol. 3, no. 11, pp. 9-15, May 1991.

[85] M. A. Pai and P. W. Sauer, "Stability analysis of power systems by Lyapunov's direct method," *Control Systems Magazine, IEEE,* vol. 9, no. 1, pp. 23-27, Jan. 1989.

[86] A. A. Fouad, V. Vittal, and K. O. Tae, "Critical energy for direct transient stability assessment of a multimachine power system," *IEEE Trans. Power Appar. Syst.,* vol. PAS-103, no. 8, pp. 2199-2206, Aug. 1984.

[87] H. D. Chiang, F. F. Wu, and P. P. Varaiya, "Foundations of the potential energy boundary surface method for power system transient stability analysis," *IEEE Trans. Circuits Syst.,* vol. 35, no. 6, pp. 712-728, Jun. 1988.

[88] H. D. Chiang, F. F. Wu, and P. P. Varaiya, "A BCU method for direct analysis of power system transient stability," *IEEE Trans. Power Syst.,* vol. 9, no. 3, pp. 1194-1208, Aug. 1994.

[89] A. Llamas, J. De La Ree Lopez, and L. Mili, et al., "Clarifications of the BCU method for transient stability analysis," *IEEE Trans. Power Syst.,* vol. 10, no. 1, pp. 210-219, Feb. 1995.

[90] H. D. Chiang and C. C. Chu, "Theoretical foundation of the BCU method for direct stability analysis of network-reduction power system models

with small transfer conductances," *IEEE Trans. Circuits Syst.,* vol. 42, no. 5, pp. 252-265, May 1995.

[91] Y. Xue, T. Van Custem, and M. Ribbens-Pavella, "Extended equal area criterion justifications, generalizations, applications," *IEEE Trans. Power Syst.,* vol. 4, no. 1, pp. 44-52, Feb. 1989.

[92] L. F. C. Alberto, F. H. J. R. Silva, and N. G. Bretas,"Direct methods for transient stability analysis in power systems: state of art and future perspectives*," in Proc. IEEE Power Tech Proceedings*, Porto, Sep. 2001, pp. 1-6.

[93] D. Ernst, D. Ruiz-Vega, and M. Pavella, et al., "A unified approach to transient stability contingency filtering, ranking and assessment," *IEEE Trans. Power Syst.,* vol. 16, no. 3, pp. 435-443, Aug. 2001.

[94] M. Pavella, D. Ernst, and D. Ruiz-Vega, *Transient stability of power systems: a unified approach to assessment and control*. Norwell, MA: Kluwer, 2000.

[95] G. A. Maria, C. Tang, and J. Kim, "Hybrid transient stability analysis," *IEEE Trans. Power Syst.,* vol. 5, no. 2, pp. 384-393, May 1990.

[96] D. Z. Fang, T. S. Chung, and Y. Zhang, et al., "Transient stability limit conditions analysis using a corrected transient energy function approach," *IEEE Trans. Power Syst.,* vol. 15, no. 2, pp. 804-810, May 2000.

[97] N. Acharya and N. Mithulananthan, "Locating series FACTS devices for congestion management in deregulated electricity markets," *Electr. Power Syst. Res.,* vol. 77, no. 3–4, pp. 352-360, Mar. 2007.

[98] F. Capitanescu, J. L. Martinez Ramos, and P. Panciatici, et al., "State-of-the-art, challenges, and future trends in security constrained optimal power flow," *Electr. Power Syst. Res.,* vol. 81, no. 8, pp. 1731-1741, Aug. 2011.

[99] G. J. Hou and V. Vittal, "Determination of transient stability constrained interface real power flow limit using trajectory sensitivity approach," *IEEE Trans. Power Syst.,* vol. 28, no. 3, pp. 2156-2163, Aug. 2013.

[100] G. J. Hou and V. Vittal, "Cluster computing-based trajectory sensitivity analysis application to the WECC system," *IEEE Trans. Power Syst.,* vol. 27, no. 1, pp. 502-509, Feb. 2012.

[101] Q. Jiang and G. Geng, "A Reduced-space interior point method for transient stability constrained optimal power flow," *IEEE Trans. Power Syst.,* vol. 25, no. 3, pp. 1232-1240, Aug. 2010.

[102] M. La Scala, M. Trovato, and C. Antonelli, "On-line dynamic preventive control: an algorithm for transient security dispatch," *IEEE Trans. Power Syst.,* vol. 13, no. 2, pp. 601-610, May 1998.

[103] Q. Jiang and Z. Huang, "An enhanced numerical discretization method for transient stability constrained optimal power flow," *IEEE Trans. Power Syst.,* vol. 25, no. 4, pp. 1790-1797, Nov. 2010.

[104] Y. Xia, K. W. Chan, and M. Liu, "Direct nonlinear primal-dual interior-point method for transient stability constrained optimal power flow," *IET Proc.-Gener. Transm. Distrib.,* vol. 152, no. 1, pp. 11-16, Jan. 2005.

[105] Y. Sun, Y. Xinlin, and H. F. Wang, "Approach for optimal power flow with transient stability constraints," *IEE Proc.-Gener. Transm. Distrib.,* vol. 151, no. 1, pp. 8- 18, Jan. 2004.

[106] L. Chen, Y. Taka, and H. Okamoto, et al., "Optimal operation solutions of power systems with transient stability constraints," *IEEE Trans. Circuits and Syst. I: Fundamental Theory and Applications,* vol. 48, no. 3, pp. 327-339, Mar. 2001.

[107] L. Tang and J. D. McCalley,"An efficient transient stability constrained optimal power flow using trajectory sensitivity*," in Proc*. *North American Power Symposium*, Champaign, IL, Sep. 2012, pp. 1-6.

[108] A. Pizano-Martínez, E. A. Zamora-Cárdenas, and C. R. Fuerte-Esquivel, et al.,"Formulation of a new constraint for transient stability constrained optimal power flow*," in Proc*. *International Symposium on Innovation and Technology*, Cusco, Perú, Dec. 2012, pp. 28-39.

[109] J. Yuryevich and P. W. Kit, "Evolutionary programming based optimal power flow algorithm," *IEEE Trans. Power Syst.,* vol. 14, no. 4, pp. 1245-1250, Nov. 1999.

[110] A. G. Bakirtzis, P. N. Biskas, and C. E. Zoumas, et al., "Optimal power flow by enhanced genetic algorithm," *IEEE Trans. Power Syst.,* vol. 17, no. 2, pp. 229-236, May 2002.

[111] H. Yoshida, K. Kawata, and Y. Fukuyama, et al., "A particle swarm optimization for reactive power and voltage control considering voltage security assessment," *IEEE Trans. Power Syst.,* vol. 15, no. 4, pp. 1232-1239, Nov. 2000.

[112] G. Zwe-Lee, "Particle swarm optimization to solving the economic dispatch considering the generator constraints," *IEEE Trans. Power Syst.,* vol. 18, no. 3, pp. 1187- 1195, Aug. 2003.

[113] A. A. A. Esmin, G. Lambert-Torres, and A. C. Zambroni De Souza, "A hybrid particle swarm optimization applied to loss power minimization," *IEEE Trans. Power Syst.,* vol. 20, no. 2, pp. 859- 866, May 2005.

[114] K. Cheng-Chien, "A Novel coding scheme for practical economic dispatch by modified Particle Swarm approach," *IEEE Trans. Power Syst.,* vol. 23, no. 4, pp. 1825-1835, Nov. 2008.

[115] W. Rong-Jong, C. Shan, and L. Yeou-Fu, et al., "Installed capacity selection of hybrid energy generation system via improved particle-swarm-optimisation," *IET Gener. Transm. Distrib.,* vol. 8, no. 4, pp. 742-752, Apr. 2014.

[116] M. Fan, V. Vittal, and G. T. Heydt, et al., "Probabilistic power flow analysis with generation dispatch including photovoltaic resources," *IEEE Trans. Power Syst.,* vol. 28, no. 2, pp. 1797-1805, May 2013.

[117] M. Hajian, W. D. Rosehart, and H. Zareipour, "Probabilistic power flow by Monte Carlo simulation with Latin supercube sampling," *IEEE Trans. Power Syst.,* vol. 28, no. 2, pp. 1550-1559, May 2013.

[118] D. Villanueva, J. L. Pazos, and A. Feijoo, "Probabilistic load flow including wind power generation," *IEEE Trans. Power Syst.,* vol. 26, no. 3, pp. 1659-1667, Aug. 2011.

[119] M. Fan, V. Vittal, and G. T. Heydt, et al., "Probabilistic power flow studies for transmission systems with photovoltaic generation using cumulants," *IEEE Trans. on Power Syst.,* vol. 27, no. 4, pp. 2251-2261, Nov. 2012.

[120] J. M. Morales and J. Perez-Ruiz, "Point estimate schemes to solve the probabilistic power flow," *IEEE Trans. Power Syst.,* vol. 22, no. 4, pp. 1594-1601, Nov. 2007.

[121] H. P. Hong, "An efficient point estimate method for probabilistic analysis," *Reliability Engineering and System Safety,* vol. 59, no. 3, pp. 261-267, 1998.

[122] R. Billinton and P. R. S. Kuruganty, "Probabilistic assessment of transient stability in a practical multimachine system," *IEEE Trans. Power Appar. Syst.,* vol. PAS-100, no. 7, pp. 3634-3641, Jul. 1981.

[123] R. Billinton and P. R. S. Kuruganty, "A probabilistic index for transient stability," *IEEE Trans. Power Appar. Syst.,* vol. PAS-99, no. 1, pp. 195-206, Jan. 1980.

[124] P. M. Anderson and A. Bose, "A probabilistic approach to power system stability analysis," *IEEE Trans. Power Appar. Syst.,* vol. PAS-102, no. 8, pp. 2430-2439, Aug. 1983.

[125] E. Chiodo, F. Gagliardi, and D. Lauria, "Probabilistic approach to transient stability evaluation," *IEE Proc. Gener. Transm. Distrib.,* vol. 141, no. 5, pp. 537-544, Sep. 1994.

[126] E. Chiodo and D. Lauria, "Transient stability evaluation of multimachine power systems: a probabilistic approach based upon the extended equal area criterion," *IEE Proc. Gener. Transm. Distrib.,* vol. 141, no. 6, pp. 545-553, Nov. 1994.

[127] E. Chiodo, F. Gagliardi, and M. La Scala, et al., "Probabilistic on-line transient stability analysis," *IEE Proc. Gener. Transm. Distrib.,* vol. 146, no. 2, pp. 176-180, Mar. 1999.

[128] Y. Hsu and C. Chang, "Probabilistic transient stability studies using the conditional probability approach," *IEEE Trans. on Power Syst.,* vol. 3, no. 4, pp. 1565-1572, Nov. 1988.

[129] F. F. Wu, Y. K. Tsai, and Y. X. Yu, "Probabilistic steady-state and dynamic security assessment," *IEEE Trans. on Power Syst.,* vol. 3, no. 1, pp. 1-9, Feb. 1988.

[130] R. Billinton and S. Aboreshaid, "Stochastic modelling of high-speed reclosing in probabilistic transient stability studies," *IEE Proc. Gener. Transm. Distrib.,* vol. 142, no. 4, pp. 350-354, Jul. 1995.

[131] J. D. McCalley, A. A. Fouad, and V. Vittal, et al., "A risk-based security index for determining operating limits in stability-limited electric power systems," *IEEE Trans. on Power Syst.,* vol. 12, no. 3, pp. 1210-1219, Aug. 1997.

[132] E. Vaahedi, W. Li, and T. Chia, et al., "Large scale probabilistic transient stability assessment using BC Hydro's on-line tool," *IEEE Trans. on Power Syst.,* vol. 15, no. 2, pp. 661-667, May 2000.

[133] D. Lauria, C. Pisani, and D. Villacci,"Probabilistic transient stability margins assessment based upon quadratic stability region approximation*," in Proc. 2012 IEEE International Energy Conference and Exhibition*, Florence, Sep. 2012, pp. 439-444.

[134] Z. Y. Dong, J. H. Zhao, and D. J. Hill, "Numerical simulation for stochastic transient stability assessment," *IEEE Trans. on Power Syst.,* vol. 27, no. 4, pp. 1741-1749, Nov. 2012.

[135] D. Z. Fang, L. Jing, and T. S. Chung, "Corrected transient energy function-based strategy for stability probability assessment of power systems," *IET Gener. Transm. Distrib.,* vol. 2, no. 3, pp. 424-432, May 2008.

[136] M. Ali, Z. Y. Dong, and P. Zhang, "Adoptability of grid computing technology in power systems analysis, operations and control," *IET Gener. Transm. Distrib.,* vol. 3, no. 10, pp. 949-959, Oct. 2009.

[137] H. Cramér, *Mathematical Methods of Statistics*. Princeton: Princeton University Press, 1946.

[138] M. J. Panik, *Advanced statistics from an elementary point of view*. Burlington, MA: Elsevier Academic Press, 2005.

[139] *Probability and Statistical Inference*. Chichester, West Sussex: Wiley, 2007.

[140] P. Sauer and G. Heydt, "A convenient multivariate Gram-Charlier type A series," *IEEE Trans. Communications,* vol. 27, no. 1, pp. 247-248, Jan. 979.

[141] P. Zhang and S. T. Lee, "Probabilistic load flow computation using the method of combined cumulants and Gram-Charlier expansion," *IEEE Trans. Power Syst.,* vol. 19, no. 1, pp. 676-682, Feb. 2004.

[142] F. A. Rahimi, M. G. Lauby, and J. N. Wrubel, et al., "Evaluation of the transient energy function method for on-line dynamic security analysis," *IEEE Trans. Power Syst.,* vol. 8, no. 2, pp. 497-507, May 1993.

[143] Y. Zhang, L. Wehenkel, and P. Rousseaux, et al., "SIME: A hybrid approach to fast transient stability assessment and contingency selection," *Int. J. Elect. Power Energy Syst.,* vol. 19, no. 3, pp. 195-208, Mar. 1997.

[144] M. J. Laufenberg and M. A. Pai, "A new approach to dynamic security assessment using trajectory sensitivities," *IEEE Trans. on Power Syst.,* vol. 13, no. 3, pp. 953-958, Aug. 1998.

[145] S. Q. Yuan and D. Z. Fang, "Robust PSS parameters design using a trajectory sensitivity approach," *IEEE Trans. Power Syst.,* vol. 24, no. 2, pp. 1011-1018, May 2009.

[146] I. A. Hiskens and M. A. Pai, "Trajectory sensitivity analysis of hybrid systems," *IEEE Trans. Circuits Syst.,* vol. 47, no. 2, pp. 204-220, Feb. 2000.

[147] I. A. Hiskens, "Power system modeling for inverse problems," *IEEE Trans. Circuits and Systems I: Regular Papers,* vol. 51, no. 3, pp. 539- 551, Mar. 2004.

[148] R. D. Zimmerman, C. E. Murillo-Sánchez, and R. J. Thomas, "MATPOWER steady-state operations, planning and analysis tools for power systems research and education," *IEEE Trans. Power Syst.,* vol. 26, no. 1, pp. 12-19, Feb. 2011.

[149] M. A. Pai, *Energy function analysis for power system stability.* Norwell, MA: Kluwer, 1989.

[150] A. A. Fouad and V. Vittal, *Power system transient stability analysis using the transient energy function method.* Englewood Cliffs, NJ: Prentice-Hall, 1992.

[151] J. Kennedy and R. Eberhart,"Particle swarm optimization*," in Proc. Proc. IEEE Int. Conf. on Neural Networks*, Perth, WA, Jan. 1995, pp. 1942-1948.

[152] A. K. David and X. J. Lin, "Dynamic security enhancement in power-market systems," *IEEE Trans. Power Syst.,* vol. 17, no. 2, pp. 431-438, May 2002.

[153] M. Basu, "Optimal power flow with FACTS devices using differential evolution," *Int. J. Elect. Power Energy Syst.,* vol. 30, no. 2, pp. 150-156, Feb. 2008.

[154] W. E. C. Council, "NERC/WECC Planning Standards. [Online]," *http://www.wecc.biz/documents/library/ procedures/ planning*.

[155] R. Lumia, "A novel method for signal energy measurement," *IEEE Trans. Instrum. Meas.,* vol. 29, no. 3, pp. 198-200, Sep. 1980.

[156] C. A. Coello Coello, "Theoretical and numerical constraint-handling techniques used with evolutionary algorithms: a survey of the state of the art," *Computer Methods in Applied Mechanics and Engineering,* vol. 191, no. 11, pp. 1245-1287, Apr. 2002.

[157] Y. Shi and R. C. Eberhart,"Parameter selection in Particle Swarm Optimization*," in Proc. Proc. of the 7th Int. Conf. on Evolutionary Programming VII*, California, USA, 1998, pp. 591-600.

[158] C. Fu and A. Bose, "Contingency ranking based on severity indices in dynamic security analysis," *IEEE Trans. Power Syst.,* vol. 14, no. 3, pp. 980-985, Aug. 1999.

[159] F. Capitanescu, M. Glavic, and D. Ernst, et al., "Contingency filtering techniques for preventive security constrained optimal power flow," *IEEE Trans. Power Syst.,* vol. 22, no. 4, pp. 1690-1697, Nov. 2007.

[160] K. R. Padiyar, *Power system dynamics: stability and control.* Singapore: John Wiley & Sons (Asia) Pte Ltd, 1996.

[161] S. He, Q. H. Wu, and J. R. Saunders,"A novel Group Search Optimizer inspired by animal behavioural ecology*," in Proc. IEEE Congress on Evolutionary Computation*, Vancouver, BC, Jul. 2006, pp. 1272-1278.

[162] S. He, Q. H. Wu, and J. R. Saunders, "Group Search Optimizer: an optimization algorithm inspired by animal searching behavior," *IEEE Trans. Evol. Comput.,* vol. 13, no. 5, pp. 973-990, Oct. 2009.

[163] H. Shen, Y. Zhu, and B. Niu, et al., "An improved Group Search Optimizer for mechanical design optimization problems," *Prog Nat Sci,* vol. 19, no. 1, pp. 91-97, Oct. 2009.

[164] L. Wang, X. Hu, and J. Ning, et al., "A modified Group Search Optimizer algorithm for high dimensional function optimization," *Communications in Computer and Information Science,* vol. 308, pp. 219-226, 2012.

[165] X. Yan, W. Yang, and H. Shi, "A Group Search Optimization based on improved small world and its application on neural network training in ammonia synthesis," *Neurocomputing,* vol. 97, pp. 94-107, Nov. 2012.

[166] L. D. S. Pacifico and T. B. Ludermir,"Improved Group Search Optimization based on opposite populations for feedforward networks training with weight decay*," in Proc. IEEE International Conference on Systems, Man, and Cybernetics*, Seoul, Oct. 2012, pp. 474-479.

[167] T. Back and H. Schwefel, "An overview of evolutionary algorithms for parameter optimization," *Evolutionary Computation,* vol. 1, no. 1, pp. 1-23, Mar. 1993.

[168] A. Papoulis, *Probability, random variables, and stochastic processes.* New York: McGraw-Hill, 2002.

[169] P. W. Sauer and M. A. Pai, *Power system dynamics and stability.* Englewood Cliffs, NJ: Prentice-Hall, 1998.

[170] R. D. Zimmerman, C. E. Murillo-Sanchez, and D. Gan, "MATPOWER: a Matlab power system simulation package 2006 [Online]," *http://www.pserc.cornell.edu//matpower/.*

[171] O. Anaya-lara, N. Jenkins, and J. Ekanayake, et al., *wind energy generation modelling and control.* West Sussex: A john Wiley and Sons, Ltd., 2009.

[172] H. Wu, M. Shahidehpour, and Z. Li, et al., "Chance constrained day-ahead scheduling in stochastic power system operation," *IEEE Trans. Power Syst.,* vol. 29, no. 4, pp. 1583-1591, Jul. 2014.

[173] Q. Wang, J. Wang, and Y. Guan, "Price based unit commitment with wind power utilization constraints," *IEEE Trans. Power Syst.,* vol. 28, no. 3, pp. 2718-2726, Aug. 2013.

[174] H. Yu, C. Y. Chung, and K. P. Wong, et al., "A chance constrained transmission network expansion planning method with consideration of load and wind farm uncertainties," *IEEE Trans. Power Syst.,* vol. 24, no. 3, pp. 1568-1576, Aug. 2009.

[175] J. Wu, J. Zhu, and G. Chen, et al., "A hybrid method for optimal scheduling of short-term electric power generation of cascaded hydroelectric plants based on Particle Swarm Optimization and chance-constrained programming," *IEEE Trans. Power Syst.,* vol. 23, no. 4, pp. 1570-1579, Nov. 2008.

[176] S. O. Faried, R. Billinton, and S. Aboreshaid, "Probabilistic evaluation of transient stability of a power system incorporating wind farms," *IET Renewable Power Generation,* vol. 4, no. 4, pp. 299-307, Jul. 2010.

[177] H. Zhang and P. Li, "Chance constrained programming for optimal power flow under uncertainty," *IEEE Trans. Power Syst.,* vol. 26, no. 4, pp. 2417-2424, Nov. 2011.

[178] F. Vallee, J. Lobry, and O. Deblecker, "System reliability assessment method for wind power integration," *IEEE Trans. Power Syst.,* vol. 23, no. 3, pp. 1288-1297, Aug. 2008.

[179] H. Huang and C. Y. Chung, "Coordinated damping control design for DFIG-based wind generation considering power output variation," *IEEE Trans. Power Syst.,* vol. 27, no. 4, pp. 1916-1925, Nov. 2012.

[180] A. Schellenberg, W. Rosehart, and J. Aguado, "Cumulant-based probabilistic optimal power flow (P-OPF) with Gaussian and gamma distributions," *IEEE Trans. Power Syst.,* vol. 20, no. 2, pp. 773- 781, May 2005.

[181] J. M. Morales, L. Baringo, and A. J. Conejo, et al., "Probabilistic power flow with correlated wind sources," *IET Gener. Transm. Distrib.,* vol. 4, no. 5, pp. 641-651, May 2010.

[182] B. Zhou, K. W. Chan, and T. Yu, et al., "Equilibrium-inspired multiple Group Search Optimization with synergistic learning for multiobjective electric power dispatch," *IEEE Trans. Power Syst.,* vol. 28, no. 4, pp. 3534-3545, Nov. 2013.

[183] D. Gautam, L. Goel, and R. Ayyanar, et al., "Control strategy to mitigate the impact of reduced inertia due to doubly fed induction generators on large power systems," *IEEE Trans. Power Syst.,* vol. 26, no. 1, pp. 214-224, Feb. 2011.

[184] "GE Power & Water, Renewable Energy [Online]," *http://www.ge-energy.com/products_and_services/products/wind_turbines*.

[185] A. M. Leite Da Silva, R. A. G. Fernandez, and C. Singh, "Generating capacity reliability evaluation based on Monte Carlo simulation and Cross-Entropy methods," *IEEE Trans. Power Syst.,* vol. 25, no. 1, pp. 129-137, Feb. 2010.

[186] H. Zhang and P. Li, "Probabilistic analysis for optimal power flow under uncertainty," *IET Gener. Transm. Distrib.,* vol. 4, no. 5, pp. 553-561, May 2010.

[187] Y. M. Atwa, E. F. El-Saadany, and M. M. A. Salama, et al., "Adequacy Evaluation of Distribution System Including Wind/Solar DG During Different Modes of Operation," *IEEE Trans. on Power Syst.,* vol. 26, no. 4, pp. 1945-1952, Nov. 2011.

[188] A. C. Xue, F. F. Wu, and Q. Lu, et al., "Power system dynamic security region and its approximations," *IEEE Trans. Circuits Syst.,* vol. 53, no. 12, pp. 2849-2859, Dec. 2006.